METEOR-BERICHTE

CAYSEIS - magma-starved oceanic crustal accretion and transform margin formation in the Cayman Trough revealed by seismic and seismological data

Cruise No. M115

April 1 – April 28, 2015,
Kingston (Jamaica) – Pointe-à-Pitre (Guadeloupe)

**I. Grevemeyer, A. Dannowski, N. W. Hayman,
C. Peirce, H. van Avendonk**

Editorial Assistance:

DFG-Senatskommission für Ozeanographie
MARUM – Zentrum für Marine Umweltwissenschaften der Universität Bremen

2016

The METEOR-Berichte are published at irregular intervals. They are working papers for people who are occupied with the respective expedition and are intended as reports for the funding institutions. The opinions expressed in the METEOR-Berichte are only those of the authors.

The METEOR expeditions are funded by the *Deutsche Forschungsgemeinschaft (DFG)* and the *Bundesministerium für Bildung und Forschung (BMBF).*

Editor:
DFG-Senatskommission für Ozeanographie
c/o MARUM – Zentrum für Marine Umweltwissenschaften
Universität Bremen
Leobener Strasse
28359 Bremen

Author:
Prof. Dr. Ingo Grevemeyer
GEOMAR Helmholtz Zentrum
für Ozeanforschung
Wischhofstraße 1-3
24148 Kiel

Telefon: +49-431-600-2336
Telefax: +49-431-600-2922
e-mail: igrevemeyer@geomar.de

Citation: I. Grevemeyer, A. Dannowski, N.W. Hayman, C. Peirce, H. van Avendonk (2016) CAYSEIS - magma-starved oceanic crustal accretion and transform margin formation in the Cayman Trough revealed by seismic and seismological data – Cruise No. M115 – April 1 – April 28, 2015 – Kingston (Jamaica) – Pointe-à-Pitre (Guadeloupe). METEOR-Berichte, M115, 56 pp., DFG-Senatskommission für Ozeanographie, DOI:10.2312/cr_m115

ISSN 2195-8475

Table of Contents

		Page
1	Summary	03
2	Participants	04
3	Research Programme	05
	3.1 Scientific background	05
	3.1.1 Ultra-slow spreading – crustal accretion and hydrothermal activity	05
	3.1.2 Transform margins – a widely unrecognized class of passive continental margins	08
	3.1.3 The Mid-Cayman spreading centre	10
	3.1.4 The Swan Island transform fault boundary	13
	3.2 Objectives and goals	13
4	Cruise narrative	16
5	Preliminary results	20
	5.1 Performance of scientific equipment	20
	5.1.1 EM122 Kongsberg echosounder	20
	5.1.2 Ocean-bottom seismographs	21
	5.1.3 Airgun array	23
	5.1.4 Marine gravimeter / gravity	24
	5.1.5 Marine magnetometer / magnetics	25
	5.2 First scientific results from shipboard data	25
	5.2.1 Local earthquake monitoring	26
	5.2.2 Passive acoustic and visual mammal observation	29
	5.2.3 Profile P1 – along the Mid-Cayman spreading centre	30
	5.2.4 Profile P2 and P3 – across the Mid-Cayman spreading centre	34
	5.2.5 Profile P4 – mature ultra-slow spreading crust and Swan Island transform	34
	5.2.6 Profile P5 – off-axis structure of ultra-slow spreading crust	35
	5.2.7 Profile P6 – off-axis structure of ultra-slow spreading crust	42
	5.3 Weather report	42
6	Station lists	44
7	Data archive and availability	53
8	Acknowledgements	53
9	References	54
Appendix 1– Gravimeter Installation		57
Appendix 2 – Report on Marine Mammal Observation		69

1 Summary

About 57% of the Earth's outer surface is oceanic crust and new ocean floor is continuously created along the 55,000-60,000 km long mid-ocean ridge (MOR) system. About 25% of MORs spread at an ultra-slow spreading rate of < 20 mm/yr. Most ultra-slow spreading ridges occur in areas of the world that are difficult to reach, like the Gakkel Ridge in the Arctic Ocean and the Southwest Indian Ridge in the Indian Ocean. It has long been recognized that crustal accretion at ultra-slow spreading rates is fundamentally different from crust generated at faster spreading rates. However, due to the remoteness of ultra-slow ridges, the formation of crust at these magma-starved centres is yet not well understood. During the CAYSEIS cruise we surveyed lithospheric formation at ultra-slow spreading rates at the Mid-Cayman spreading centre (MCSC) in the Caribbean Sea, where oceanic crust is formed at a full rate of ~17 mm/yr. To the northeast and southwest, the MCSC is bound by two major transform faults. Using active-source wide-angle seismic imaging and passive local earthquake monitoring we, studied the balance between magmatic accretion and tectonic stretching (and hence oceanic core complex formation) and the relationship between faulting and hydrothermal activity at ultra-slow spreading rates. In addition, we explored transform margin formation at a unique setting, occurring at the southern terminus of the MCSC. In total, six seismic lines surveyed crust formed at the MCSC, two of these profiles also crossed the Swan Island transform fault. The project was a collaboration between German, British and American scientists.

Zusammenfassung

Die Erdoberfläche besteht zu ca. 57% aus Ozeanischer Kruste, welche kontinuierlich an dem 55-60 tausend km langen System der Mittelozeanischen Rücken generiert wird. Rund 25% der Kruste werden bei Spreizungsraten von <20 mm pro Jahr produziert. Generell sind diese sehr-langsam spreizenden Rücken in Gegenden zu finden, welche nur schwierig zu erreichen sind, wie der Gakkel Rücken in der Arktis und der Südwestindische Rücken im Indischen Ozean. Die Tatsache, dass sich der Spreizungsprozess fundamental bei sehr langsamen Raten ändert, macht diesen Typ von Spreizungsachsen jedoch besonders bedeutsam. Aus diesem Grund wurde die Bildung neuer Ozeanischer Kruste an der Cayman Spreizungsachse (MCSC) in der Karibik untersucht. Am MCSC wird mit einer Rate von 17 mm pro Jahr kontinuierlich neuer Meeresboden produziert. Im Nordosten und Südwesten wird das Becken durch Transformverwerfungen begrenzt. Das Ziel der durchgeführten Untersuchungen war es, entlang von sechs seismischen Profilen und durch die passive Überwachung der lokalen Erdbebenaktivität, die Generierung von Kruste an magmatisch-unterversorgten Spreizungszentren, sowie die Beziehung zwischen hydrothermaler Aktivität und aktiven Störungen zu untersuchen. Darüber hinaus wurde entlang von zwei Profilen am südlichen Ende des MCSC die Entwicklung eines gescherten passiven Kontinentalrands erkundet. Die durchgeführten Messungen wurden in Kooperation mit Partnern aus Deutschland, Großbritannien und den USA durchgeführt.

2 Participants

Name	Discipline	Institution
Grevemeyer, Ingo, Prof. chief scientist	OBS	GEOMAR
Dannowski, Anke, Dr., scientist	OBS	GEOMAR
Gaida, Timo, student	Airguns / OBS	CAU
Gausepohl, Florian, scientist	OBS	GEOMAR
Merz, Michaela, student	OBS	CAU
Papenberg, Cord, Dr. scientist	OBS	GEOMAR
Reußwig, Rabea, student	OBS	CAU
Steffen, Klaus-Peter, technician	Airguns	GEOMAR
Völsch, Ann-Marie, scientist	OBS	GEOMAR
Wehner, Daniel, student	Airguns / OBS	CAU
Wieprich, Margit, scientist	OBS	GEOMAR
Hall, Kapleton Kirk, observer	Observer	Jamaica
Peirce, Christine, Prof. scientist	OBS	Durham
Bird, Anna, technician	Mammal observation	Durham
Clegg, Andrew Paul, technician	OBS	OBIF
Erfanian-Mehr, Mahshid, technician	OBS	OBIF
Pitcairn, Ben, technician	OBS	OBIF
Hayman, Nicholas, Dr. scientist	OBS	UTIG
van Avendonk, Harm, Dr. scientist	OBS	UTIG
Harding, Jennifer, graduate student	OBS	UTIG
Mironov, Anatoly, technician	OBS	UTIG
Saustrup, Steffen, technician	OBS	UTIG
Snyder, Rebecca. technician	Mammal observation	Seiche
Raeke, Andreas, technician	Met technician	DWD

GEOMAR	Helmholtz Zentrum für Meeresforschung, Kiel, Germany
CAU	Christian-Albrchts Universität zu Kiel, Gemany
Durham	Department of Earth Sciences, Durham University, UK
OBIF	Ocean Bottom Instrument Facility, UK
UTIG	Institute for Geophysics, The University of Texas at Austin, U.S.A
DWD	Deutscher Wetter Dienst, Offenbach, Germany
Seiche	Seiche Limited, UK

3 Reseach Programme

3.1 Scientific background

In 2010 the island of Haiti was hit by one of the most deadly earthquakes occurring in the last 100 years. The moment magnitude Mw=7.0 earthquake occurred along a fault system that connects the Puerto Rico trench and the Swan Island transform fault, marking the northernmost boundary of the Caribbean plate (Fig. 3.1). The Swan Island transform generated recently one of the largest events in the Caribbean Sea: a Mw=7.3 strike-slip earthquake, occurring in 2009 offshore of Honduras. Motion along these major strike slip faults is caused by seafloor spreading in the Cayman Trough. The Cayman Trough hosts an ultra-slow spreading centre, generating new seabed at a full rate on 17 mm/yr, over the last 45 Myr (Fig. 3.1a). In 2009-10, research activities at the Mid-Cayman spreading centre (MCSC) discovered the deepest known black-smoker hydrothermal vents [German et al., 2009]. Cruise M115 was focused on two main topics:

(i) the crustal accretion process at the MCSC, surveying the relationship between crustal structure, fault activity, and hydrothermal venting; and
(ii) the effects of spreading on the evolution of the Swan Island transform fault.

The Swan Island transform fault (and the parallel Oriente transform fault to the northeast) provides a rare opportunity to study the drift phase of a transform margin, where newly accrete oceanic crust occurs on one side and continental crust on the other.

3.1.1 Ultra-slow spreading – crustal accretion and hydrothermal activity

The world's oceanic crust is accreted at mid-ocean ridges leading to a feedback between magmatism, volcanism, faulting, and hydrothermal fluid flow. Many studies of mid-ocean ridges revolve around presumed relationships between:

(1) spreading rate and crustal thickness,
(2) faulting of axial crust and magmatic intrusion,
(3) axial depth and the thickness of the upper mantle thermal boundary layer, and
(4) abundance of hydrothermal activity and spreading rate.

These relationships are especially relevant at ultra-slow spreading centres. Ultra-slow ridges spread at <20 mm/yr (full rate), a rate at which the melt supply to ridges is thought to dramatically decrease [e.g., Reid and Jackson, 1981; Grevemeyer et al., 1997]. Thus, many ultra-slow spreading centres are in a phase of amagmatic spreading, resulting in the surface exposure of the upper mantle at the seabed [Dick et al., 2003], and low hydrothermal activity [Baker et al., 1996]. However, several ultra-slow ridge segments have locally abundant magmatism and hydrothermal activity [e.g., Michael et al., 2003; Baker and German, 2004; Cannat et al., 2006]. The wide range in magmatic and tectonic styles points to dynamic relationships between these ridge processes at ultra-slow spreading rates.

Recent work on the Southwest Indian ridge (SWIR) has led to a new model for the relationship between tectonic faulting, magmatism, and crustal thickness at ultra-slow spreading centres [Cannat et al., 2006]. In this model (Fig. 3.2), as the amount of melt transported to the

crust decreases, symmetric spreading of faulted, magmatic crust is interrupted by the exhumation of smooth seafloor comprising predominantly mantle peridotite. In the transition between these two styles of seafloor spreading, domal massifs rise kilometres above the adjacent ridge valleys. These massifs are called oceanic core complexes (OCCs) and, in some places comprise exhumed mantle peridotite and in others, crustal gabbroic rocks [e.g., Dick et al., 2000; Karson et al., 2006; Escartin et al., 2003; Ildefonse et al., 2007]. In current models and drill-core studies from key areas of the SWIR and Mid-Atlantic Ridge (MAR), the basaltic hanging wall is stripped away by detachment faulting and the OCC rotates in response to the unloading and extension [e.g., Dick et al., 2000; Karson et al., 2006].

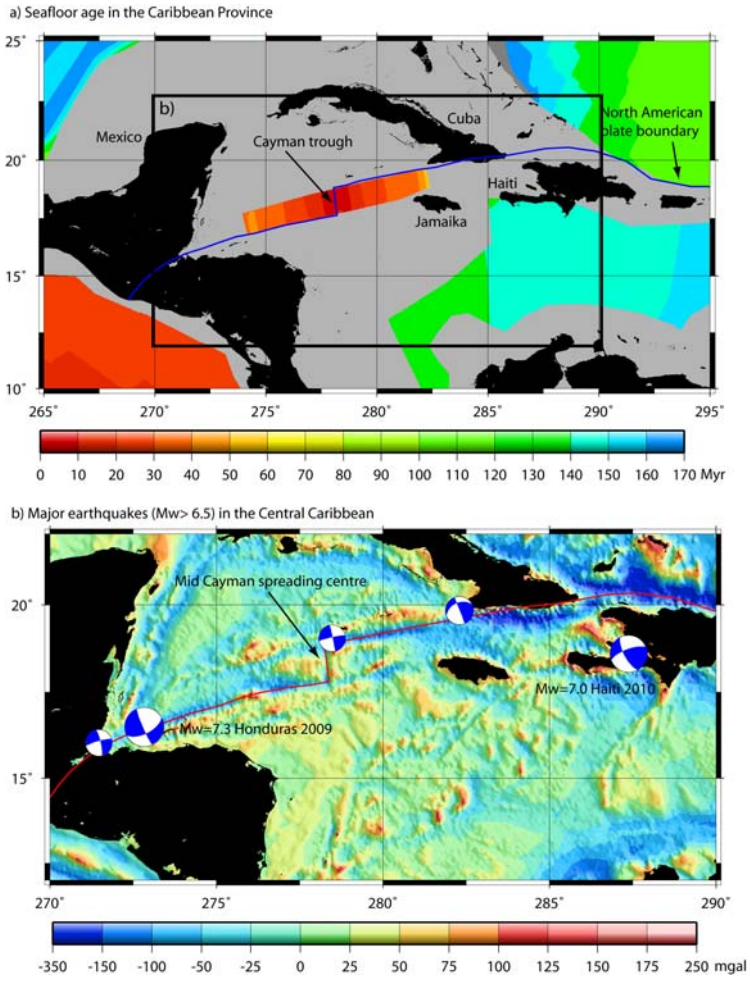

Fig. 3.1 Location map of the study area in the Caribbean Sea. a) Seafloor age in Myr. (b) Satellite-derived gravity field and regional earthquakes.

What is particularly interesting about the OCC model is that it requires dynamic interactions between magmatism, hydrothermal activity, and faulting. Many of the aspects of OCC development, and particularly detachments slipping at low angles, require crustal weakening by either melting in the upper mantle and lower crust [e.g., Yoshinobu and Hirth, 2002] and/or hydrothermal alteration, such as serpentinization in the upper crust [e.g., Escartin et al., 2003].

The 'life-cycle' of an OCC is, therefore, dependent on patterns of melting and hydrothermal alteration. Workers are beginning to understand these dynamics in slow-spreading centres such as the MAR. A frontier area is to now test the OCC model at an ultra-slow spreading rate, where the patterns of melting and hydrothermal fluid flow are thought to be at a low-flux end-member. Seismic imaging is key to this task given its success at imaging of OCC structure and crustal properties around hydrothermal systems [deMartin et al., 2007].

OCC development is also linked to patterns of volcanism and hydrothermal venting [Dick et al., 2008; Escartin et al., 2008]. The identification of the Lost City Field on the Atlantis Massif (MAR) [Kelley et al., 2001], and role of detachment faulting in positioning vents along the MAR [Escartin et al., 2008], led to the recognition of OCCs as key sites for hydrothermal systems. OCC-related faulting may provide fluid conduits, serpentinization provides heat and chemical

exchange with fluids, and hypothesized off-axis magmatism in slow- and ultra-slow spreading centres likely drives much of the fluid flow.

The most detailed studies of ultra-slow spreading ridges, to date, have been carried out along the SWIR, and indicate along-strike changes (over hundreds of kilometres) in upper mantle thermal structure that leads to differences in axial bathymetric structure [e.g., Cannat et al., 2008]. Seismic modelling by Muller et al. [1997] verified crustal thickness changes in the 66°E area of the SWIR that correspond to gravity and bathymetry variations. When viewed on the segment scale (tens of kilometres), the SWIR has well-defined OCCs [Dick et al., 2000; Cannat et al., 2006]. The seismically most studied SWIR OCC is the Atlantis Bank.

Muller et al. [1997] studied four wide-angle seismic profiles across Atlantis Bank and the adjacent Atlantis Platform around Ocean Drilling Program (ODP) Hole 735B [Dick et al., 2000]. Muller et al. [1997] were able to determine that the intact crust away from the OCC had a high velocity gradient in oceanic crustal layer 2 and a lower velocity gradient in layer 3, with a total crustal thickness of 4 km. In contrast, the OCC around Hole 735B was missing layer 2, but had a 5 km deep Moho. In the context of the crustal geochemistry, it is noteworthy that this area of the SWIR has comparable Na8 values and REE compositions to that of the MCSC (see section 3.1.3), with an inferred overall ~3 km thick crust and a >15 km deep melt column [Muller et al., 1997].

In effect, the Atlantis Bank area of the SWIR is, therefore, confronted with the same problem as the MCSC (see section 3.1.3). On one hand, there is an apparently straightforward connection between the ultra-slow spreading rate, deep axial bathymetry, basalt geochemistry, and gravity and velocity anomalies indicating a very thin crust. On the other hand, there is a structural un-roofing of crustal material by detachment faulting, and potential trapping of melt in the lower crust [e.g., Dick et al., 2000] leading, locally, to anomalously thick (5 km) areas of crust. The structure is further complicated by variable serpentinization of exhumed upper mantle.

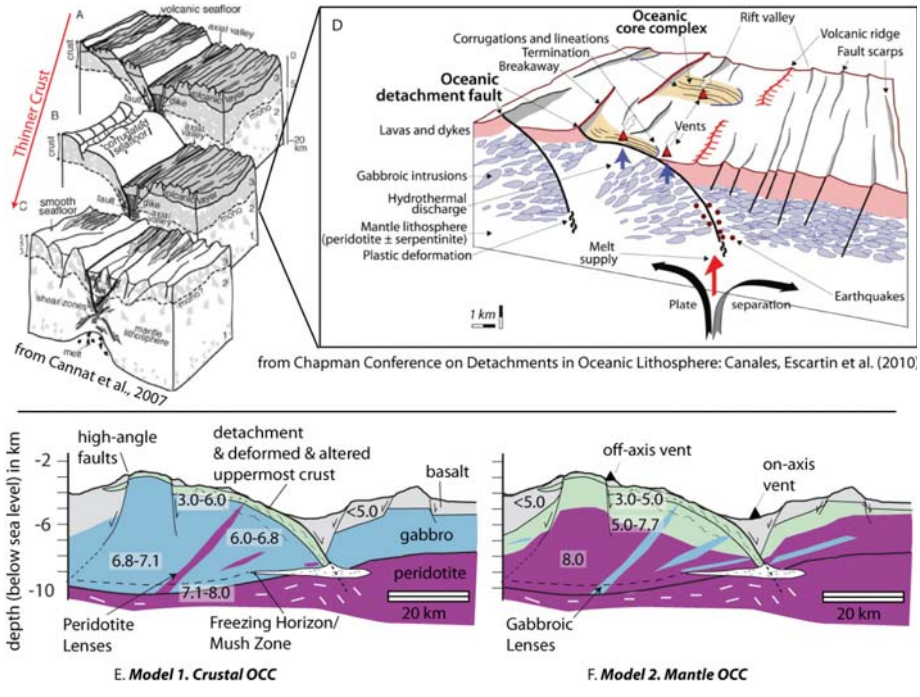

Fig. 3.2 (top) Models for oceanic core complex formation. (bottom) Models to be tested with the proposed experiment.

Seismic refraction studies of OCC formation have been constrained using dredge samples and rock samples from IODP Hole 1309D [e.g., Ildefonse et al., 2007] to ground truth the models with lithological constraints [e.g., Canales et al., 2008; Collins et al., 2009; Dannowski et al., 2010]. High-resolution tomographic images of the Atlantis Massif OCC obtained from MCS

streamer refractions, have been used to infer the presence of fresh peridotite, serpentinized mantle rock, or igneous crust [Canales et al., 2008; Blackman et al., 2009]. Collins et al. [2009], using the NOBEL near-seafloor explosion source to get good shallow refractions on OBSs, obtained a comparable results to the aforementioned streamer refraction studies. The 6 km long streamer of the R/V Maurice Ewing was sufficient to image the top ~1.5 km of this ~1 km deep bathymetric high [Canales et al., 2008]. Seismic velocities increase rapidly from 2 to 4 km/s near the seafloor to just over 7 km/s at 1.0-1.5 km depth [Blackman et al., 2009]. To image deeper into the basement would have required longer source-receiver offsets.

The absolute P-wave velocities, imaged from the arrival times of streamer refractions, are difficult to interpret because the velocities up to 7 km/s could represent either serpentinized mantle rock or gabbro. A similar problem was experienced by Muller et al. [1997] at the SWIR. However, Blackman et al. [2009] noted that seismic velocities higher than 6 km/s in the top 500 m of the basement of Atlantis Bank (SWIR) and Atlantis Massif (MAR) coincide with the gabbroic sections recovered by scientific drilling [e.g., Dick et al., 2000; Ildefonse et al., 2007]. Lower seismic velocity gradients presumably represent predominantly serpentinized ultramafic rocks.

A key lesson learnt from the Atlantis Massif seismic experiments [Canales et al., 2008; Collins et al., 2009] is that while unaltered gabbros have lower velocities than peridotite, they may have comparable, or even higher velocities than serpentinized peridotite because of more extensive alteration of ultramafic rock. The near-surface seismic structure can be determined at high resolution by streamer tomography, but such short source-receiver offsets do not provide coverage of the deeper parts of the OCC.

To date, the deep structure of OCCs, where rocks are assumed to be unaltered, has been best resolved by two surveys conducted with the German RV METEOR using active-source OBS data. At the MAR near 22°N, Dannowski et al. [2010] found a continuous oceanic crustal layer 3 extending from an OCC to the adjacent crust, but with a pronounced change in Moho depth. Planert et al. [2009; Reston et al., 2002] undertook a similar survey at the MAR and found relatively thick oceanic crust (6-10 km) on a spreading segment with an OCC at 5°S. Both studies yielded a profound asymmetry between the conjugated ridge flanks, favouring model 1 of Fig. 3.2.

Lastly, we note that local earthquake monitoring and tomographic images across the TAG field on the MAR have been essential to understanding the hydrothermal systems [deMartin et al., 2007]. The refraction study at TAG shows a pronounced lateral change in velocity across an inferred detachment (based upon earthquake distributions along a high-angle fault plane at depth). The velocity change is attributed to a change in the relative proportions of volcanics and gabbros.

3.1.2 Transform margins – a widely unrecognized class of passive continental margins

In a broad sense, continental margins are either active or passive, depending on the degree of observed volcanic and/or tectonic activity [for a review see Reston, 2009; Fig. 3.3]. Active margins display significant activity associated with the convergence of two lithospheric plates, whilst passive margins are much less expressive and subside thermally or under the load of the great thickness of sediment which accumulates there.

Early studies of passive continental margins included multi-channel seismic (MCS) reflection surveys, which imaged two distinctive styles of sedimentation and basement geometry. The first showed large, rotated fault blocks infilled by small sedimentary basins, whereas the second revealed a wedge-shaped body of seaward-dipping reflectors (SDRs) primarily within the sediment column. These SDRs were thought to result from eruption of massive volumes of basaltic lava. In addition, wide-angle seismic refraction studies observed that some margins also exhibited large extents of sub-crustal, high velocity (7.2-7.7 km/s) magmatic material, termed underplating. Consequently, margins are classified as either volcanic at which SDRs and underplating are observed, or nonvolcanic where they are not.

The along-strike continuity of these rifted margins is often punctuated by significant lateral offsets, known as transform margins. Despite the relative abundance of transform margin segments along passive margins, they remain less well studied and, hence, less well understood than rifted margins. Transform margins represent zones of sheared continental crust, which offset adjacent rifted margin segments. They are associated with fracture zones in the oceanic crust which can often be traced in gravity free-air anomaly data from the transform margin itself to an offset in the associated mid-ocean ridge (MOR) axis. Consequently, at the MOR, the spreading centre is offset in a similar manner to along-strike continental margin structures. In addition to their accompanying fracture zones, transform margins are most readily distinguished by their characteristically steep continental slopes, observed adjacent to, in many cases, an elevated section of the basement surface known as a marginal ridge. The ridge is most likely a result of thermal expansion resulting from heat flow across the margin, between adjacent old cold continental and young hot oceanic lithosphere, or might be caused by compressional tectonics, sharp variations in degree of subsidence and/or magmatic underplating.

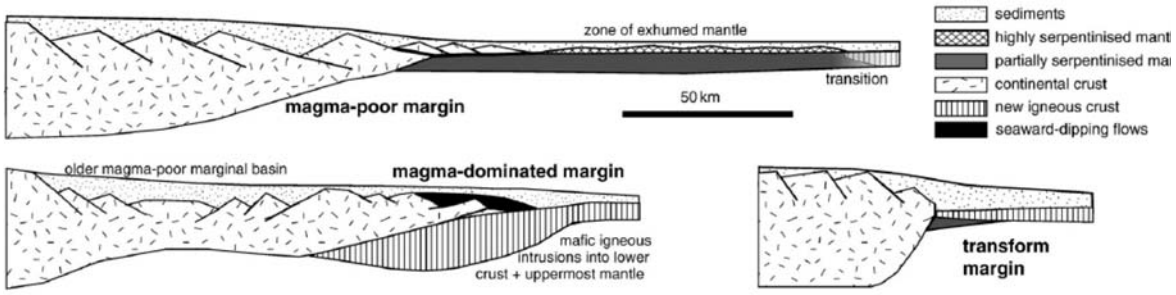

Fig. 3.3 Classification of passive continental margins based on extension direction and magma production rate [Reston, 2009].

The heat flow explanation is consistent with conceptual models of transform margins that suggest that they formed and evolved in a series of stages [e.g., Peirce et al., 1996]:

(1) initial intracontinental rifting. On a small scale, initial rifting consists of many small faults that, as rifting progresses, link together to form larger-scale rift- and transform-style structures. As rifting continues the continental crust thins orthogonal to the rift axis and several distinct rift segments form, each separated by a transform;
(2) crustal thinning proceeds to such an extent that plate separation finally occurs and oceanic spreading centres form; thus, spreading results in the juxtaposition of old

continental lithosphere against young oceanic lithosphere across a transform and the continental plates continue to drift apart; and

(3) later transform motion stops and the transform margin becomes inactive, placing aged oceanic crust next to continental crust.

Consequently, thinned continental crust may ultimately be juxtaposed against normal thickness oceanic crust across a fracture zone. The resultant margin structure is also dependent on the degree to which the oceanic and continental crustal blocks are mechanically coupled. However, in order to improve estimates for the degree of coupling, thermal history and lithospheric strength, more observations of deep crustal structure are required. Furthermore, transform faults are believed to be sites where mantle is highly hydrated. The effect of transform-related serpentinization is unknown. It is possible that serpentinization may reduce the effect of friction between the two plates and, hence, facilitate the evolution of structurally segmented margins. This mechanism might be similar to that proposed for the motion of crustal blocks along low-angle detachment faults at non-volcanic rifted margins.

The deep structure of transform margins has been modelled with both gravity and wide-angle seismic refraction data, suggesting that the continental crust thins sharply over a distance of less than 10-40 km. For example, the Ghana [Edwards et al., 1997] and French Guiana [Greenroyd et al., 2008] margins exhibit continental crustal thinning over zones of 10-20 km and ~40 km in width respectively. Edwards et al. [1997] also note the presence of a zone of high density (3100 kg/m3), high velocity (5.8-7.3 km/s) and high magnetization (1.10-1.25 A/m) at the ocean-continent boundary of the Ghana transform margin. They suggest that this zone may be a consequence of either intrusion by basic igneous rocks or serpentinization of upper mantle material. In the latter case, the serpentinzation occurs as a result of water ingress at the transform, a characteristic that is also observed at oceanic fracture zones [Detrick et al., 1993].

Studies in which such observations of transform margins have been made are relatively few, and it is uncertain if they are sufficiently diverse to encompass all the characteristic features. The study of newly accreted oceanic crust juxtaposed against continental crust, and the effect of active relative motion between them is, therefore, critical to further advance our knowledge of ho transform margins evolve.

3.1.3 The Mid-Cayman spreading centre

The Mid-Cayman spreading centre (MCSC) is spreading at a full rate of 15-17 mm/yr [Holcombe and Sharman, 1973] and was first recognized during early studies of the North American-Caribbean plate boundary. Its ultra-slow spreading rate has been confirmed by more recent geodetic solutions [DeMets et al., 2007]. Magnetic anomalies have been identified back to at least 45.6 Ma (anomaly 20) [Rosencrantz et al., 1988; Leroy et al., 2000], just after rifting of the Caribbean Large Igneous Province (CLIP), and Mayan and Chortis continental crustal blocks [e.g., Mann, 2007].

Recent efforts discovered the deepest known black smoker hydrothermal vents [German et al., 2009] at the MCSC. These vents are of particular interest because the great water depths impose anomalously high pressures on the seafloor for a ridge setting, potentially giving rise to unusually high vent fluid temperatures. Biologists are also particularly interested in these vents because any vent-associated biota at the MCSC may have evolved independently from East Pacific Rise (EPR) and MAR vent biota, thereby placing constraints on time-scales and conditions of increasing biodiversity on vent systems worldwide. An off-axis, moderate-temperature sulphide vent was also discovered, attesting to an extensive hydrothermal system, likely requiring some combination of faulting to enhance permeability and/or an off-axis heat source.

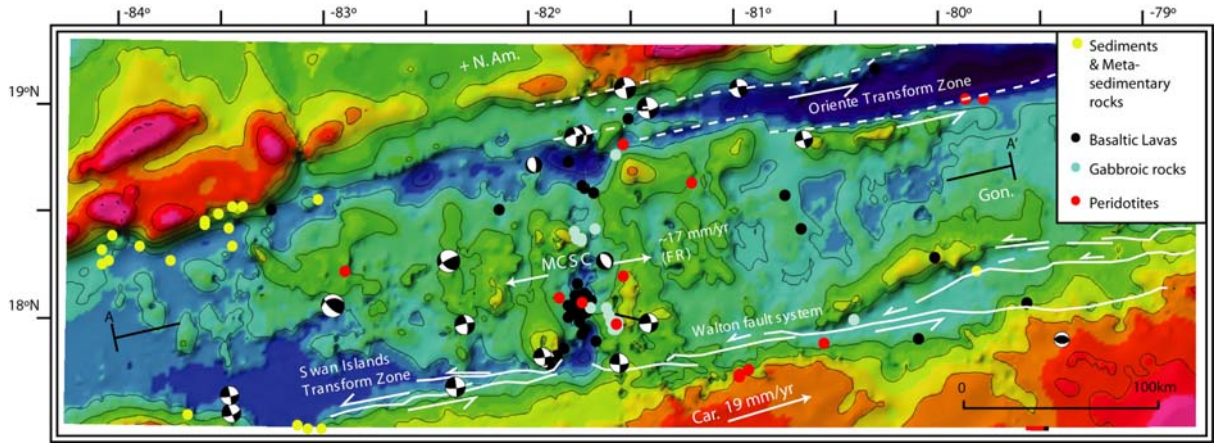

Fig. 3.4 Detailed bathymetry of the Mid-Cayman spreading centre (MCSC) and dredged rock types [Hayman et al., 2011].

Much of the evidence for the OCC model in the MCSC comes from the bathymetric structure (Fig. 3.4) [e.g., Hayman et al., 2011]. The MCSC is defined by 5-6 km deep basins within an intra-ridge rift bound by curvi-planar massifs and more planar rift walls that approach ~2 km below sea level. There are few constraints on the geology of the steeper-walled rift flanks, with at least one of the rift walls (to the southeast) appearing to be dominated by basalt. In contrast, the shallowly dipping massifs, such as the east-central massif called Mt Dent, appear to be dominated by a mix of gabbro and peridotite, though the proportion is only constrained by a few submersible dives. The other two massifs are at the northeast ridge-transform intersection and the southeastern area of the rift wall. The relatively smooth, locally corrugated (in TOBI and AUV data; N. Hayman pers. Comm.) surface of Mt Dent is cut by a series of NS fault scarps [Stroup and Fox, 1981], similar to other OCCs such as Atlantis Massif on the MAR [Karson et al., 2006]. Stroup and Fox [1981] recovered basalt at the eastern edge of Mt Dent, which may correspond to the 'breakaway' in current OCC models (Fig. 3.2). There are also important spatial relationships between the basement massifs (OCCs) and what appear to be predominantly volcanic fields in the adjacent, deeper basins. As our motivating questions revolve around the crustal thickness and interaction between mantle melts and detachment faults, it is critical to understand the seismic structure across these volcanic systems as well. Additionally, the along-strike changes in volcanism and tectonism highlight the three-dimensional nature of the crust.

Regarding the melt history of the MCSC, an important aspect of MCSC rocks that highlights the need for seismic data is that they have end-member high Na8.0 and low Fe8.0

values (Na2O and FeO composition normalized to MgO of 8.0 wt%) indicative of low extents of melting from a relatively homogenous 'cold' mantle [Klein and Langmuir, 1987]. Additionally, MCSC peridotites are extremely depleted in light rare earth element (REE) compositions [Hayman et al., 2011]. These observations, detected in basalt compositions, support proposed relationships between thin crust, cold mantle, and a deep axial depth [Klein and Langmuir, 1987], and are also born out in seismic experiments in places such as the SWIR [Muller et al., 1997].

The critical tectonic problem in OCC development is determining how once deep-seated gabbros and peridotites are exhumed. The OCC model envisions a detachment fault that bounds the surface of massifs such as Mt Dent, and continues to depth as a high-angle fault (Fig. 3.2). For the MCSC, evidence for detachment faulting on Mt Dent includes its bathymetric structure as outlined above, and also amphibolite grade (<~850°C) deformation fabrics in many of the recovered rocks [Karson and Fox, 1986]. Futher geological research is required to refine the tectonic history of the MCSC, but evidence to date shows a potential multiphase exhumation history with, at first, deep-seated deformation followed by exhumation on structures that are either highly localized or else not preserved. Subsequent upper crustal deformation is solely recorded by the corrugated, curvi-planar surface of massifs like Mt Dent. Therefore, seismic data is required to image the detachment and its relationship to the deeper crustal structure and Moho.

Identification of hydrothermal vents both on-axis and on the flanks of Mt Dent [German et al., 2009; Hayman, pers. Comm.] highlights another outstanding problem for both ultra-slow spreading centres, and all OCCs. Black smoker vents on the northern volcanic field of the MCSC point to sufficient heat sources and high crustal permeability to allow high-flux, high-temperature venting. These discoveries support earlier work demonstrating deep crustal fluid flow in MCSC gabbroic crust [Ito and Anderson, 1983]. Yet, in a presumably cold ridge environment such as the MCSC, what is the specific relationship between magmatism, faulting, and hydrothermal fluid flow?

While new observations from the MCSC have brought this ultra-slow spreading centre into focus, there is still a paucity of geophysical data. Magnetic anomaly data have received the most attention over the years, primarily because they show changes in spreading rate over time that inform plate reconstructions of the entire Caribbean plate. These spreading rate changes, however, occurred >20 Myr ago and, therefore, do not bear on the active spreading-centre processes, though in general these have been ongoing since late Eocene time.

In contrast, geophysical constraints on crustal thickness of the MCSC are neither of the vintage or resolution to answer the key questions. For example, short seismic refraction profiles [Ewing et al., 1960] in the eastern Cayman Trough show crustal velocities and thicknesses within the range of typical oceanic crust or extremely thin continental (or island arc) crust. The mean thickness of the crust beneath the eastern trough is 5.4 km (mean thickness of Layer 2 = 1.8 km and Layer 3 = 3.6 km). To date, this is the only existing seismic constraint on crustal thickness. Later, based on satellite gravity, ten Brink et al. [2002] suggested that the Cayman Trough is underlain by oceanic crust that is markedly thinner (only 2-3 km thick) than normal oceanic crust (6 km thick) between the MCSC axis to a distance of approximately 50 km from the MCSC. However, neither the Ewing et al. [1960] seismic data nor the gravity data are of sufficient resolution to confidently constrain crustal thickness, let alone evaluate hypotheses that hinge on imaging the deep crustal structure.

3.1.4 The Swan Island transform fault boundary

The Swan Island transform fault is a segment of the boundary between the North American and Caribbean plates and accommodates about 20 mm/yr of slip. The largest recent earthquake occurred northward of Honduras on 28th May 2009, causing a Mw=7.3 earthquake. Its focal mechanism indicates left-lateral strike-slip faulting on the Swan Islands transform fault. Previous strong earthquakes along the North America-Caribbean plate boundary include the destructive Guatemala earthquake of 4th February 1976, a Mw=7.5 event which resulted in more than 23,000 fatalities. The 1976 earthquake occurred on the Motagua fault, a segment of the plate boundary that lies in southern Guatemala, several hundred kilometres southwest of the plate boundary that ruptured in the 28th May 2009 shock.

Models for the formation of the Swan Island transform fault suggest that 2-3 km thick oceanic crust created at the Mid-Cayman spreading axis [ten Brink et al., 2002] occurs to the north of the plate boundary while continental crust of unknown thickness occurs to the south. Thus, along the Swan Island transform fault extremely thin zero-age to 45 Myr old oceanic crust occurs next to perhaps 20-30 km thick continental crust, resulting in a profound contrast in the strength and thermal state across this fault. Dredging of rocks from the fault scarp sampled sediments and meta-sedimentary rocks (Fig. 3.4). However, along the eastward continuation of the fault – the Walton faults system linking the Mid-Cayman spreading centre with Jamaica and Haiti – peridotites and basalt have been sampled.

Little is known of the seismic structure of the Swan Island transform fault. However, seismic studies at the slow spreading Mid-Atlantic Ridge (for a review see Detrick et al. [1993]) established that large-offset transforms exhibit anomalous crustal structures that fall well outside the range typically associated with oceanic crust. Seismically, fracture zone crust in the North Atlantic is extremely heterogeneous in both thickness and internal structure. It is frequently quite thin (<1-2 km thick) and is characterized by low compressional wave velocities and the absence of a normal seismic layer 3. The geological interpretation of the available seismic observations is that the crust within transform faults consists of a thin, intensely fractured, and hydrothermally altered basaltic section overlying ultramafic rocks that are extensively serpentinized. The existence of a thin crustal section can be explained by a reduced magma supply. Thus, in the case of an ultra-slow spreading centre, the already starved magma supply at the segment ends in the vicinity of the faults might be even lower.

Seismic studies across fossil transform margins – like the Ghana transform margin or the French Guiana transform margin – suggest that the transition between continental and oceanic crust occurs quite abruptly [Edwards et al., 1997; Greenroyd et al., 2008]. However, across most now extinct transform margins, thick layers of sediments cover the igneous crust, placing it several kilometres below the seafloor. Thick sediment layers strongly attenuate seismic signals. Therefore, the study of a thinly sedimented and still “drifting“ transform margin is expected to yield seismic data of a much high quality than we have obtained in all previous studies, and reveal the dynamics of evolution of transform margins from active through to the relic phases.

3.2 Objectives and goals

The importance of focusing research efforts on ultra-slow spreading centres is underscored by the fact that they comprise ~25% of the 55,000-60,000 km of global ridge system. Work at the Gakkel Ridge in the Arctic is hindered by ice covered sea and poor weather conditions. It thus

requires special equipment to reach and survey the area. However, due to the ice conditions, ocean-bottom-seismographs are generally not used as the risk of losing the instruments in difficult ice conditions is too large. The Southwest Indian ridge is located in the southern ocean. Sea conditions are generally rough and, because of its remoteness, it is difficult to reach. In contrast, the Cayman Trough is located in the Caribbean and is, thus, the ultra-slow spreading centre that is most easy to access and which has the best prospects for good weather year round.

In addition, the Cayman Trough is one of the rare examples on our planet where an active transform fault separates continental from oceanic crust and is, thus, also a natural laboratory to study the process of passive transform margin formation. Furthermore, the relatively thin sedimentary cover of the study area will permit detailed bathymetric mapping of the shallow tectonic structure, which is fundamental to understanding regional deformation in 3D, and to properly plan the seismic data acquisition. Finally, previous studies in the Cayman Trough have provided the reconnaissance information to design a project entirely focused on studying processes. Therefore, a number of wide-angle seismic refraction profiles were shot in the Cayman Trough (see Fig. 3.5) and a micro-earthquake survey was conducted to address a number of goals/objectives:

1. *Characterization of the structure and physical properties of the crust and uppermost mantle over both conjugated ridge flanks*. To further test models for the formation of OCCs and to interrogate their importance at ultra-slow spreading centres, we need geophysical observations that show the spatial relation between an OCC, any detachment, the volcanics, and the deep crustal structure beneath the intra-ridge rifts is required. Here, we focus on two widely discussed, but rarely tested hypotheses and their alternatives (see Figure 3.2, bottom):

(1) Ultra-slow OCCs and overlying detachment faults have a curviplanar geometry, with a shallowly-dipping upper crustal structure that strips away the volcanics, and a steeply-dipping middle-to-lower crustal structure that is rooted in a melt-rich zone near the spreading axis. Alternatively, OCCs form by the exhumation of mantle rock with limited and ephemeral magmatism and hydrothermal venting in ultra-slow environments.

(2) Several kilometres beneath the seafloor, ultra-slow OCCs develop a freezing horizon for melts that is roughly coincident with the present-day Moho. Alternatively, ultra-slow OCCs are amagmatic and the Moho is at the base of a mantle serpentinization front.

2. *Study of the mantle melting process and the generation of oceanic crust at the Cayman Trough*. To characterize the process of mantle melting and to estimate the relative importance of mantle temperature, upwelling rate and composition, the seismic structure of the oceanic crust and the relation between seismic and petrologic parameters (pressure, rock melting fractions) need to be determined and understood. These properties most likely change significantly from the centre of the Mid-Cayman spreading centre axis towards the segment ends, where the transform faults couple the newly generated oceanic crust to thick and cold continental lithosphere.

3. *Characterization the time-dependence phases in the activity of the Mid-Cayman spreading centre*. The activity of nearly all spreading centres changes through time and, at the

MCSC, it has been suggested that this results in profound changes in crustal thickness (derived from gravity data) at ~10 Myr and 20 Myr ago [ten Brink et al., 2002]. Mapping variations in crustal thickness as a function of time and spreading rate will be used to refine existing empirical relationships. Furthermore, we will then be able to study the impact such variation may have had on the thickness of crust generated at the segment ends in the transform fault.

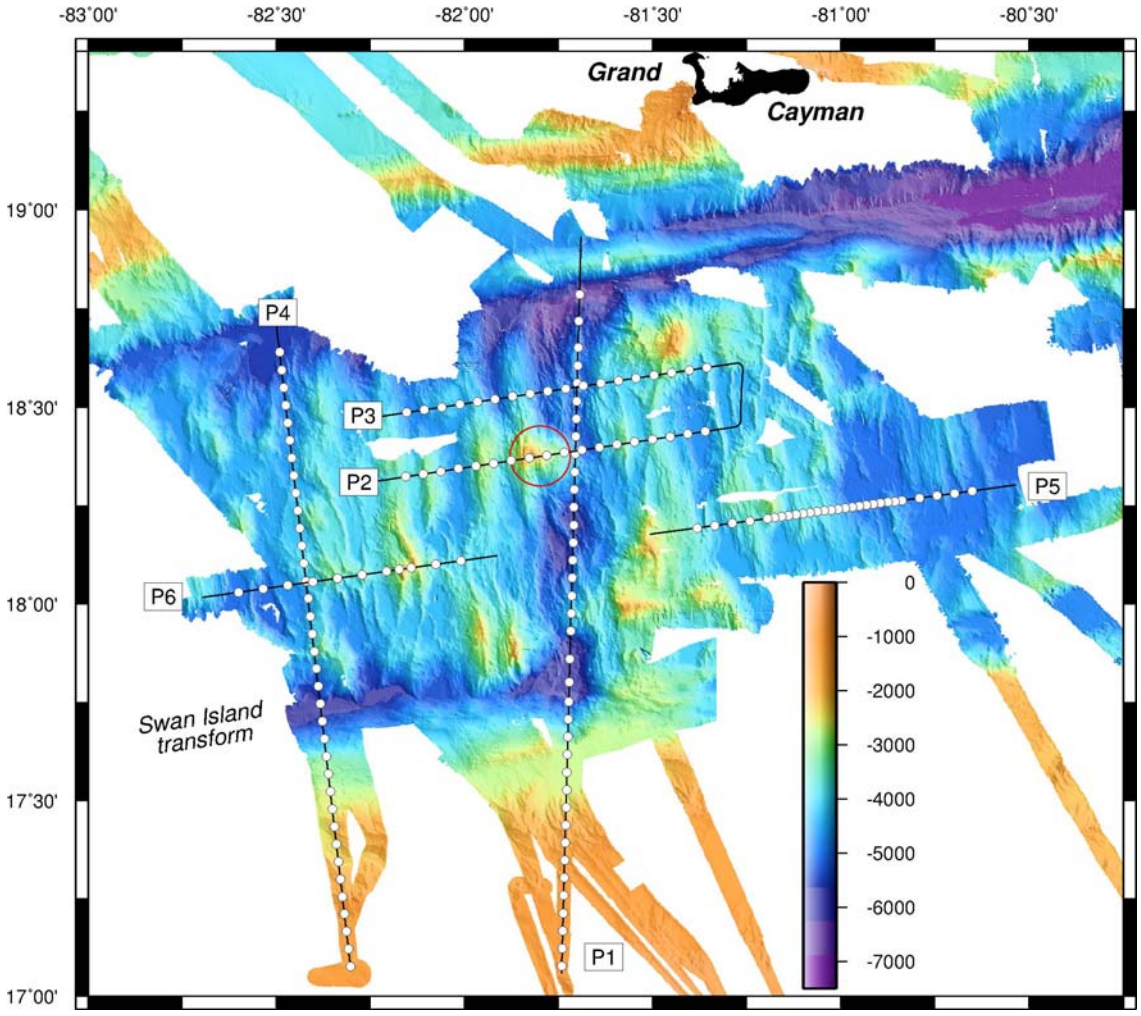

Fig. 3.5 Wide-angle seismic refraction lines of M115. Depth in metres. Red circle mark Mt. Dent.

4. *Tectonics of the active transform fault as crust ages and is transported westward*. In the Cayman Trough new oceanic crust is formed at the segment ends near to the transform fault. With time, the crust is transported westward and cools as it ages. Within 10 Myr we would expect the crust to subside by approximately 1 km. This study aims to determine how is this vertical motion on only one side of the transform fault is accommodated.

5. *Width of the ocean-continent boundary along the Swan Island transform fault*. Most transform margins studied to date are located in the Atlantic ocean, where rifting occurred more than 100 Myr ago. A huge thickness of sediments have since accumulated and, hence, affect the ability of seismic surveys to image to full crustal depth due to the high degree of attenuation caused by the sediments or the degree of flexure of the lithosphere caused by their loading. In the

Swan Island transform fault sediment thickness is thought to be rather low. We have, therefore, an ideal opportunity to study the nature and width of the ocean-continent boundary in detail, unhindered by thick sediment cover.

6. *Seismotectonics of the Mid-Cayman spreading centre in the vicinity of hydrothermal vent sites*. During spreading at slow- and ultra-slow spreading rates a significant portion of plate separation is not accommodated by magmatism but by faulting, which is manifest by local earthquakes. By recording local seismicity it is possible to delineate active faults and obtain focal mechanisms and, hence, yielding fault motion. In addition, earthquakes are generally limited to crustal temperatures below 600°C, and so the depth distribution of local earthquakes is a first-order proxy for temperature in a highly faulted tectonic crustal setting.

4 Cruise narrative

The CAYSEIS cruise, M115, of the German RV METEOR began on 1st of April 2015. All times quoted are local times that, for the duration of the cruise, was UTC-5. At 09:20 the METEOR left the pier. The pilot, Captain Hammacher and his crew safely left the harbour of Kingston, Jamaica. At 10:15 the pilot left the vessel and METEOR started its transit to the Cayman Trough to the west of Jamaica. At 11:00 we left the 15 nm zone and began to record underway geophysical data, namely swath bathymetry, with the hull mounted Kongsberg EM122 echosounder, and gravity data with a LaCoste marine gravimeter.

At 17:10 we carried out the first releaser test, testing the release units used to release each ocean-bottom seismograph (OBS) from the seabed, just leaving a small anchor behind. Over the next few days of the order of 50 releaser tests were conducted, testing releasers of OBS from GEOMAR and the UK OBS pools.

At 04:40 on the 2nd of April METEOR left the territorial waters of Jamaica and entered the EEZ of the Cayman Islands (a UK overseas territory). The rain showers of the first two days stopped, and we sailed towards the Cayman Trough with forecast perfect weather conditions of force 4-5 winds and swell of just 1-1.5 m. The excellent weather remained stable during the entire cruise.

At 01:17 on the 3rd of April, the first OBS was deployed in the median valley of the Mid-Cayman spreading centre. The first 25 OBS were deployed for local earthquake monitoring along the spreading axis and to record offline shots to gain a 3-D coverage for tomographic data analysis. Five of the OBS, however, would also record inline shots from the first seismic profile. Instruments were deployed on seabed in water deeper than 5500 m, and three were deployed in water deeper than 6000 m.

On the 3rd of April at 19:18, we started to deploy OBS101 to OBS132 at 5 km station spacing along active-source seismic profile P1, running along the median valley of the Cayman Trough. The last 15 of these stations were located on the continental slope to the south of the Cayman Trough, with some of these within the territorial waters of Honduras. The last OBS of P01 was deployed at 09:38 on the 4th of April. After a short mapping survey, another releaser test and a test of the magnetometer were conducted. Thereafter, we deployed the passive acoustic monitoring (PAM) system at 15:02 to listen for whales and other marine mammals. In addition, a visual watch searched for marine mammals contemporaneously. Neither the PAM nor the visual

watch detected any marine mammal and so, after an hour, the soft start of the airguns would be initiated. At 15:31 the airgun arrays were deployed and were ready for first shot by 16:15. At 16:18 the soft start instruction was issued, adding at 5 min intervals, another airgun to the array. After 30 min all 12 airguns (six clusters) were switched into the array, although one gun did not operate. This provided a total array volume of 5000 in^3 (82 litres). Once the full array was firing, the PAM was recovered and a marine magnetometer deployed from the stern of the vessel. At 14:40 on the 5th April, the last shot was fired along P1 and magnetometer and airguns were recovered. At 17:58 the first OBS201 was released, it surfaced at 19:31, and was on deck at 19:56. Over the next 2.5 days we recovered all of the OBS from profile P1, except for UTIG OBS117. This OBS was unresponsive to acoustic communications and remained so at all further attempts made throughout the cruise. On the 7th of April at 07:42 the last OBS132 was on deck.

After a transit of about 5 hours, we deployed 20 OBS along profile P2 (OBS201 to 218, plus two OBSs to test new data loggers, i.e., OBS206B and OBS208b) and 18 OBSs (OBS301 to OBS318) along P3. Station spacing was 5 km. The first OBS (OBS201) of P2 was deployed at 00:36 on the 8th of April 2015; the last OBS318 along P3 was installed at 16:08 on the 8th of April. Both profiles run across the axis of the Cayman Trough and survey two different domains, including an oceanic core complex. Again, we first deployed the PAM to listen for mammals and, in addition, kept a visual watch using binoculars. The airguns and magnetometer were then deployed. Neither the PAM nor the visual watch sighted any mammals for the entire 1 hr observation period. Therefore, the airgun operations started with a soft start on 18:00 on the 8th of April. After about 30 minutes, the array reached full volume of 5250 in^3 (86 litres) firing at 190 bar. At 05:45 on the 9th April shooting along profile P3 was completed and METEOR changed course to approach the start of profile P2. During the change of profile the airguns where continuously fired to fan shoot into the OBSs deployed along both profiles. About 45 min later METEOR commenced shooting along P2, completing this profile about 12 hours later, when the airgun and magnetometer and airguns were recovered. Over the next 2.5 days all 38 OBS were also safely recovered.

A short transit of just 2 hours brought METEOR to the northernmost OBS position of profile P4. At 03:55 on 12th April, the deployment of 36 OBSs commenced at a spacing of 5 km, running approximately in a NNW-SSE direction across the oceanic crustal basin floored and the Swan Island transform fault, and on into the continental margin of Honduras. At 17:00, all OBS were deployed and the pre-profiling procedure of PAM deployment and mammal observations commenced. Whilst this process was on-going, the airguns and the magnetometer were deployed. As no mammals were observed, the airgun soft start procedure was initiated and at 20:30 the airguns were in full operation and the profile was shot at a speed of 5 kn with a shot interval of 1 min. At 18:30 on the 13th of April, the magnetometer and airguns were recovered and we began OBS recovery along P4. Unfortunately, neither OBH408 at 4400 m water depth nor OBH421 at 5600 m depth responded to acoustic commands. By 13:49 on the 15th April, the last OBS (OBS436) was on deck. After a transit of 40 nm, we returned to OBS421 and tried releasing it again. However, we neither received any answer nor did the OBS surface.

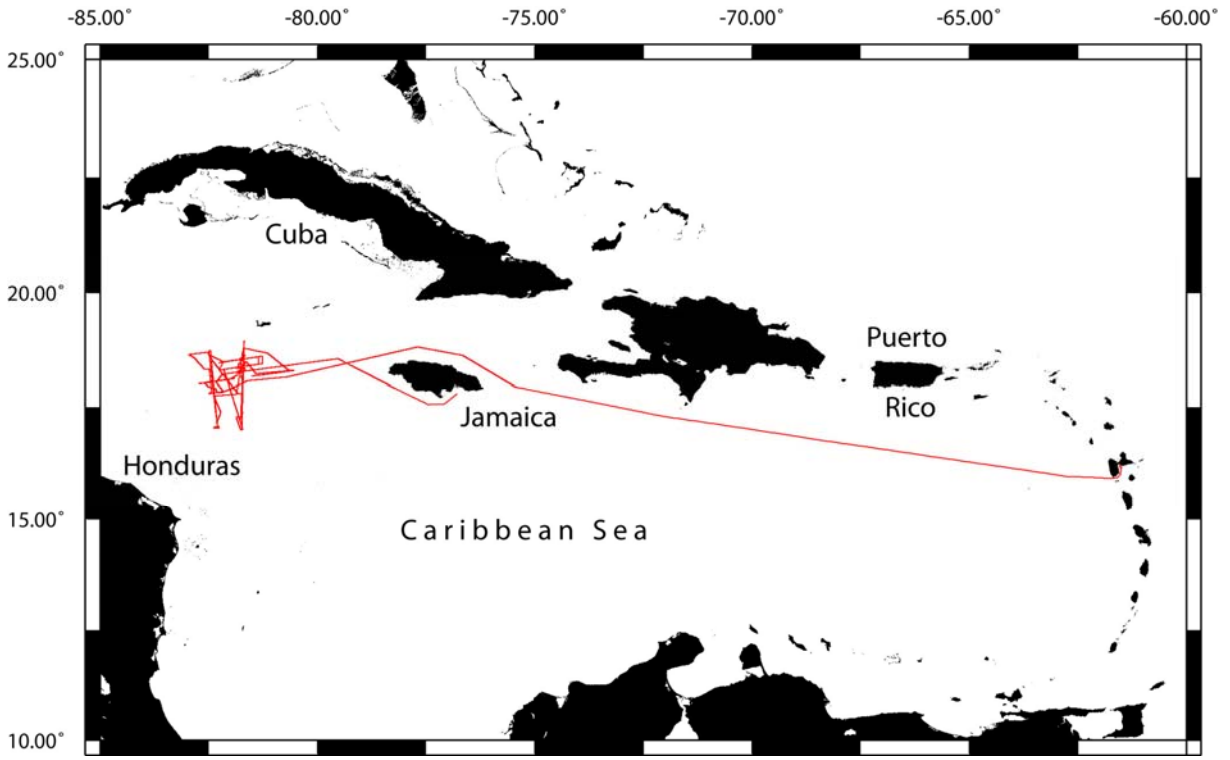

Fig. 4.1 Track chart of RV METEOR cruise M115.

METEOR then sailed to the east to recover the first 11 OBSs of those deployed in the median valley, that had been recording local earthquakes; namely OBS01 to OBS06, OBS17, OBH18, and OBS23 to OBS25 that were recovered from water depth of 4800 m to 6600 m. At 00:08 on the 17th April the 11th OBS25 was on deck. A transit of 70 nm to the SE brought METEOR to the most eastward deployment location, OBS501, of profile P5. Seismic profile P5 was located off-axis, surveying mature crust along a flow line on the eastern flank of the Mid-Cayman spreading centre. In total 28 OBSs were deployed along P5 at variable intervals of 2 to 5 km. At 15:39 on Friday 17th of April the PAM system was deployed to observe for marine mammals. Magnetometer and airgun deployment occurred 15 min later. After 60 min, with no mammals observed, the airgun soft start procedure was initiated; 30 min later the airgun array was in full operational mode. The profile was shot at a speed of 3.8 kn and a shot interval of 1 min. At 08:00 on the 18th of April, the profile was completed and the magnetometer and airguns were recovered. Over the next 28 hours all OBSs from profile P5 were recovered. At 13:14 on the 19th April, the last OBS, OBS528, was on deck.

METEOR then sailed west, approaching the northern median valley of the Cayman Trough to recover the remaining OBSs from the earthquake monitoring network. At 03:06 on the 19th April, OBS22 was released, it surfaced at 16:47 and was recovered by 16:59. Over the next ~10 hr we recovered OBS21, OBS19, OBS20, OBS15, OBS16, OBS11 and OBS10, all deployed in the spreading centre. OBS10 was on deck by 02:14 on the 20th of April.

Operations along the last seismic line, profile P6, began with the deployment of OBS601 at 04:07 on the 20th April. Profile P6 was located on the western ridge opposite P5, and targeted at studying the crustal structure of the conjugated ridge flank. In total 10 OBSs were deployed at intervals of 7 km. In addition, a further OBS (OBS604) was deployed 3.5 km to the west of OBS603, to test a new seismic data logger. At 09:11 the PAM was deployed. Over the next hour no marine mammals were observed, neither acoustically using the PAM nor visually. It is

noteworthy that, from the first OBS deployment in the passive array to the last OBS recovery, no marine mammals were observed.

Having observed no marine mammals during the observation period for P6, the airguns were deployed, soft started and in full operational mode by 10:45. About 10 hr later, airgun operations were complete and both the airgun array and magnetometer were recovered. During the night of the 20th to 21st of April the last passive OBSs were recovered from Mt Dent on the western flank of the Cayman Trough (OBS12 to OBS14, and OBS07 to OBS09), and by 22:22 on the 21st April all 11 OBS from P6 were back on deck.

In total, 170 OBS sites were occupied during the CAYSEIS cruise. Unfortunately, three OBS failed to return in response to acoustic release command. However, all three stations, two GEOMAR OBH and one UTIG OBS, had an independent timer release programmed for the 22nd April. In the intervening time we filled gaps in the swath bathymetric coverage of the Cayman Trough and adjacent ridge flanks. At 13:00 METEOR approached the deployment site of OBS408 and, 15 min later, the OBS surfaced and was recovered by 13:30. We then sailed south towards OBS421. About 5 nm from the deployment location we briefly picked up the OBS's VHF radio beacon. We searched for 20 min until we got a trustworthy reading from the direction finder and by 17:43 the OBS was on deck. Thereafter, we searched for OBS117 deployed near the southern end of the Cayman Trough along profile P1. Unfortunately, we did not receive any signals from its VHF radio beacon. We, therefore, deemed it lost on the seabed and deployed the magnetometer at 21:20 to record, in addition to bathymetry and gravity, the Earth's magnetic field during our transit out of the Cayman Trough.

At noon on the 23rd April, METEOR left the territorial waters of the Caymans (UK) and entered the EEZ of Jamaica. At 11:00 on the 24th April, at 74°40'W to the southeast of Jamaica, the magnetometer was recovered. About one hour later we left the territorial waters of Jamaica and recording of underway geophysical data (swath bathymetry and gravity field) ended.

On the evening of 27th April, METEOR reached the pilot station of the port of Pointe-à-Pitre, Guadeloupe. At 20:00, METEOR was alongside at the end of a successful cruise.

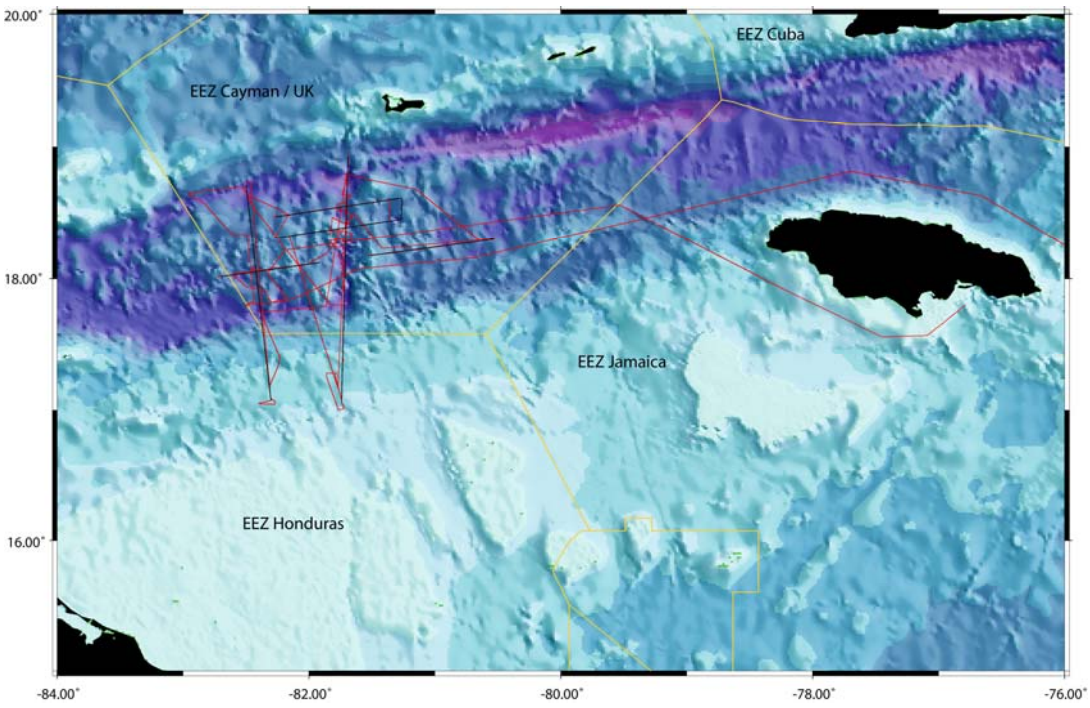

Fig. 4.2 Track chart of M115 and the exclusive economic zones (EEZ) visited during the cruise.

5 Preliminary results

5.1 Performance of scientific equipment

5.1.1 EM122 Kongsberg echosounder

The METEOR is fitted with a Kongsberg EM122 1°x2° multi-beam deep ocean echosounder, with two transducer arrays fixed to the ship's hull operating at 12 kHz. Data acquisition is based on successive transmit-receive cycles of this signal. The transmit beam is 150° wide across-track and 1° along-track direction. The system has 288 beams and emits 2 swaths per ping, providing 864 soundings per ping. The beam spacing can be defined as equidistant or equiangular, and the maximum seafloor coverage fixed or adjusted according to seabed and weather conditions. Seabed depth and reflectivity are recorded against UTC and GPS location. The raw depth data are processed to obtain depth contour maps, and the acoustic amplitude processed to obtain backscatter amplitudes. Swath bathymetry and backscatter data were acquired within the territorial waters of Jamaica, the Caymans, and Honduras.

During M115 we obtained 3972 nm of along-track swath bathymetry data that were combined with data of opportunity, most of which were downloaded from NOAA's National Centers for Environmental Information (NCEI), Boulder, USA. Fig. 5.1 outlines the coverage obtained during the METEOR cruise and Fig. 5.2 shows the combined bathymetry map using all available swath data.

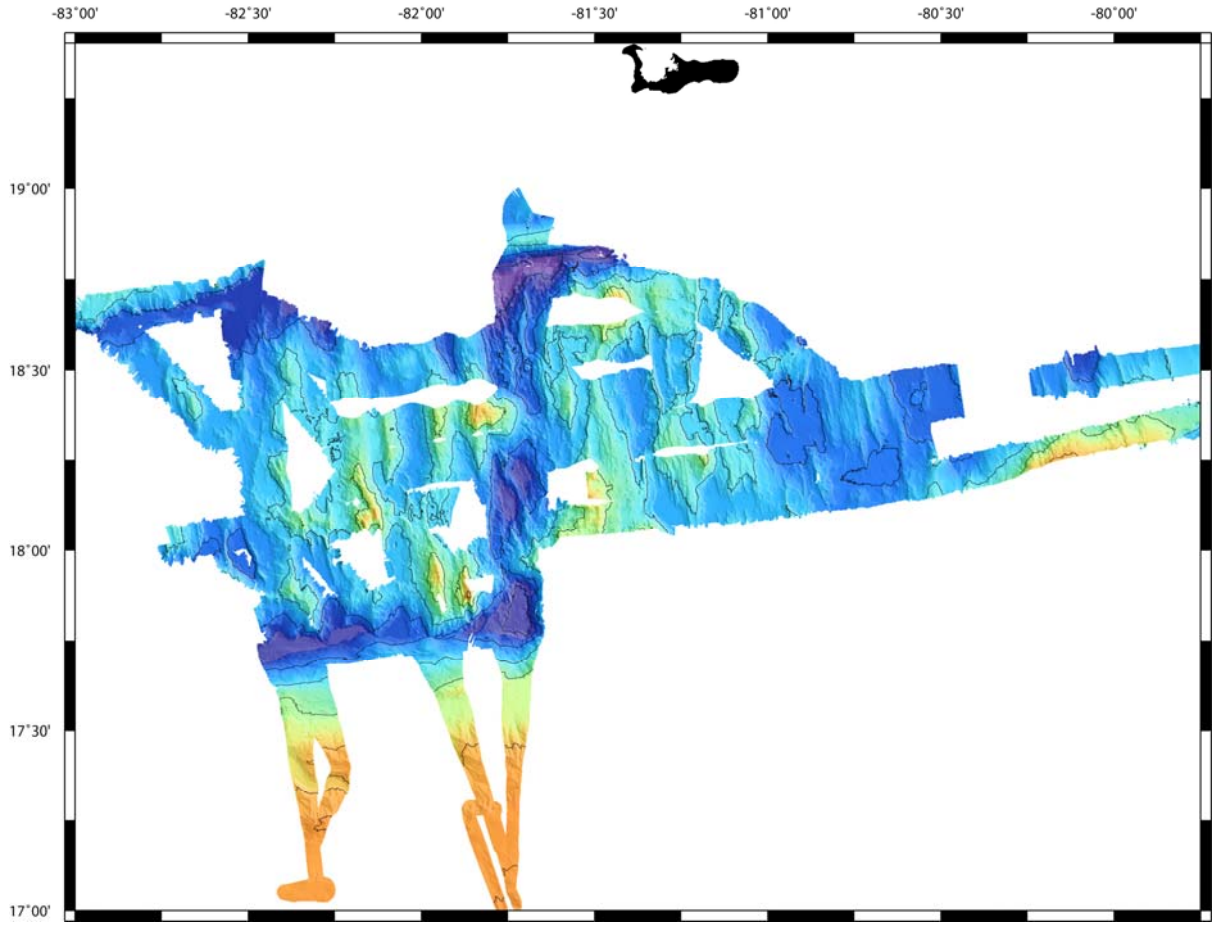

Fig. 5.1 EM122 echosounder swath bathymetry coverage obtained during M115. Colour scale as in Fig. 3.5.

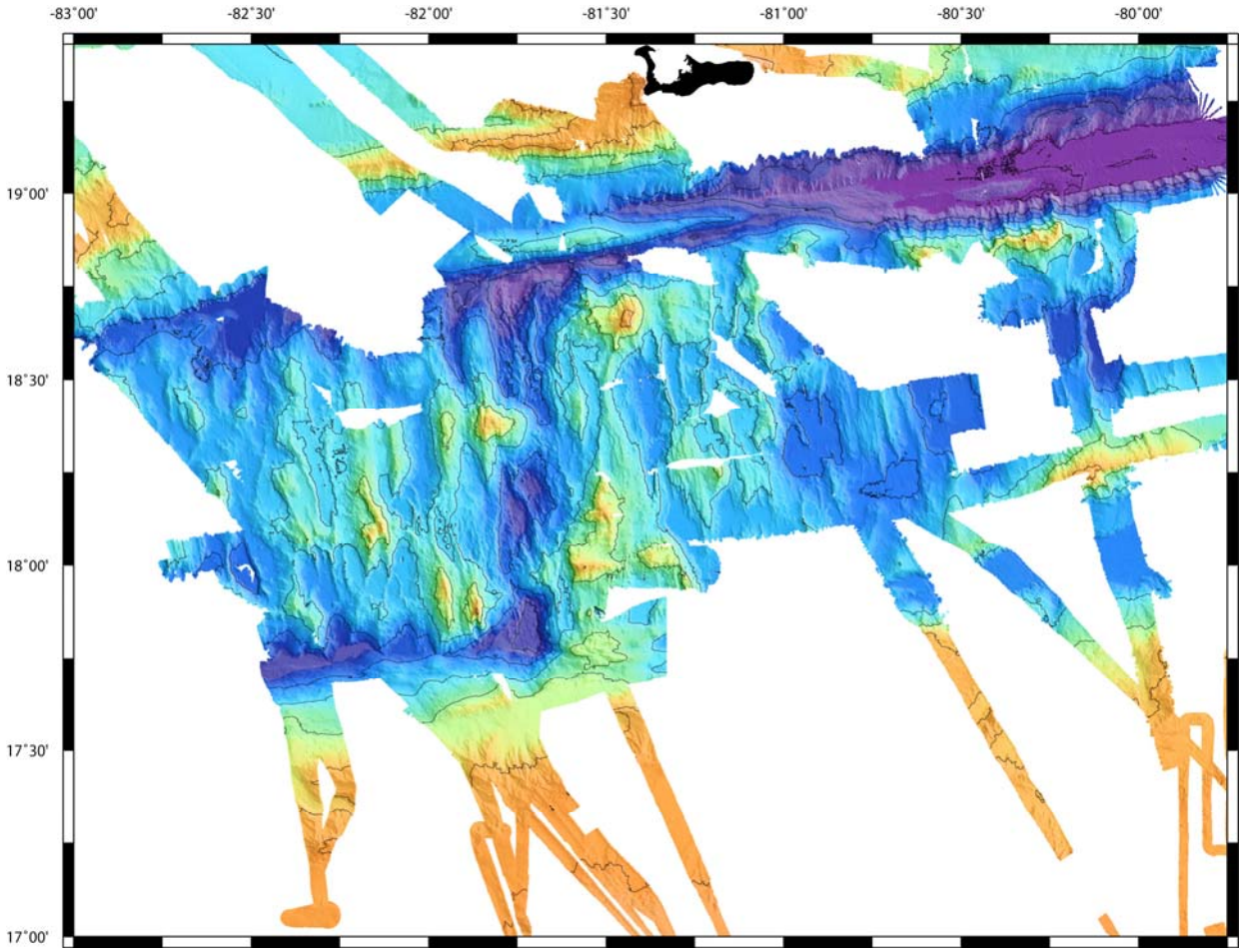

Fig. 5.2 Swath bathymetry coverage obtained by combining data from M115 and that archived at the NCEI/NOAA.

5.1.2 Ocean-bottom seismographs

During the survey different types of ocean-bottom seismographs where deployed. UK OBSs where LC4x4s, UTIG OBSs where GeoPro SEDIS 4-channel OBSs and GEOMAR provided ocean-bottom hydrophones (OBHs) and three different generations of OBSs built in Kiel.

The UK OBSs were provided by the UK's Natural Environment Research Council's (NERC) Ocean-Bottom Instrumentation Facility (OBIF) under NERC grant NE/K/011162/1. Eighteen LC4x4-type platforms were available for deployment during the cruise. These instruments were four-channel OBSs that record to compact flash, and were configured to record both three-component geophone (Sercel L-28 4.5 Hz) and hydrophone (HiTech HTI-90-U) sensor data. Data were digitized within the datalogger at 24-bit resolution at a sampling rate of 250 Hz. Buoyancy of the OBIF' OBS is provided by four small glass spheres, which limits their depth of operation to a water depth of <5500 m. Like all the other OBSs, these instruments are released using acoustic communication.

GEOMAR operated both OBSs and OBHs. The OBHs just had a single hydrophone while the OBSs were equipped like the OBIF' OBSs with a geophone and a hydrophone. The hydrophone was either an E-2PD hydrophone from OAS Inc. or a HTI-04-PCA/ULF from High Tech Inc.; geophones where 4.5 Hz SM6 B-coils in a pressure protected housing manufactured by KUM GmbH, Kiel, modified from a package designed by Carrack Measurement Technologies. In addition, for earthquake monitoring, four GEOMAR OBSs were equipped with

a Güralp 3-component broadband seismometers (CMG 40T-60s). German OBSs and OBHs had various generations of datalogger manufactured by SEND Offshore GmbH. First generation *MBS, MLS and MTS* recorders sampled at 16 to 18 bit (depending on sample rate), while the second generation *MES* sampled at 24 bit. Depending on the data logger, the sampling rate was set to either 200 or 250 Hz. As for the UK' OBSs, GEOMAR used separate pressure housings for the acoustic release and seismic data loggers. Buoyancy was provided by syntactic foam. Most OBSs were rated to 6000 m water depth. However, eight OBSs of the LOBSTER-type were rated to 8000 m. The deepest OBS to be deployed was located in 6431 m (OBS25) water depth.

UTIG provided 14 GeoPro SEDIS 4-channel OBSs. Thirteen of the instruments were of

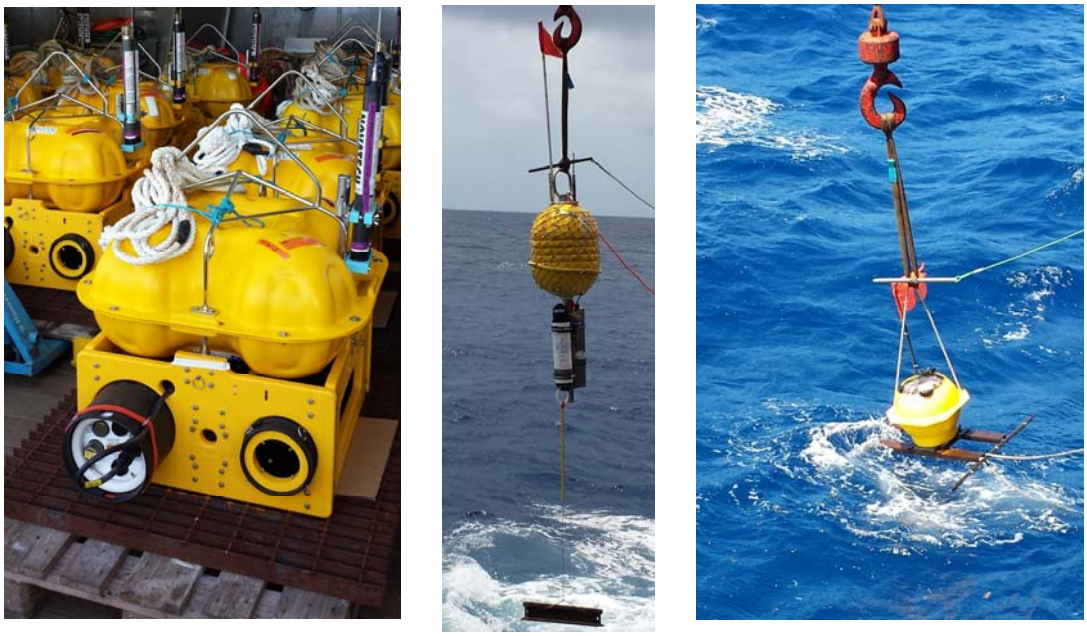

Fig. 5.3 **(**left) UK' OBIF OBS; (middle) GEOMAR' OBH; (right) UTIG' OBS.

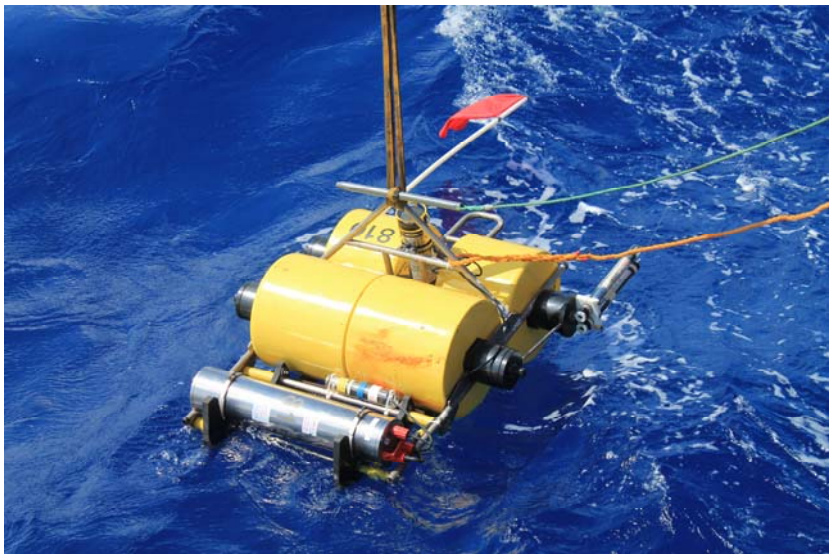

Fig. 5.4 GEOMAR' OBS, LOBSTER-type.

the older (pre-2010) SEDIS-V design, and one (S10) was a newer SEDIS-VI model. The main differences between these two generations of OBSs lie in the data logger, the raw data output, and the SEGY data conversion programs. Nine of the thirteen SEDIS-V OBSs were housed in older Benthos spheres, whereas all other OBSs had newer Nautilus spheres. The data loggers operated at 24-bit. The hydrophone was a HTI-01-PCA from High Tech Inc.. The geophones where 4.5 Hz SM6 B-coils.

All OBSs, regardless of type or supplier, were synchronised to GPS-derived UTC time before deployment and after recovery and the data corrected for clock drift prior to conversion to SEG-Y format.

In total, 170 deployments were made throughout the cruise. OBIF, UTIG, and GEOMAR deployed 55, 41, and 74 OBSs, respectively. The UK OBIF facility had a perfect run; all OBSs recorded data suitable for geophysical data analysis. Each of these OBSs was recovered after the first acoustic release command sent to it. Both UTIG and GEOMAR had a number of OBSs that did not record data. Two UTIG and five GEOMAR OBSs failed to record any data at all (UTIG: OBS107, OBS602; GEOMAR: OBS109, OBS422, OBS512, OBS517, OBS604) and one UTIG OBS remains deployed (OBS117).

5.1.3 Airgun array

The seismic source comprised six G-gun clusters (12 guns) manufactured by Sercel Marine Sources Division (formerly SODERA) and Seismograph Services Inc. configured as two sub-arrays. Six guns were set up in 3 clusters. Each cluster comprises two G-guns of 4x8 l and in the middle either 2x6 l or 2x4 l (see Figs 5.5 and 5.6). The cluster arrangement provides a good primary-to-bubble signal ratio. Operating all twelve guns provides a total volume of 84 l (5440 in^3). The G-guns were operated at 210 bar (3000 psi), towed at 7.5 m depth, and fired at 60 s intervals for OBS acquisition. The airgun array was fired using a Longshot gun controller. METEOR's external compressors provided the air supply, which were mounted in a container located on the main deck. In total, 5374 shots were fired.

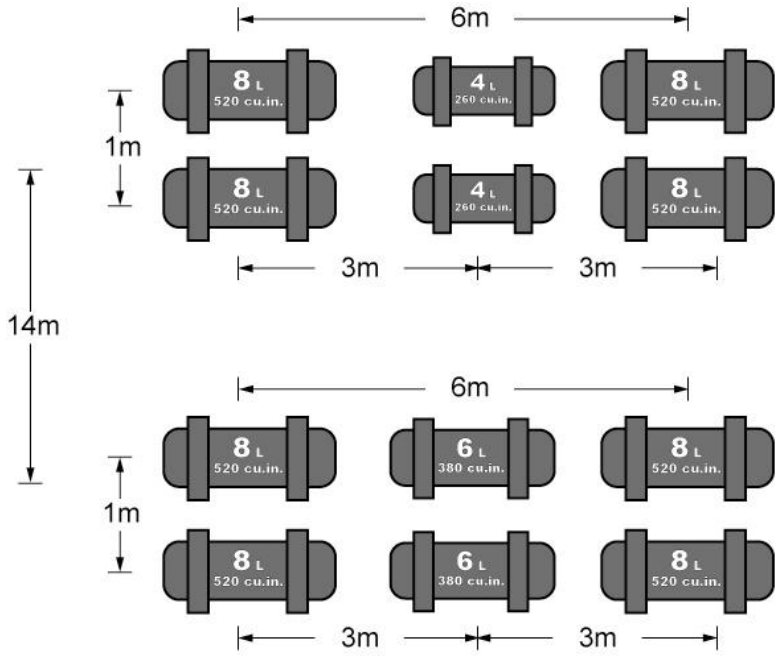

Fig. 5.5 Airgun array configuration.

Fig. 5.6 Starboard airgun sub-array.

5.1.4 Marine gravimeter / gravity

A LaCoste Micro-G marine gravimeter (serial number S40) was run throughout the cruise. This meter was provided by the NERC's National Marine Equipment Pool (NMEP) under NERC grant NE/K/011162/1. The meter was installed in Kingston by Mark Maltby from the NMEP assisted by the technical staff from OBIF. A tie-in was performed in Montego Bay at the start of the cruise (18° 28.423'N / 77° 55.383'W) and in Pointe-a-Pitre at the end (16° 13.978'N / 61°

Fig. 5.7 LaCoste-Romberg Micro-G marine gravimeter.

32.782'W). Base station ties were completed using a portable LaCoste-Romberg land gravimeter (model G-484).

The marine meter, located in the "Gravimeterraum", was provided with a NMEA navigation stream from the ship's network and ran without issue or loss of data for the entire cruise. Fig. 5.7 shows the installation of the meter and the data monitoring screen. During the survey in total 4560 nm of gravity field measurements were obtained providing, in addition to the seismic data, constraints on the sub-surface structure.

5.1.5 Marine magnetometer / magnetics

A SeaSpy magnetometer (SN 13358) of the NERC's National Marine Equipment Pool (NMEP) was deployed throughout all seismic surveying and along part of the transit to Pointe-a-Pitre within the territorial waters of the Caymans and Jamaica. The sensor lay-back from the ship's GPS reference point was input into the data acquisition "BOB" software and the correction applied during profiling. Fig. 5.8 shows the deck installation of the tow fish and winch, and the data monitoring screen. During M115, 620 nm of magnetic data were acquired.

Fig. 5.8 The SeaSpy magnetometer.

5.2 First scientific results from shipboard data

During the cruise, we acquired wide-angle seismic refraction and local micro-earthquake data to study the balance between magmatic accretion and tectonic stretching (including oceanic core complex formation), and the relationship between faulting and hydrothermal activity at ultra-slow spreading rates (see section 3). In addition, we explored transform margin formation at the unique setting of the Swan Island transform fault at the southern terminus of the MCSC. At the beginning of the cruise, 25 OBSs were deployed monitoring local earthquakes in the vicinity of the Mt Dent oceanic core complex and along the neo-volcanic ridge within the median valley. Additionally, 145 OBS were deployed to record 5374 shots fired along six seismic profiles with a total length of 480 nm (Fig. 3.5).

Here, we report data quality and first results obtained from shipboard data.

5.2.1 Local earthquake monitoring

The seismological network in the Cayman Trough (Fig. 5.9) was operated between 3rd of April 2015 to 19th of April 2015, monitoring seismicity along this ultra-slow spreading ridge. Raw data recorded in the spreading centre on the 25 OBSs (22 GEOMAR OBS/H; 3 OBIF OBS) were converted to pseudo-SEGY (or PASSCAL-SEGY) format of IRIS. To generate more manageable files sizes and for applying time corrections, the files were cut into 25 hours records with one hour overlap between adjacent records, such that each record generally begins at 0:00:01. For all stations, timing errors of the internal clock against GPS time were corrected.

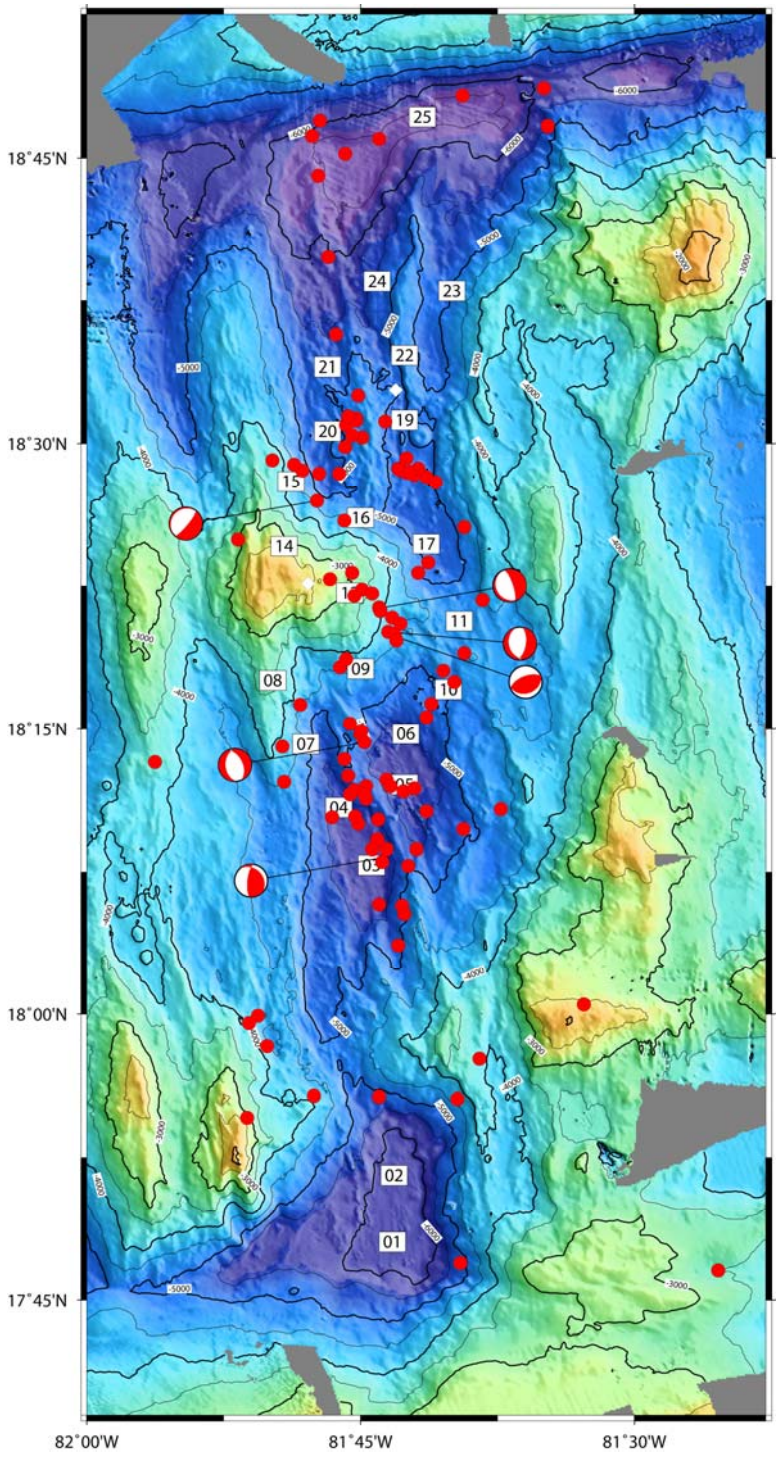

Fig. 5.9 Local micro-earthquake survey (OBS01 to OBS25) and initial earthquake locations (red dots). White diamonds mark hydrothermal fields.

To automatically detect seismic events in the daily records, a short-term-average versus a long-term-average (STA/LTA) trigger algorithm was applied. The code used was REFTRIG from the IRIS PASSCAL program library. The trigger parameters include: the length of the short term (s) and long term (l) time window, the mean removal window length (m), the trigger (t) and de-trigger ratio (d), minimum number of stations (S) and the network trigger time window length (M). The trigger parameters were applied to unfiltered vertical component data of good quality. To test the trigger parameters a continuous 24 hr data stream of all stations was visually checked. Moreover, we tested the parameters for a number of days and transferred the data into the SEISAN package used to analyse and locate the local earthquakes. Applying these trigger parameters, we obtained in total 310 local earthquakes.

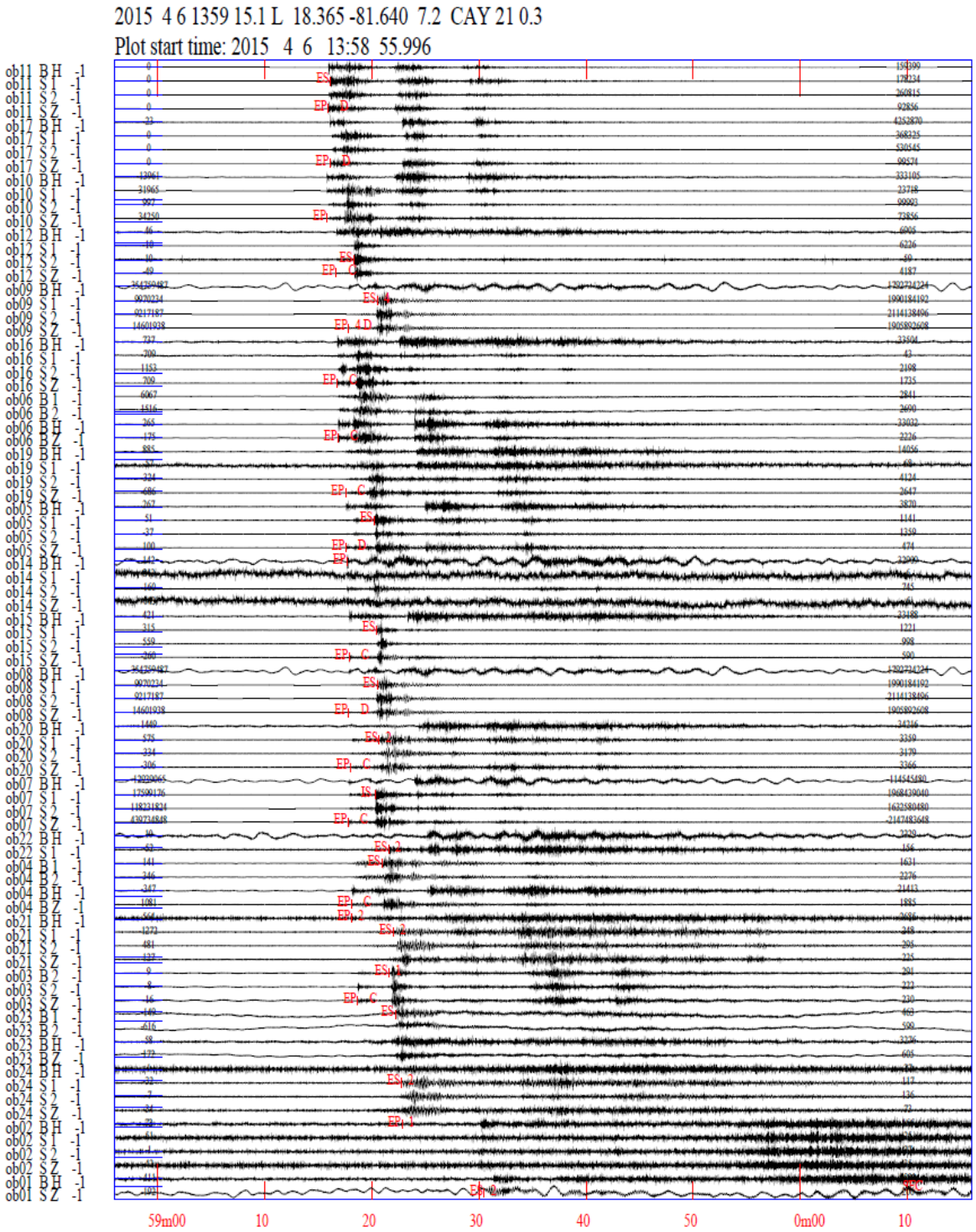

Fig. 5.10 Recorded local earthquakes occurring on 6th of April 2015.

After finding event triggers, the events were cut from the 25 hr files and stored into subdirectories, one per event. As we are only investigating local earthquakes, the appropriate time window length for the events is 3 min, starting 30 s prior to trigger time. The SEGY traces in the event directories are converted first into SAC, and then into MiniSEED waveform format, which makes it possible to store all traces associated with an event into a single waveform file. After conversion the data are registered into the SEISAN database (Havskov and Ottemöller, 2005). *P*-wave and *S*-wave arrival times are picked and events were located with NonLinLoc of Lomax et al. [2000], which employs a non-linear probabilistic location procedure.

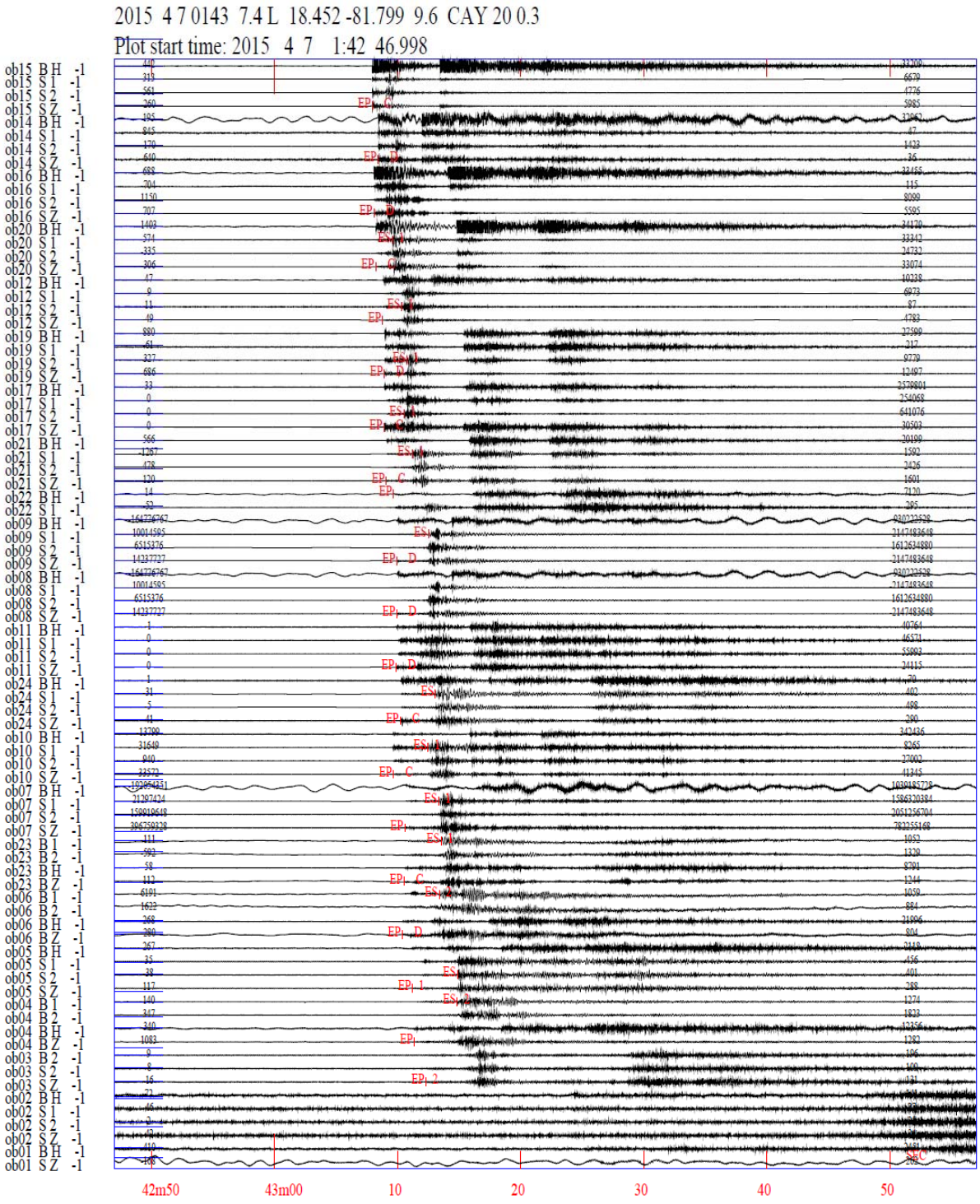

Fig. 5.11 Recorded local earthquakes occurring on 7th of April 2015.

Travel times were calculated using a 1-D velocity model used to record micro-earthquakes at the Logatchev oceanic core complex at the Mid-Atlantic Ridge [Grevemeyer et al., 2013]. Note that the location procedure iteratively updates station corrections and hence minimizes the misfit, facilitating clustering of events along the neo-volcanic zone. Furthermore, a number of focal mechanisms were derived, using first motion polarities. For this report, 106 of the 310 triggered earthquakes have had a preliminary location determined.

Examples of two local earthquakes, Figs 5.10 and 5.11, show that the data are generally of very good quality. These initial locations suggest that most earthquakes occurred along the

neo-volcanic ridge. However, events were generally offset by several kilometres to the east and west with respect to the axial ridge, suggesting that they might be associated with faults bounding the neo-volcanic ridge. In addition, some earthquakes occurred at the flanking rift mountains and at the Mt Dent oceanic core complex. With respect to other oceanic core complexes, like the Logatchev Massif at the MAR [Grevemeyer et al., 2013], the rate of seismicity is clearly reduced. Most focal mechanisms suggest normal faulting is predominant as might be expected. However, some compressional earthquakes occurred, which might relate to dyke injection.

5.2.2 Passive acoustic and visual mammal observations

Throughout the entire cruise visual marine mammal observation was conducted by Rebecca Snyder from Seiche Measurements Inc. and Anna Bird from Durham University. Both were certified acoustic and visual marine mammal observers. In total, about 240 hr of visual observations can be used to characterise the abundance of mammals during the survey; 50 of these hours comprised the actual seismic profiling. However, the only time marine mammals were observed was on 7th of April 2015 while recovering OBS, when a small pod of bottlenose dolphins was observed about 50 m off the METEOR, and during the transit to Pointe-á-Pitre, well outside the work area located to the west of Jamaica.

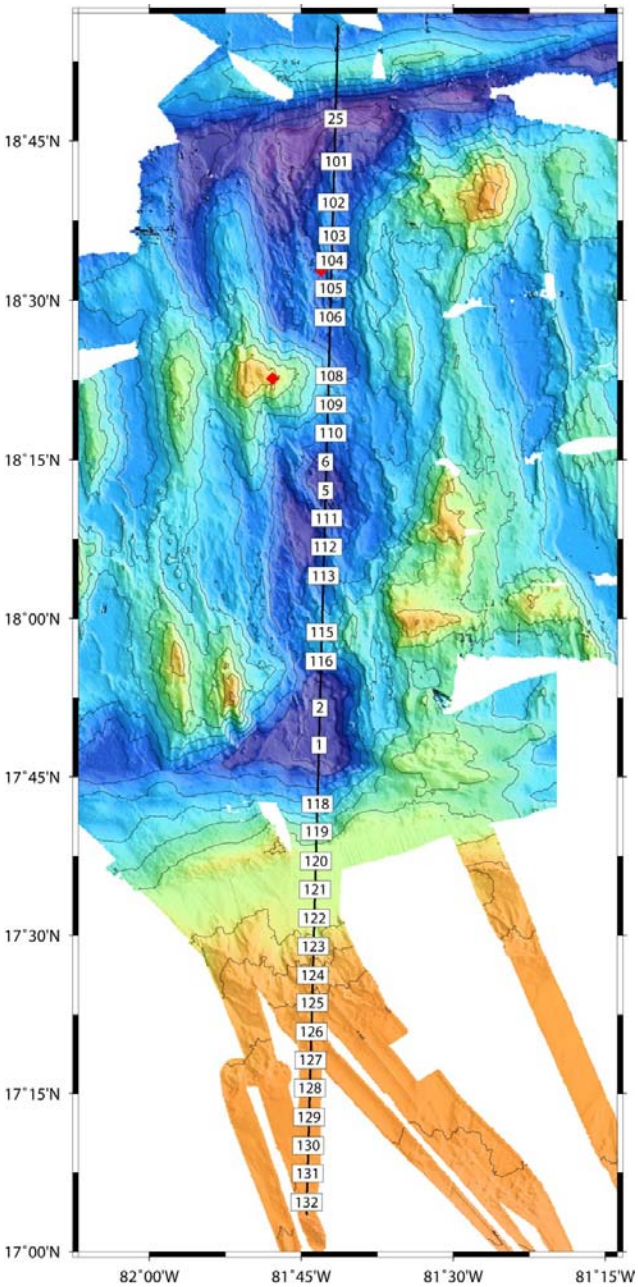

Fig. 5.12 Layout of P1 along the median valley of the Mid-Cayman Spreading Centre.

Before any airgun operations could commence, the research permit granted by the Cayman Islands required the following of the Joint Nature Conservancy Council's guidelines with, in addition, one hour of passive acoustic monitoring (PAM) of any mammals in the area. When no mammals were observed, a soft start procedure of the airguns could be issued, with the array reaching full volume and power only after no less than 20 min and no more than 40 min. During the entire survey, not a single marine mammal was detected acoustically. A detailed report of the PAM and visual mammal observations is provided in the Appendix.

5.2.3 Profile P1 – along the Mid-Cayman spreading centre

Along profile P1 32 OBS were deployed (OBS101 to OBS132). In addition, five OBS from the passive network were effectively inline with P1 and deployed at water depths ranging between 5500 m to 6500 m. Thus, 37 stations recorded the 1307 shots fired along P1 (Fig. 5.12). Most

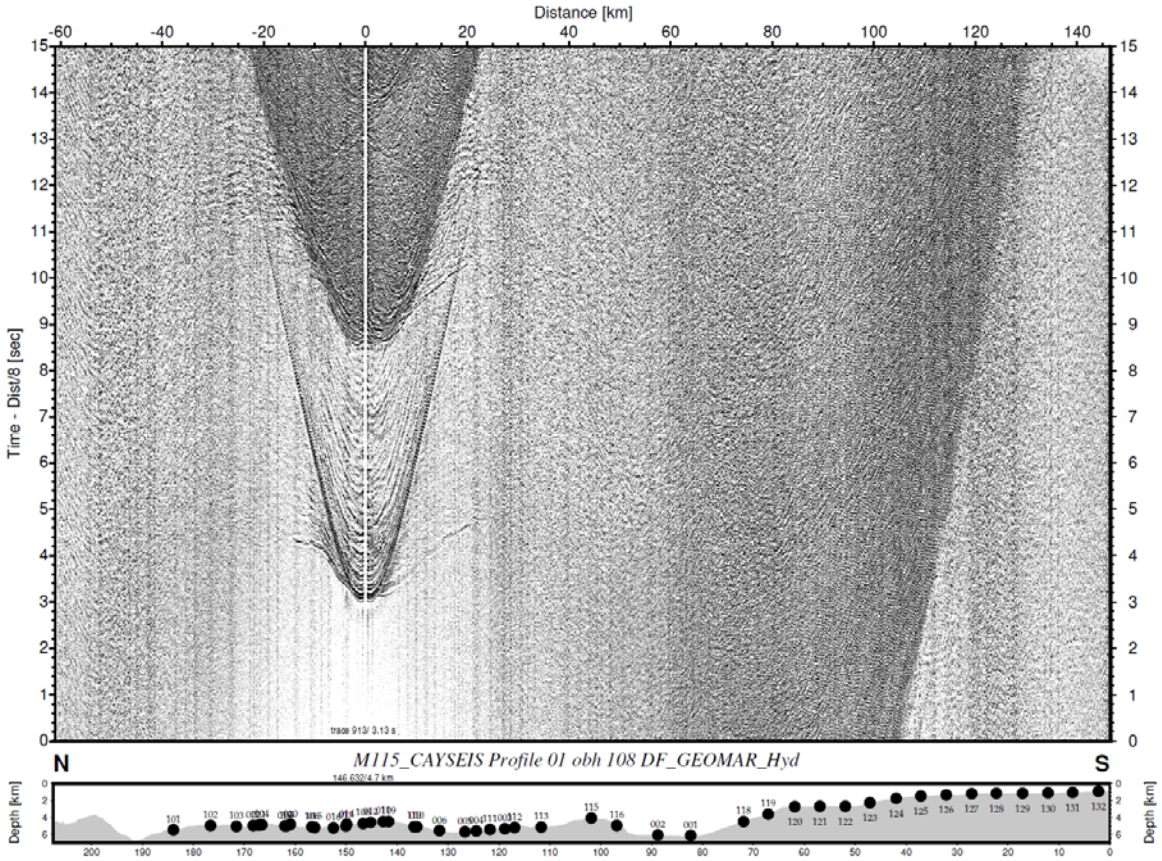

Fig. 5.13 P1 – OBH108 – hydrophone. Record section from a GEOMAR ocean-bottom hydrophone.

OBSs/Hs were deployed at a spacing of 5 km, with some in the deeper water spaced at 7.5 km. The profile runs from the Oriente transform fault in the north, along the median valley, crossing the Swan Island transform fault, onto the continental slope of Honduras. The aim of the profile was to study the variability of crustal accretion as a function of ridge crest segmentation along the ridge axis and to characterise zero-aged ultra-slow spreading lithosphere. Furthermore, the profile will provide the reference velocity structure for locating the local earthquakes and image the structure of the Swan Island transform fault and the structure of the southern continental margin bounding the basin.

Two OBSs along the profile failed to record data (OBS107, OBS114) and one OBS (OBS117) was lost. In addition, OBS101 to OBS104 recorded rather poor data. In general, data quality along the median valley was rather poor (Figs 5.13 & 5.14) with maximum recorded offsets of ~20 km. Data quality improved father south (Fig. 5.15) and was best on the continental slope (Fig. 5.16). Initial interpretation suggests the existence of fast apparent velocities of >7.5 km/s at small offsets which, in return, implies that the crust is relatively thin at the Mid-Cayman spreading centre. The larger offset arrivals recorded on the continental slope have been interpreted as Pn, sampling the uppermost mantle. Wide-angle reflections from the continental Moho (PmP), observed by instruments deployed on the continental slope, will constrain the thickness of the continental crust. Therefore, we believe that the goals of P1 will be achieved.

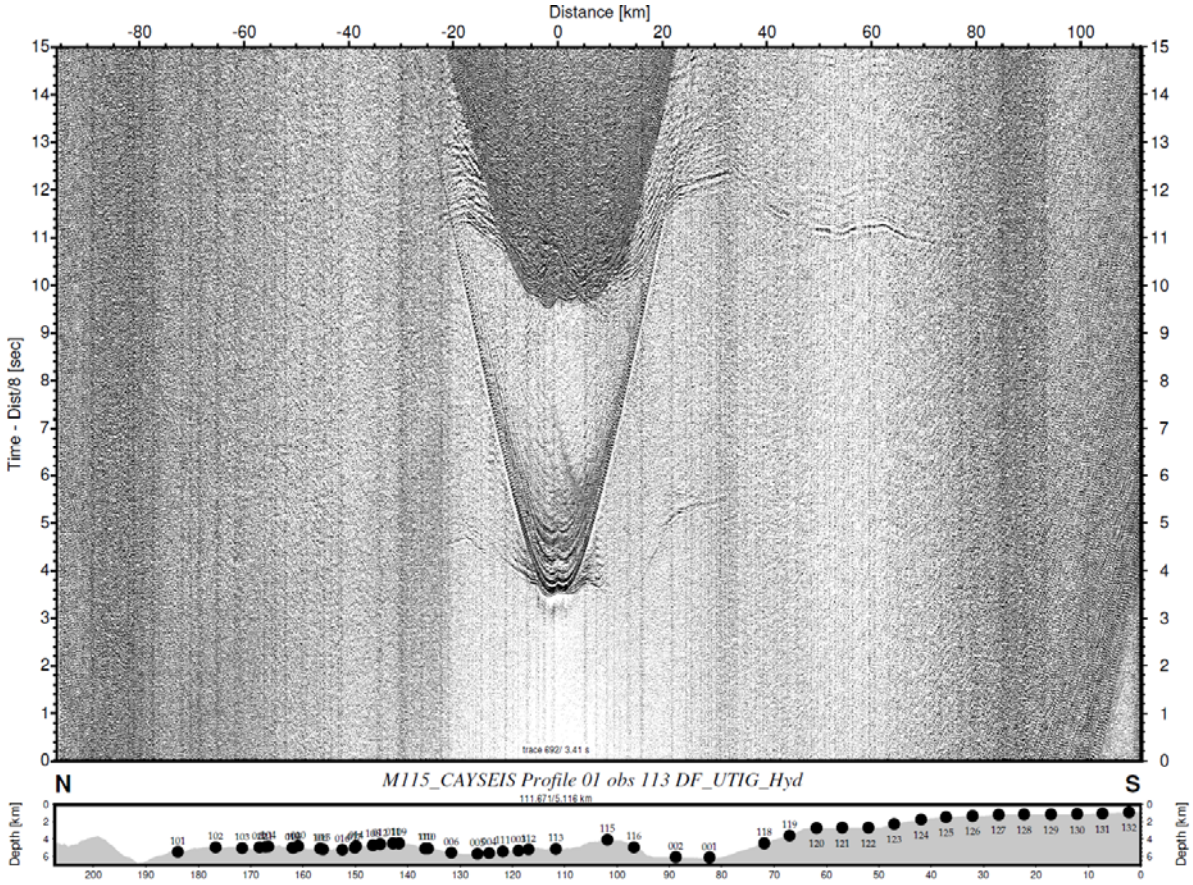

Fig. 5.14 P1 – OBS113 – hydrophone. Record section from a UTIG ocean-bottom seismograph.

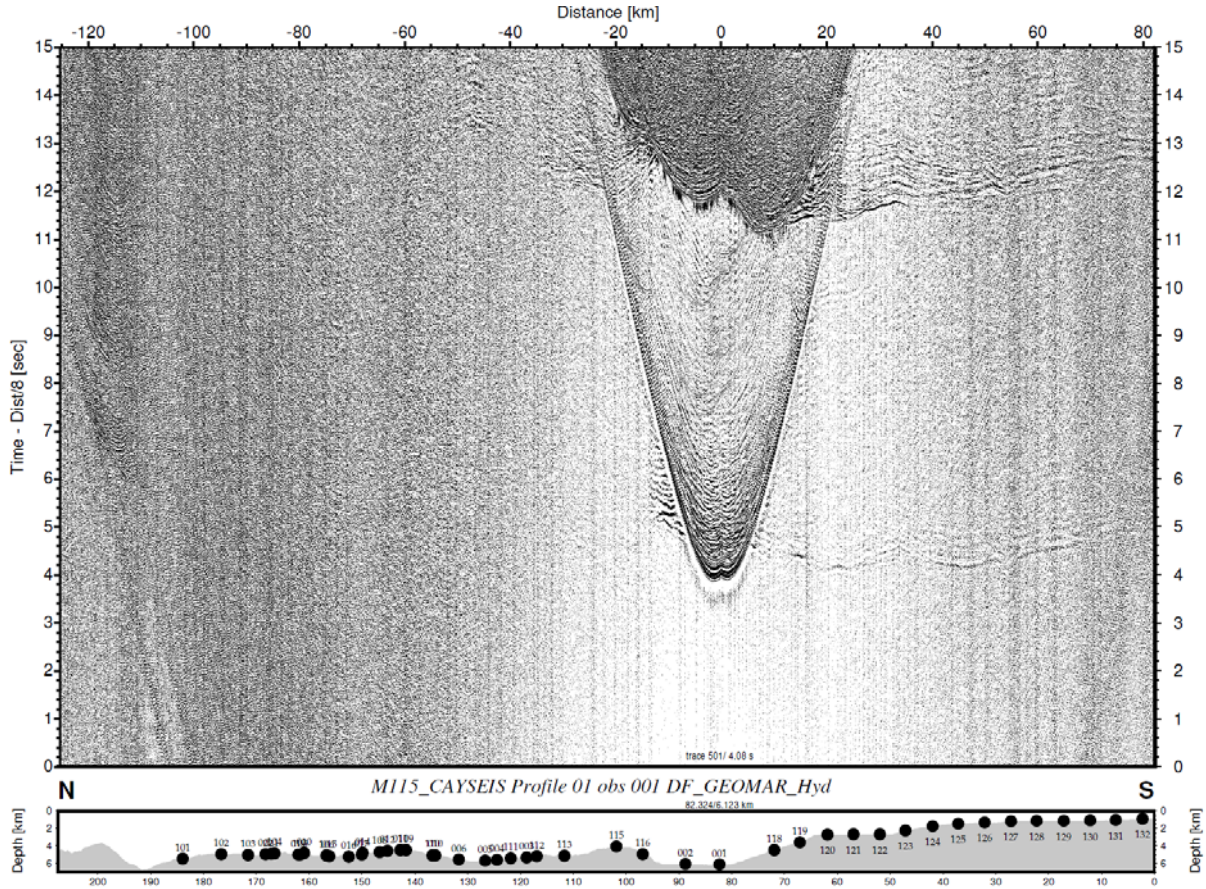

Fig. 5.15 P1 – OBS01 – hydrophone. Record section from a GEOMAR ocean-bottom seismograph.

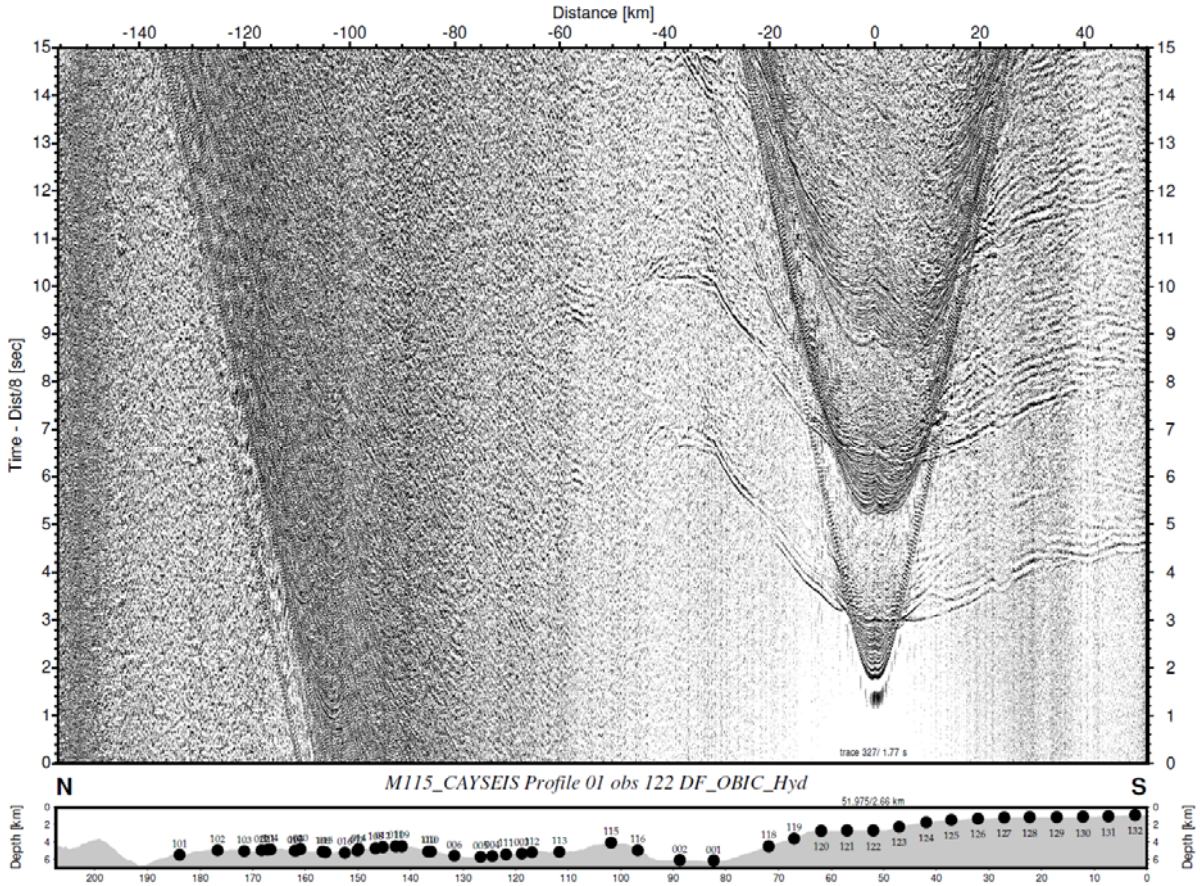

Fig. 5.16 P1 – OBS122– hydrophone. Record section from a UK OBIF ocean-bottom seismograph.

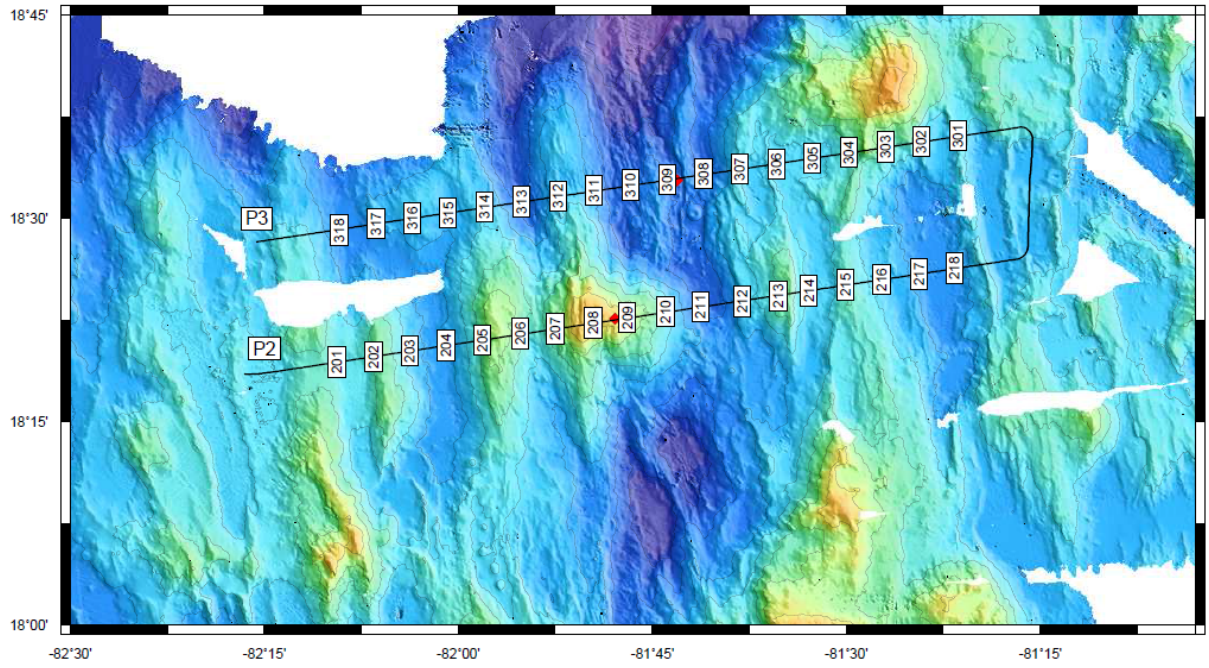

Fig. 5.17 Layout of P2 and P3 across the Mid-Cayman spreading centre. Hydrothermal sites are marked by red diamonds.

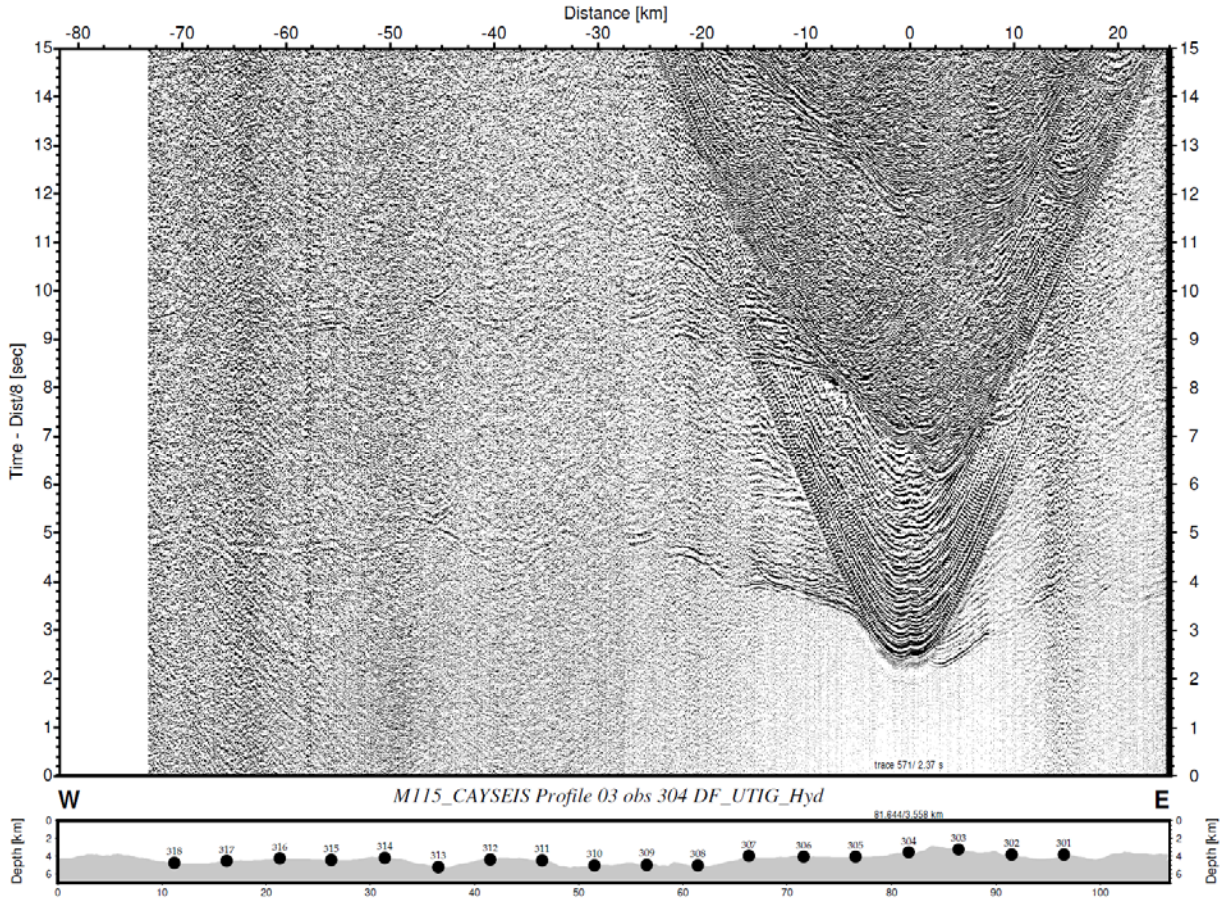

Fig. 5.18 P3 - OBS304 – hydrophone. Record section from a UTIG ocean-bottom seismograph.

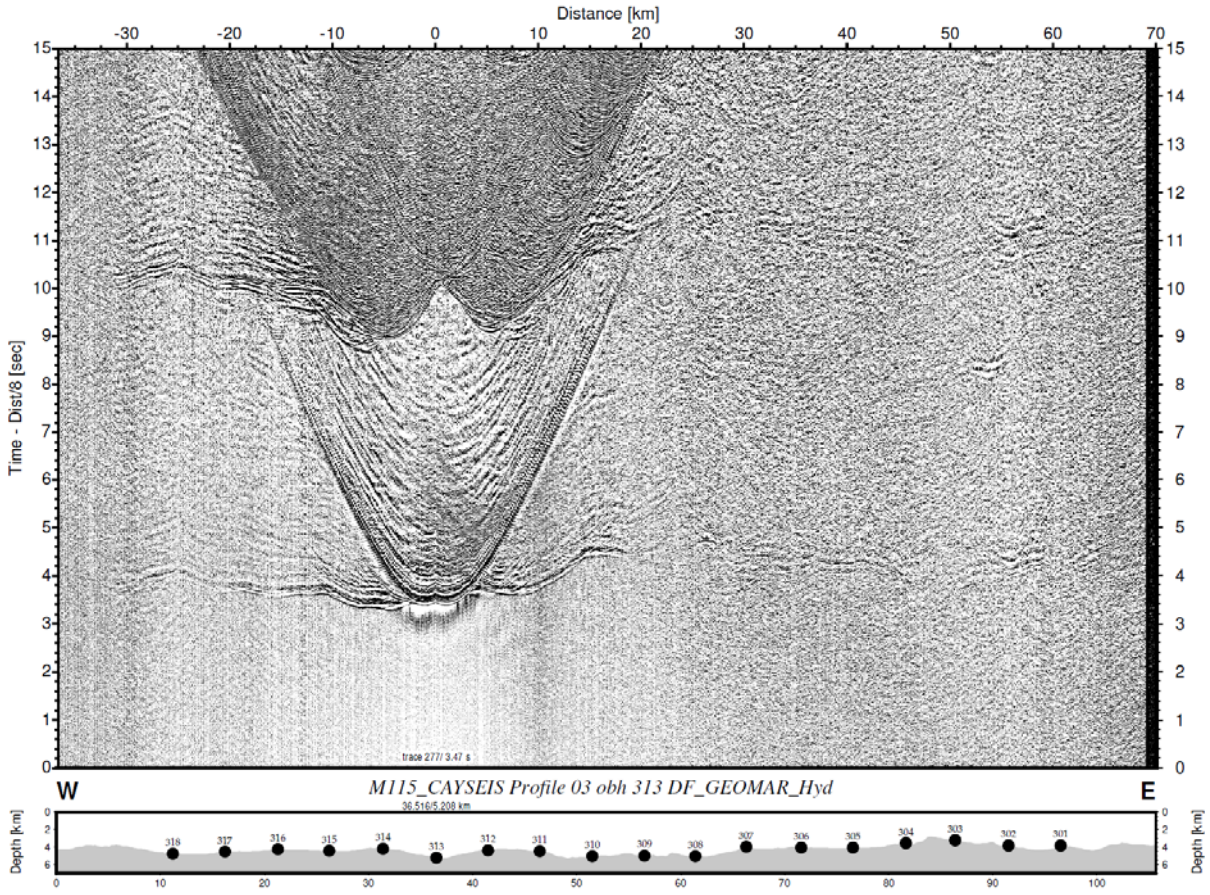

Fig. 5.19 P3 - OBS313 – hydrophone. Record section from a GEOMAR ocean-bottom seismograph.

5.2.4 Profiles P2 and P3 – across the Mid-Cayman spreading centre

The structure and tectonics of the Mid-Cayman spreading centre were surveyed by two profiles P2 and P3. We deployed 36 OBSs at 5 km spacing, along these two across-axis profiles (Fig. 5.17). Profile P2 crossed the Mt Dent oceanic core complex and the associated hydrothermal vent site on the summit of this dome-like feature. Profile P3 was located 10 km to the north, crossing the ridge-axis at the location of the deepest known hydrothermal vent field. The profiles were acquired to study the structure of an oceanic core complex formed at ultra-slow spreading rates by asymmetric spreading (P2), and the structure of "normal" crust formed by symmetric spreading to the north of the OCC (P3). In addition, we sought to characterise the crustal structure at both hydrothermal vent sites to determine how the fluid flow is facilitated at such water pressures. All instruments deployed along P2 (OBS201 to OBS218) and along P3 (OBS301 to OBS318) recorded data. Along P2 and P3 we fired 701 and 734 airgun shots, respectively. Overall, data quality is poorest for OBSs located in the median valley but, in general, even these data are of a much better quality than data recorded in the median valley of P1. Typical offsets were of the order of 40 to 70 km. Apparent velocities of ~8 km/s suggest that the arrivals propagated through both the crust and upper mantle. Interestingly, we did not observe any clear wide-angle phase from the oceanic crust-mantle boundary, or seismic Moho. Examples are shown in Figs 5.18 & 5.19.

5.2.5 Profile P4 – mature ultra-slow crust and the Swan Island transform margin

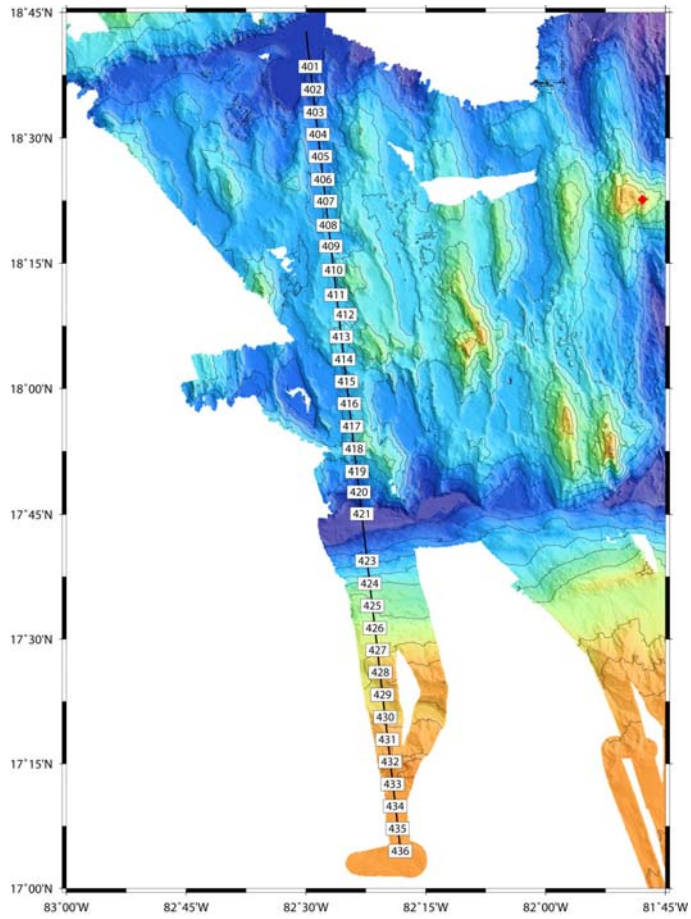

Fig. 5.20 Layout of P4, sampling mature oceanic crust ~ 50 km to the west of the MCSC, and crossing the Swan Island transform fault.

Profile P4 was located ~50 km to the west of the spreading axis, running along an isochron. The profile gathered to study the variability of crustal accretion as a function of ridge crest segmentation away from the ridge crest/median valley, characterizing mature ultra-slow spreading lithosphere. Furthermore, it also aimed to study the structure of the Swan Island transform fault and the structure of the continental margin of Honduras to the south, to investigate how the transform margin crustal structure develops with age.

We deployed 36 OBSs/Hs at 5 km intervals (OBS401 to OBS436), recording 1169 shots (Fig. 5.20). One OBH, OBH422,

failed to record any data. All other OBSs/Hs recorded excellent quality data, recording refraction

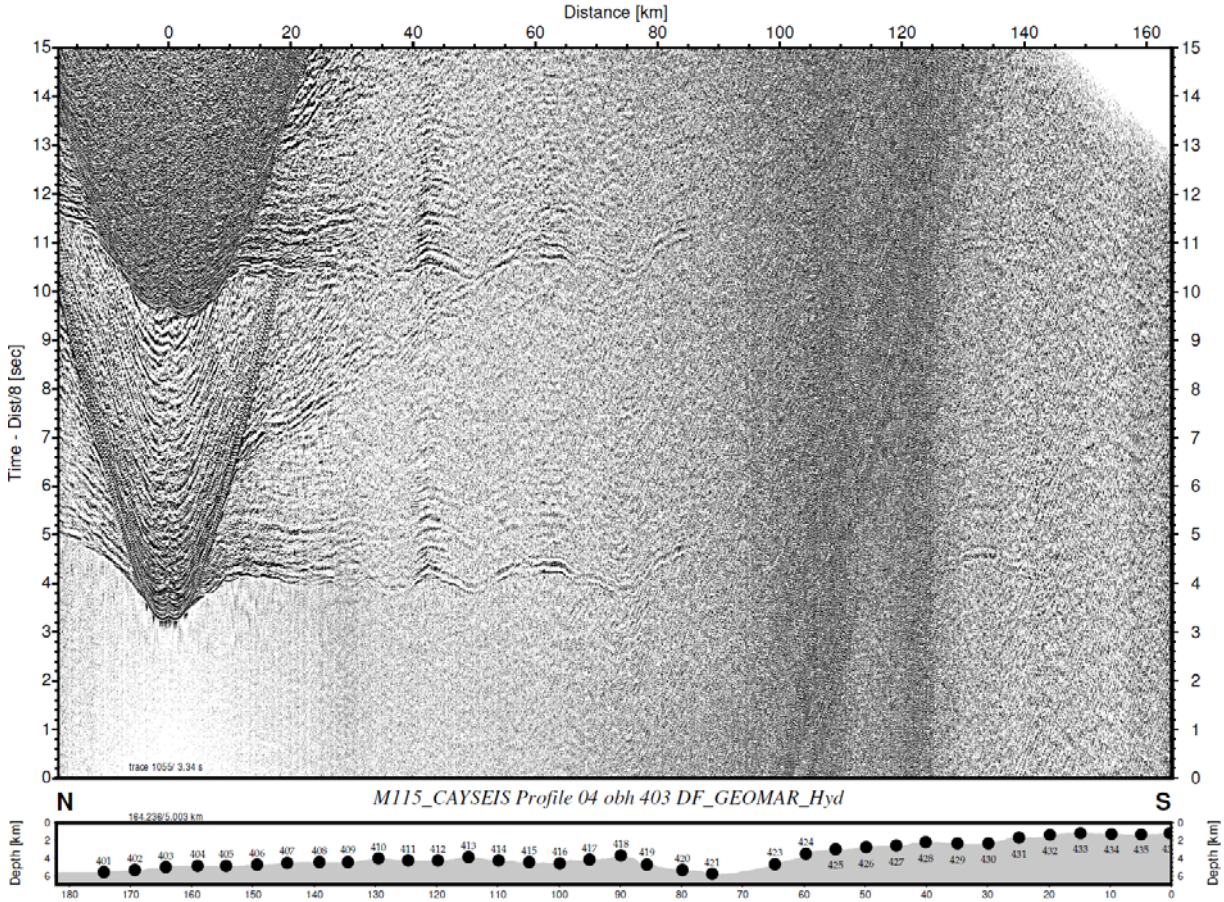

Fig. 5.21 P4 – OBS403 – hydrophone. Record section from a GEOMAR ocean-bottom seismograph.

phases of all shots at all offsets. The largest offsets where 120 to 150 km. In general, crust generated at the MCSC did not show any clear evidence for a PmP wide-angle reflection, except perhaps at 30 to 40 km offset to the south of OBS416. In contrast, OBSs on the continental slope did record a PmP reflection at >25 km offset to the south of OBS430. Fast apparent velocities at >10 km offset, like those observed by OBH403, suggest that crust in the basin is also rather thin. Example record sections are shown in Figs 5.21 to 5.24.

5.2.6 Profile P5 – off-axis structure of ultra-slow spreading crust, eastern flank

Profile P5 was located along a flow line in an off-axis setting, running between 15 to 100 km off-axis. The aim of this profile was to study the variability in crustal accretion as a function of time, and to characterise mature ultra-slow spreading lithosphere and the structure of the mantle. Furthermore, we aimed to study the effects of crustal and lithospheric ageing. In addition, this profile provided the conjugate to profile P6, located on the opposite ridge flank, enabling investigation of asymmetry in accretion.

We deployed 28 OBSs/Hs along P5, located at 2 to 5 km intervals, with smaller instrument spacing in the centre of the profile (Fig. 5.25). Two OBHs failed to record data, namely OBH514 and OBH517. All other stations recorded data of good-to-very good quality, with arrival offsets of 40 to 70 km. Again, we did not record a clear PmP arrival. Scattering of energy from the rough seabed generated some arrivals resembling wide-angle phases though.

However, due to the dense instrument spacing and good bathymetric coverage, we could identify likely features causing the observed scattering. As with the other profiles, we observed fast apparent velocities at offsets of <20 km, again suggesting a thinner than normal crust. Example record sections are shown in Figs 5.26 to 5.29.

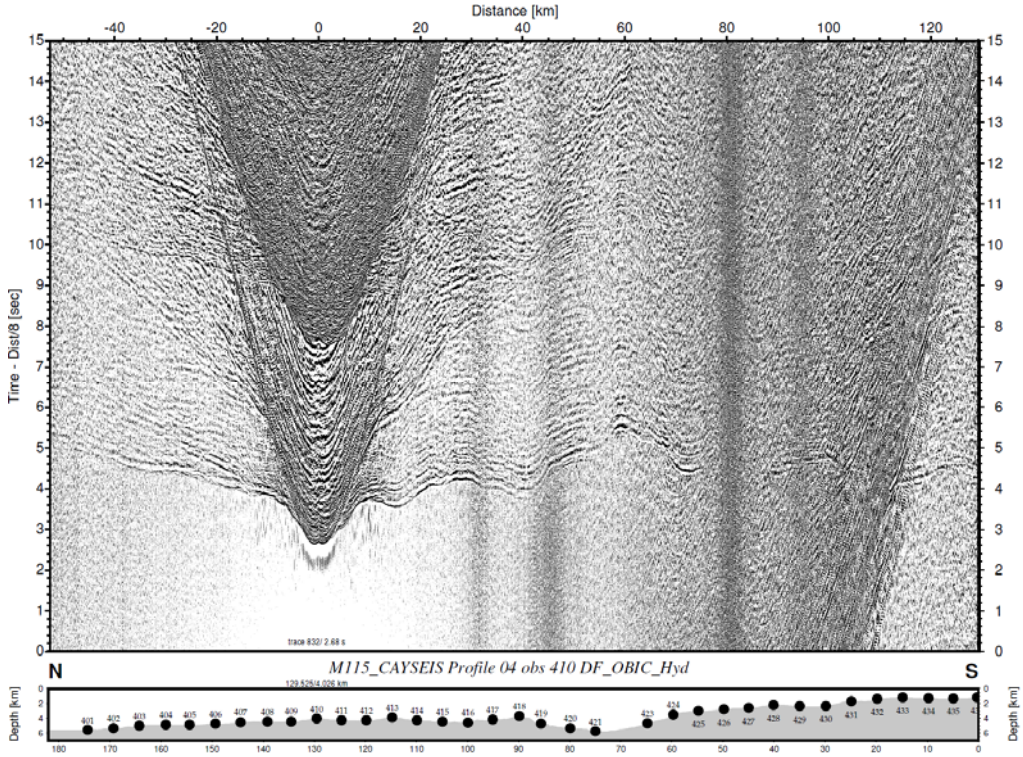

Fig. 5.22 P4 - OBS410 – hydrophone. Record section from a UK OBIF ocean-bottom seismograph.

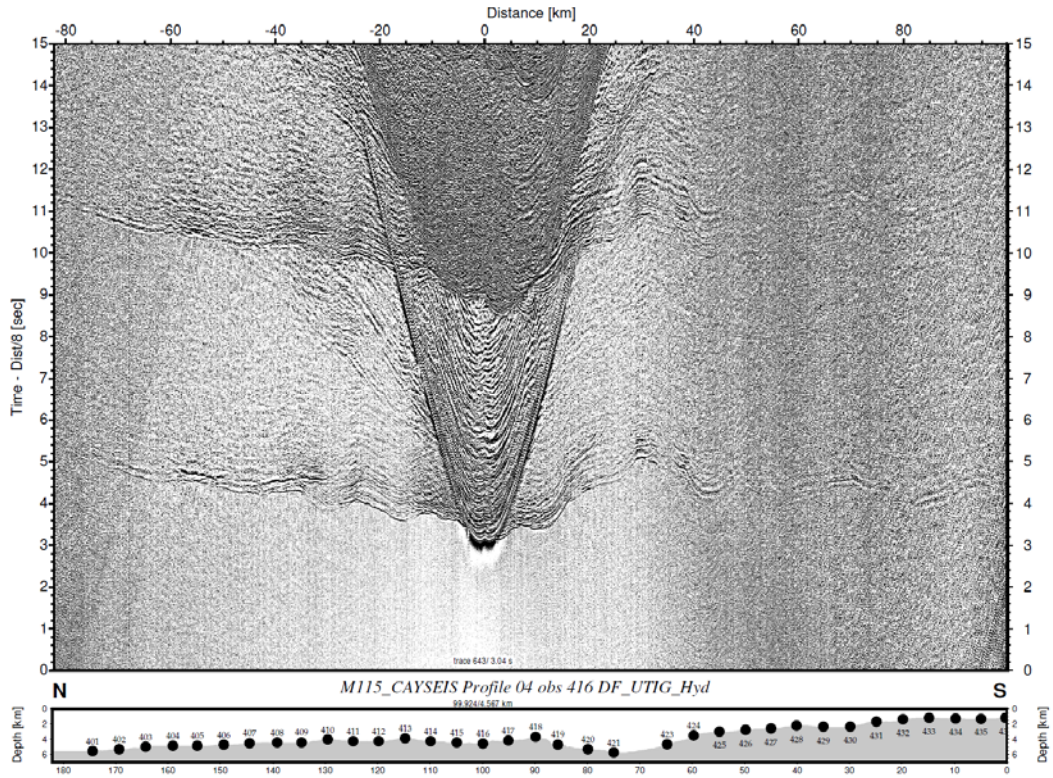

Fig. 5.23 P4 – OBS416 – hydrophone. Record section from a UTIG ocean-bottom seismograph.

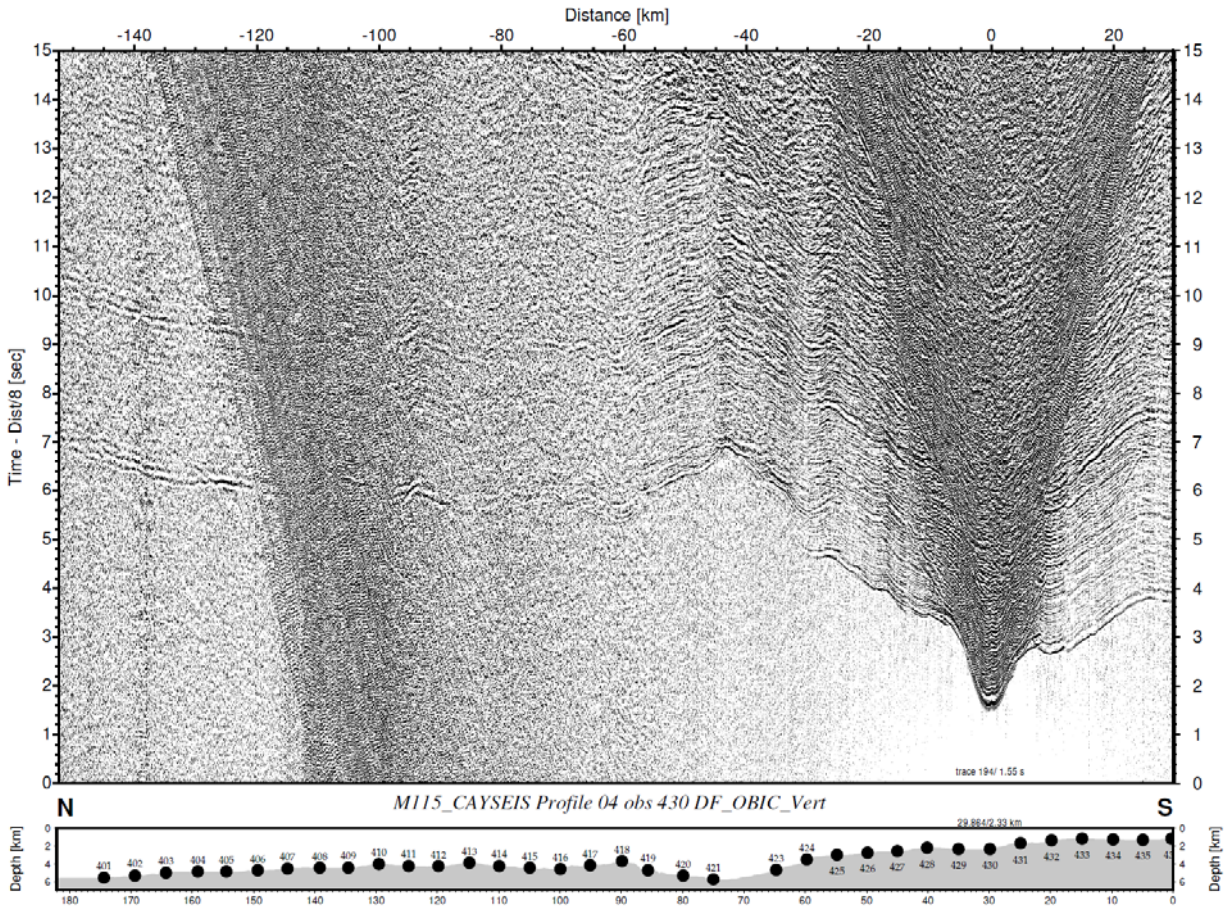

Fig. 5.24 P4 - OBS430 – vertical geophone. Record section from a UK OBIF ocean-bottom seismograph.

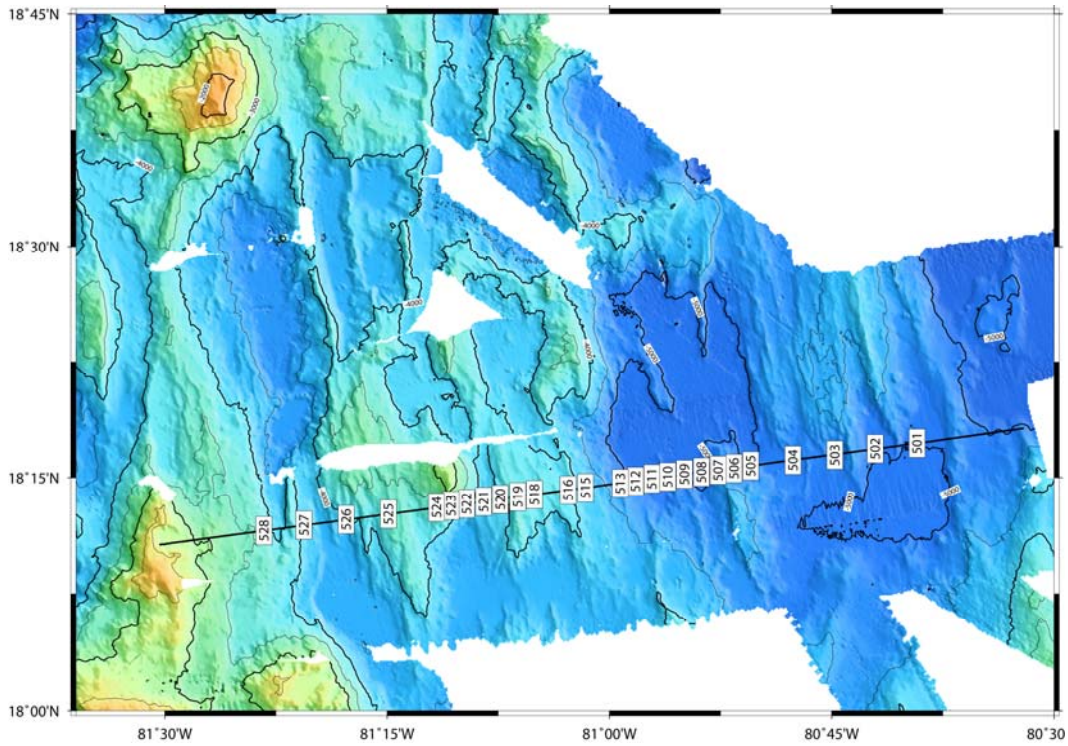

Fig. 5.25 Layout of P5, surveying mature oceanic crust in an off-axis setting. This profile is conjugate to P6.

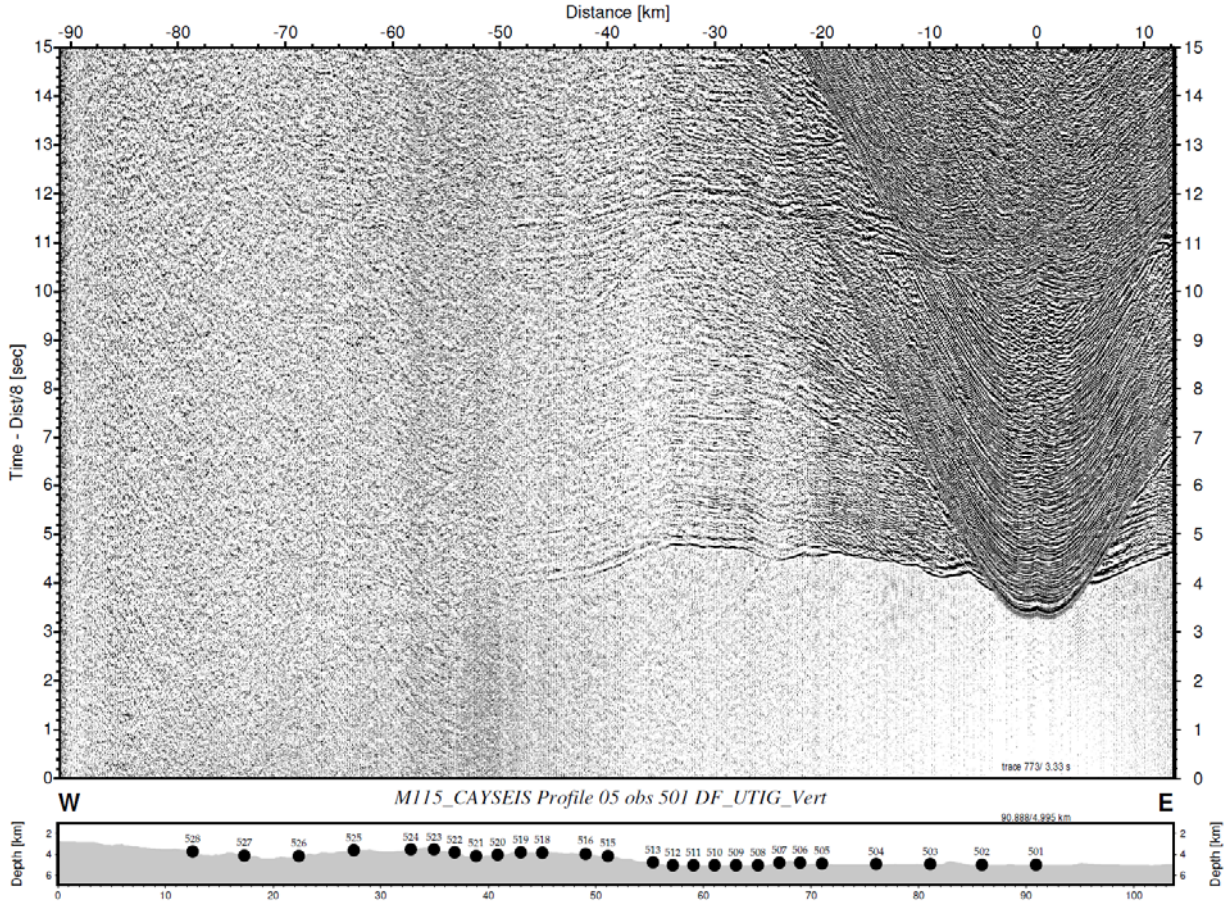

Fig. 5.26 P5 – OBS501– vertical geophone. Record section from a UTIG ocean-bottom seismograph.

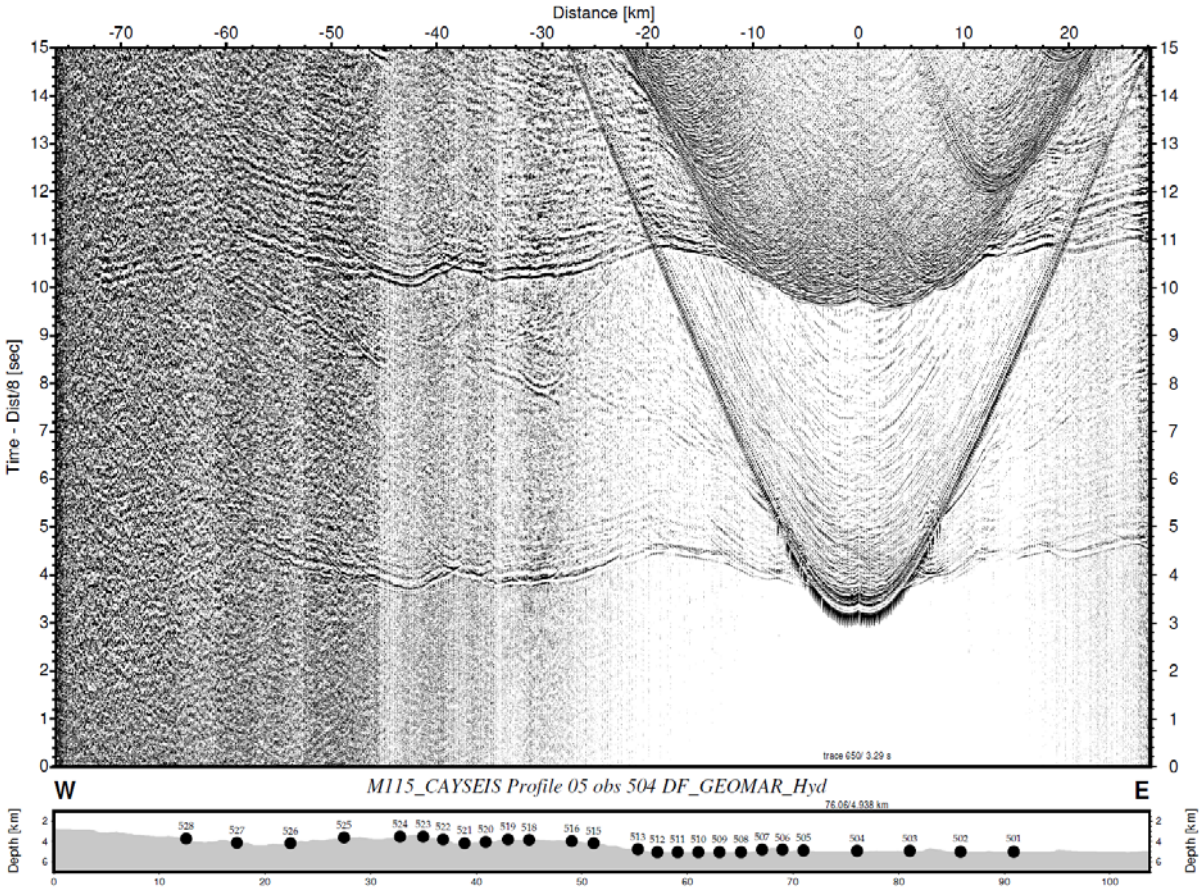

Fig. 5.27 P5 – OBS504 – hydrophone. Record section from a GEOMAR ocean-bottom seismograph.

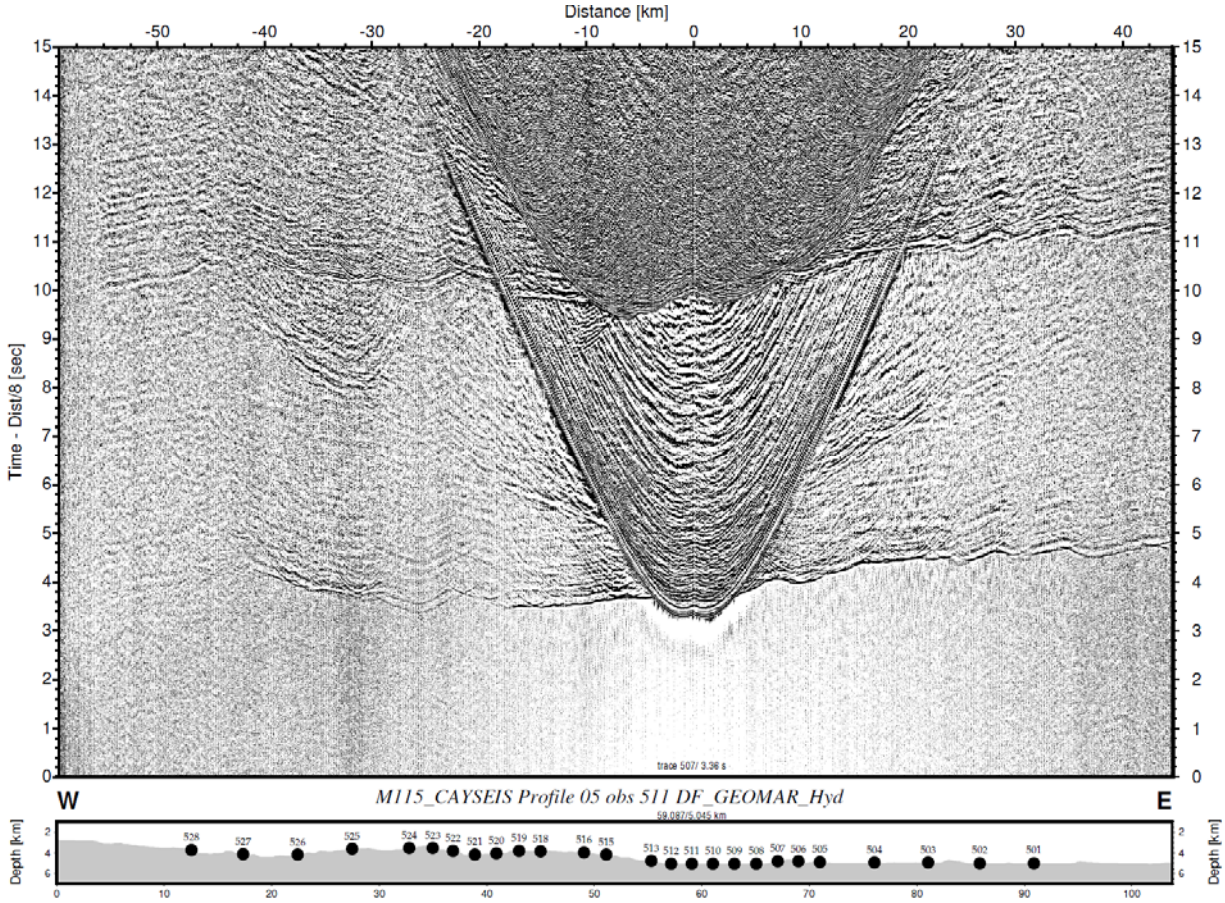

Fig. 5.28 P5 – OBS511 – hydrophone. Record section from a GEOMAR ocean-bottom seismograph.

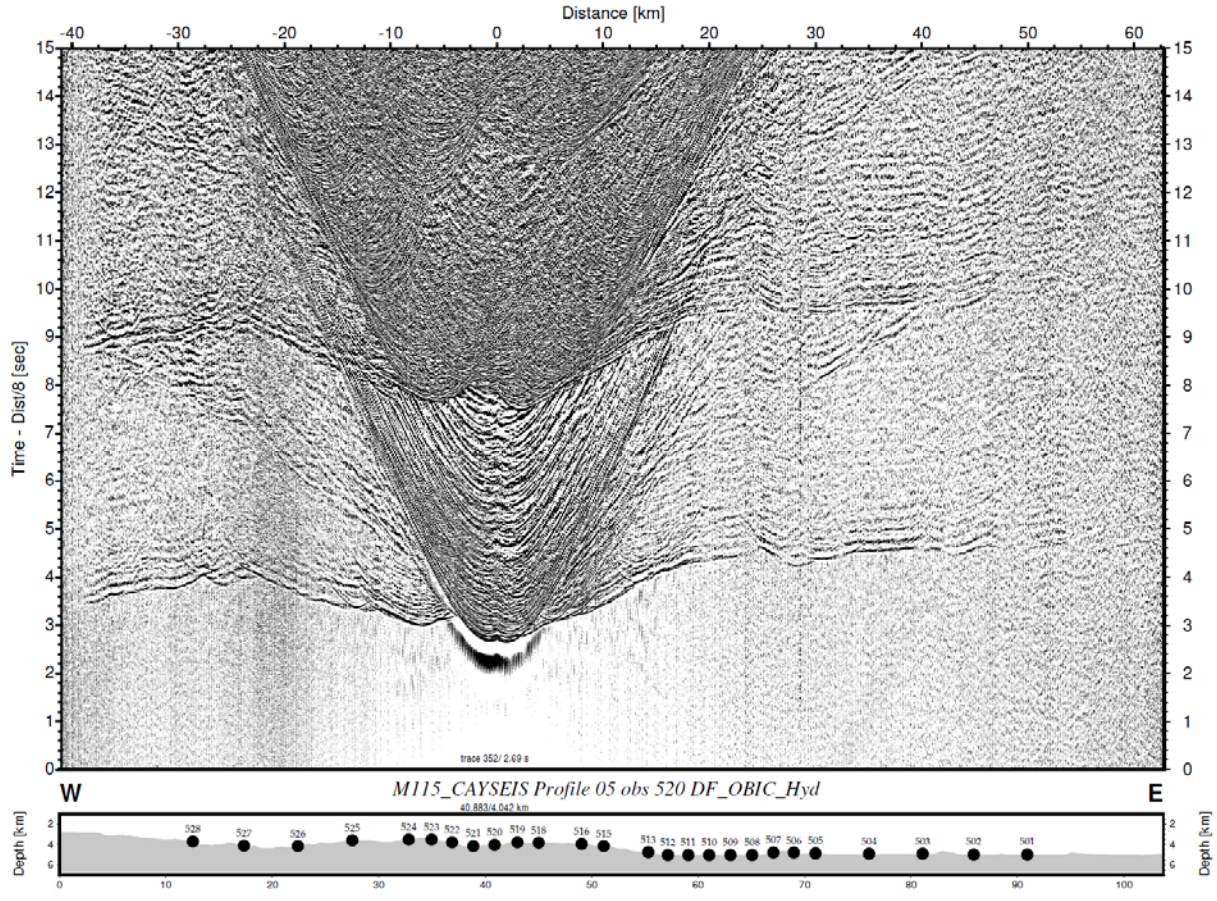

Fig. 5.29 P5 – OBS520 – hydrophone. Record section from a UK OBIF ocean-bottom seismograph.

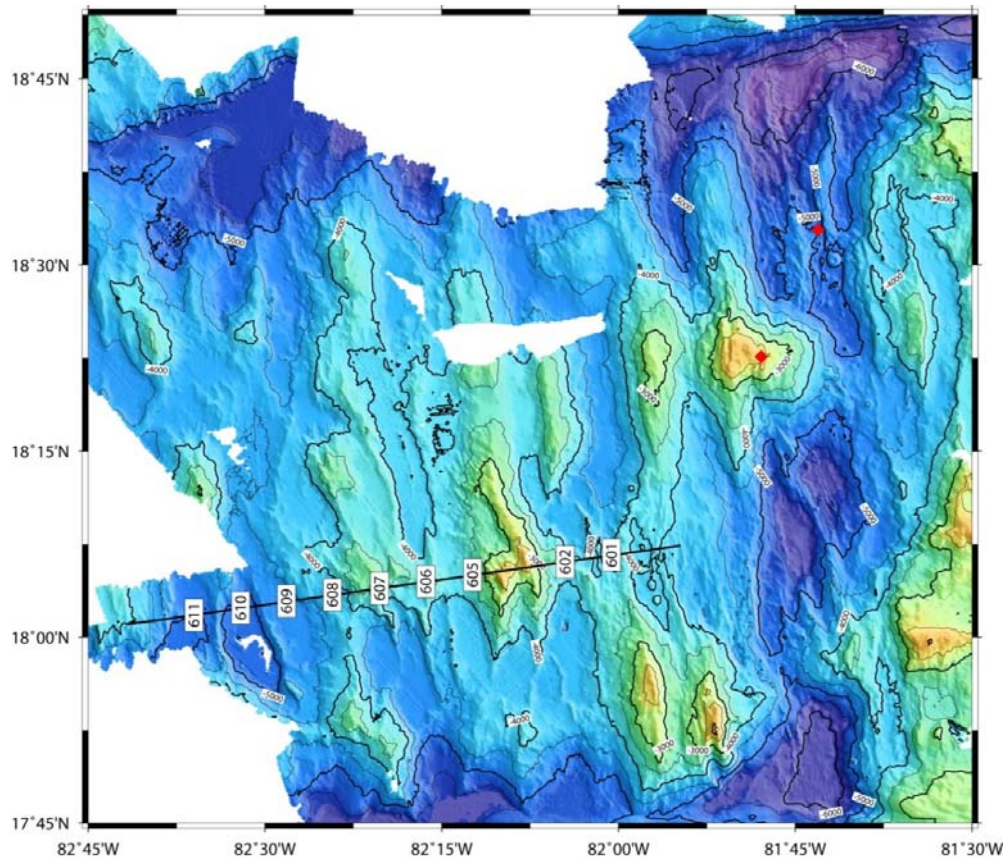

Fig. 5.30 Layout of P6, surveying mature oceanic crust in an off-axis setting. This profile is conjugated to

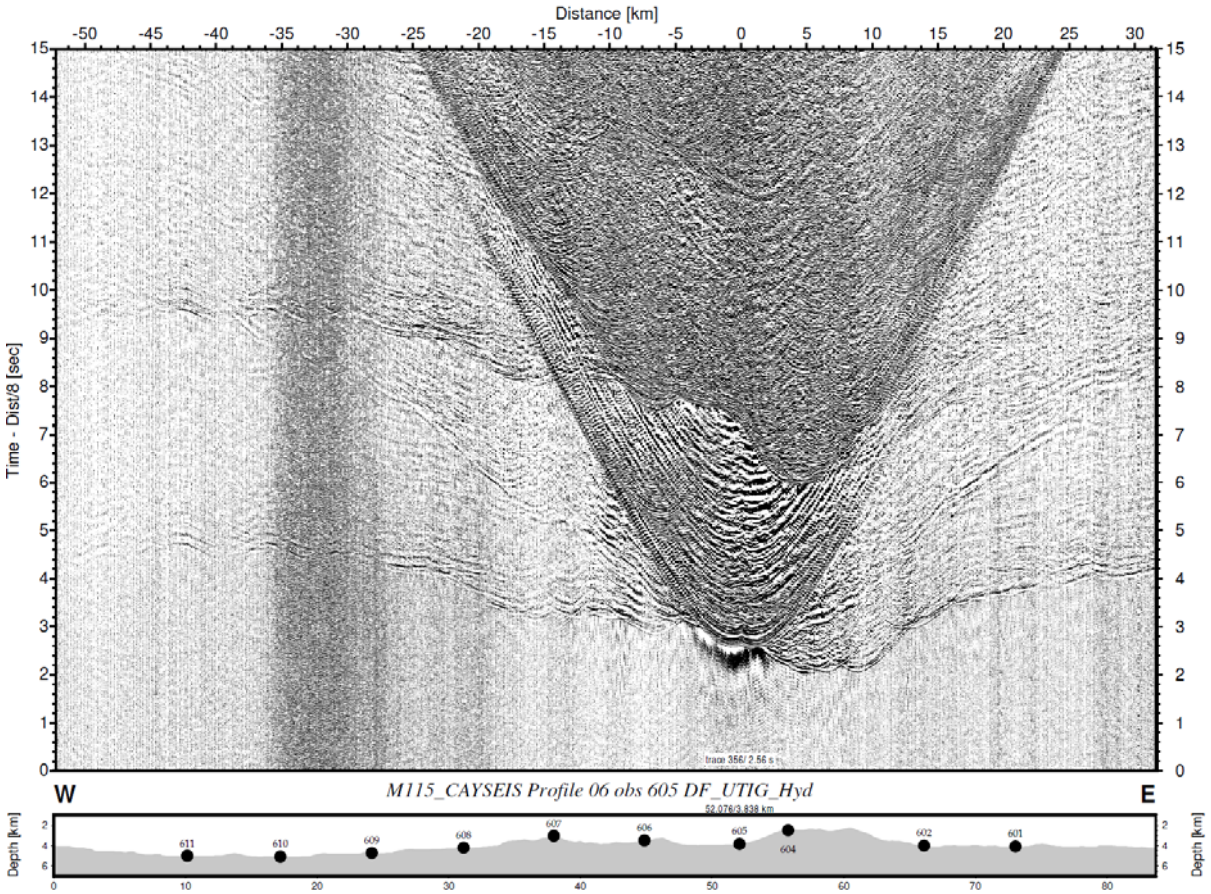

Fig. 5.31 P6 – OBS605 – hydrophone. Record section from a UK OBIF ocean-bottom seismograph.

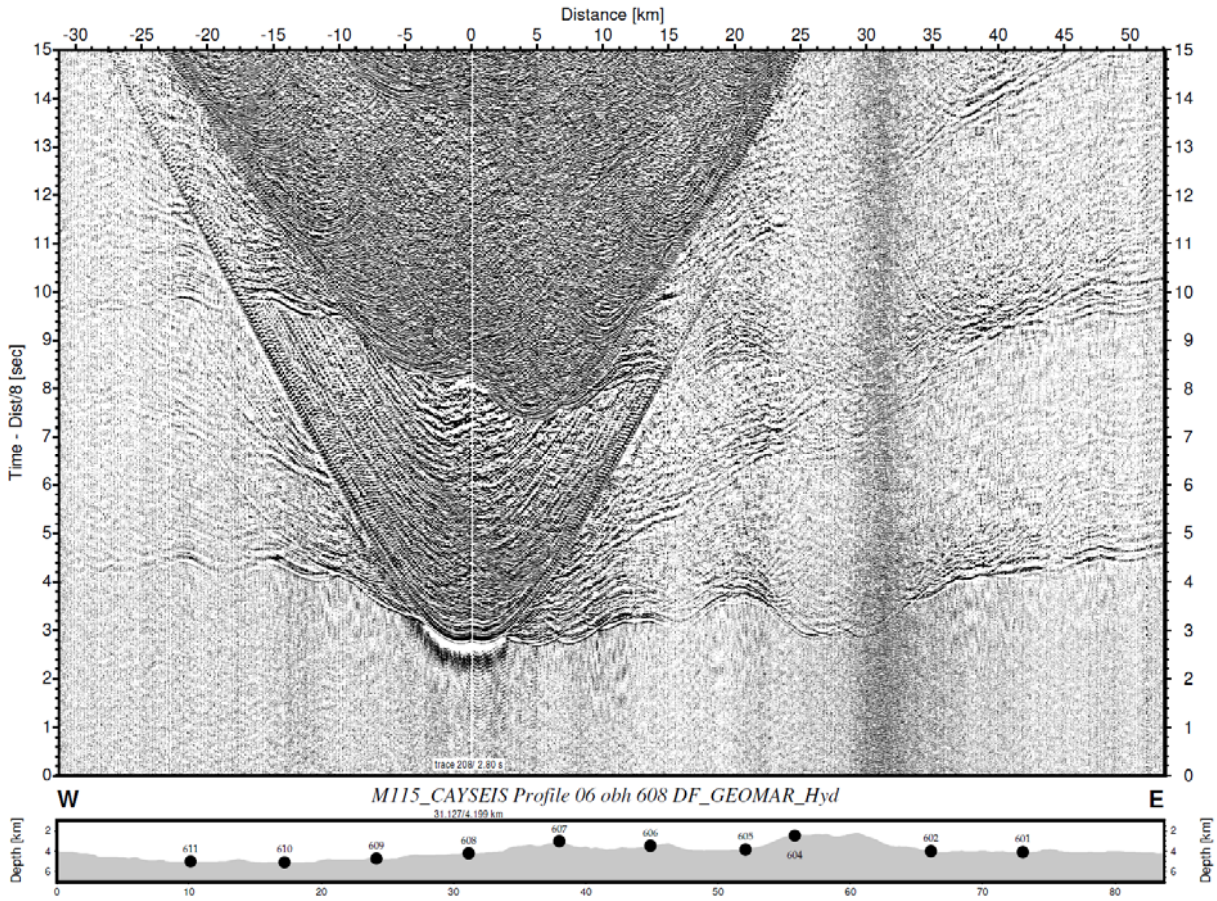

Fig. 5.32 P6 – OBS608 – hydrophone. Record section from a GEOMAR ocean-bottom seismograph.

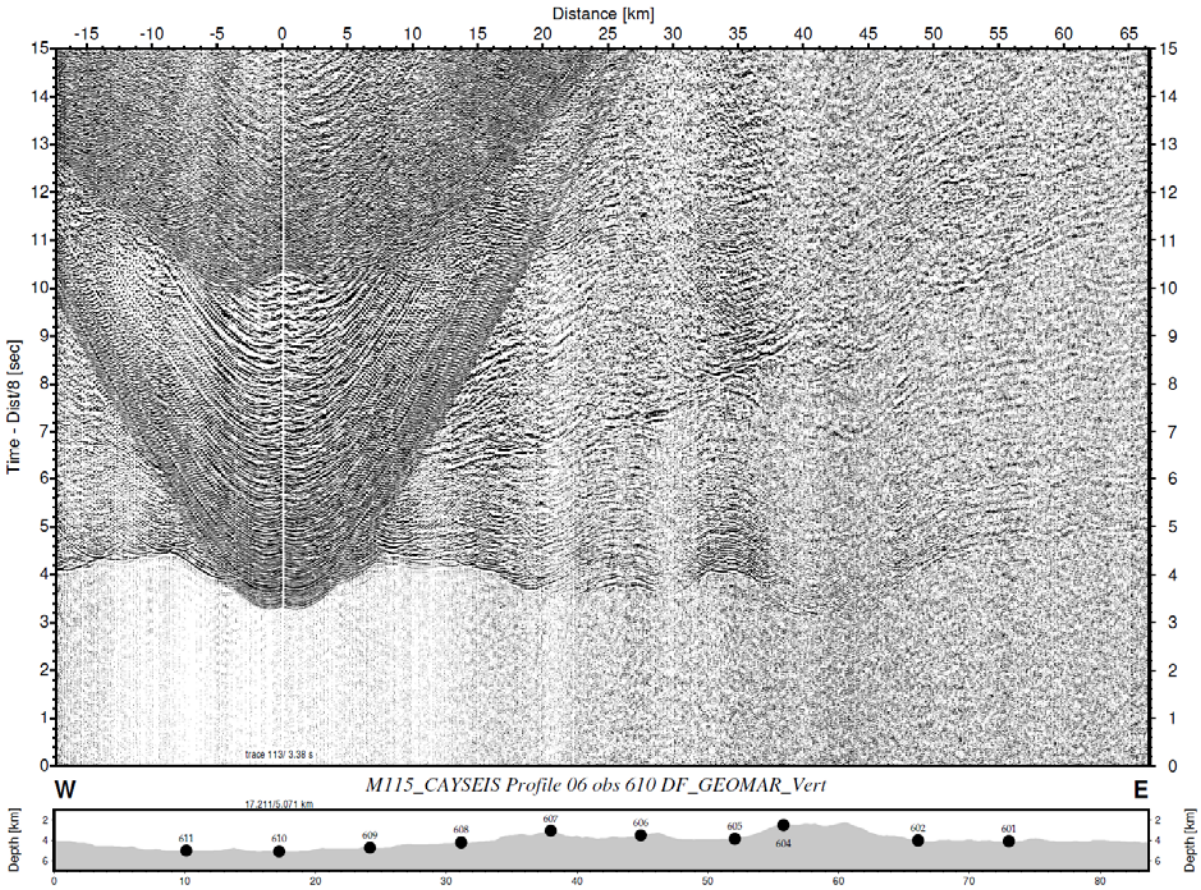

Fig. 5.33 P6 – OBS610 – vertical geophone. Record section from a GEOMAR ocean-bottom seismograph.

5.2.7 Profile P6 – off-axis structure of ultra-slow spreading crust, western flank

Profile P6 was the last profile shot during the survey. It is conjugated to P05 and hence located on the western side of the Cayman Trough (Fig. 5.30). As in the case of profile P05, the aim of this profile was also to study the variability of crustal accretion as a function of time, to characterise mature ultra-slow spreading lithosphere, the structure of the mantle, and to study ageing of lithosphere. Furthermore, together with its conjugated we aimed to reveal an asymmetry in crustal accretion. Due to time constraints at the end of the cruise, only 11 OBSs/Hs were deployed along the profile, namely OBS601 to OBS611. Unfortunately, two stations, including a test instrument, failed to record any data, namely stations OBS603 and OBS604. Stations were deployed at 7 km intervals instead of the 5 km norm along the other profiles.

Similar to profile P5, data were of good-to-very good quality, with refractions visible over offsets of up to 40 to 70 km. Again, we did not sample a clear wide-angle PmP arrival. As with the other profiles, we observed fast apparent velocities at offsets of <20 km, again suggesting a rather thin crust. Example record sections are shown in Figs 5.31 to 5.33.

5.3 Weather report

At 09:00 on the 1st April, METEOR left the Kingston harbour. At the beginning of the cruise a force 4-5 easterly wind blew between a high close to Florida and a tropical low pressure zone. During the transit the sea height reached 1 to 1.5 m in the wider working area south of the Cayman Islands.

During the night 2nd-3rd April, the of many first occasional rain showers appeared. This weather pattern at the southwestern edge of a high pressure ridge, persisted throughout the working area. Thus, good weather conditions persisted while the seismic instruments were deployed along the first north-south profile. Until the 6th April, fine and mostly dry weather continued with force 4 east-to-northeast winds and a sea of 1 to 1.5 m. The easterly swell averaged mostly about 1 m.

A low over northwestern Columbia extended a trough to 12N 78W. Thus the pressure gradient increased a little for a time. From the 7th of April the wind decreased to force 5 at times with the sea hovering around 1.5 m. Over the following days, until the 8th April, the high pressure ridge from the Azores persisted in the local area. Thus no significant weather change was experienced. However from the 9th April, humid and cooler air entered the area up to altitude levels of 3 km. Until the 13th April, in the earlier part of the day, local showers developed. This restricted deck repainting activities. On the 9th and 10th April, to the north of METEOR lightning was observed. On the 12th April at 22:47, a strong showery gust of about 36.4 kn occurred. Along the edge of the high and the tropical low pressure trough, mostly force 4-5 easterly winds were experienced. The sea reached a height of 1 to 1.5 m. On the 14th-15th April dry weather was experienced.

From the 16th April, in the northern parts of the working area, local shower activity increased a little. From the 18th April, drier and warmer air from higher levels entered the area and partly cloudy conditions developed. The wind decreased to force 3 to 4, and shifted to the east-to-southeast. The sea reached only up to 1 m.

On the 20th April, a ridge extended over the Bahamas to the eastern Gulf of Mexico and intensified for a while. The wind increased to about force 5 and the sea to 1.5 m. The visibility

reduced to about 5 nm due to dust from the Sahara. The sky was white-coloured even without clouds. On METEOR, small fine deposits of Saharan dust were encountered.

During the transit on the 22th April, the wind in the lee of Jamaica shifted briefly to the northeast with force 2 to 3. Over the following days, the Atlantic high wandered a little to the east with the pressure gradient between the tropical low pressure trough weakening. The wind was blowing at force 3-4 and mostly from the east. From the 26th April, the trade wind shifted to the southeast and increased to force 4. The sea, east of Jamaica, showed values of 1 to 1.5 m in Guadeloupe. The swell direction shifted from southeast to east. The air temperature, beside showers, was always around 26 to 27ºC with the higher values towards the end of cruise M115. The water temperature increased from 27 to 28ºC.

6 Station lists

METEOR-Station	Gear Station	Latitude		Longitude		Depth in m	Type	Remarks
M115_118-1	**OBS01**	17°48.061'	N	81°43.249'	W	6133	GEOMAR	CMG-40T
M115_119-1	**OBS02**	17°51.573'	N	81°43.176'	W	6080	GEOMAR	
M115_120-1	**OBS03**	18°07.862'	N	81°44.405'	W	5804	GEOMAR	
M115_121-1	**OBS04**	18°10.859'	N	81°46.207'	W	5709	GEOMAR	CMG-40T
M115_122-1	**OBS05**	18°12.088'	N	81°42.621'	W	5735	GEOMAR	
M115_123-1	**OBS06**	18°14.777'	N	81°42.619'	W	5579	GEOMAR	CMG-40T
M115_124-1	**OBS07**	18°14.210'	N	81°48.011'	W	4200	OBIF	
M115_125-1	**OBS08**	18°17.587'	N	81°49.855'	W	3400	OBIF	
M115_126-1	**OBS09**	18°18.144'	N	81°49.964'	W	4493	OBIF	
M115_127-1	**OBS10**	18°17.109'	N	81°40.205'	W	4892	GEOMAR	
M115_128-1	**OBS11**	18°20.690'	N	81°39.604'	W	4678	GEOMAR	
M115_129-1	**OBS12**	18°22.155'	N	81°45.586'	W	3119	GEOMAR	Paroscientific
M115_130-1	**OBS13**	18°20.967'	N	81°50.483'	W	2435	GEOMAR	
M115_131-1	**OBS14**	18°24.567'	N	81°49.204'	W	2635	GEOMAR	
M115_132-1	**OBS15**	18°27.983'	N	81°48.801'	W	4235	GEOMAR	
M115_133-1	**OBS16**	18°26.102'	N	81°45.004'	W	4740	GEOMAR	
M115_134-1	**OBS17**	18°24.730'	N	81°41.405'	W	5235	GEOMAR	
M115_135-1	**OBH18**	18°28.513'	N	81°39.614'	W	4273	GEOMAR	bad DPG, no data
M115_136-1	**OBS19**	18°31.252'	N	81°42.624'	W	5069	GEOMAR	
M115_137-1	**OBS20**	18°30.646'	N	81°46.813'	W	5029	GEOMAR	
M115_138-1	**OBS21**	18°34.017'	N	81°46.798'	W	5139	GEOMAR	
M115_139-1	**OBS22**	18°34.637'	N	81°42.605'	W	4719	GEOMAR	Paroscientific
M115_140-1	**OBS23**	18°38.019'	N	81°40.008'	W	4993	GEOMAR	CMG-40T
M115_141-1	**OBS24**	18°38.509'	N	81°44.112'	W	5324	GEOMAR	
M115_142-1	**OBS25**	18°47.125'	N	81°41.641'	W	6431	GEOMAR	

Table 6.1 Ocean-bottom seismograph passive network.

METEOR station	Gear Station	Latitude		Longitude		Depth in m	Type	Remarks
M115_143-1	**OBH101**	18°43.078'	N	81°41.759'	W	5484	GEOMAR	bad hydrophone
M115_144-1	**OBS102**	18°39.052'	N	81°41.871'	W	4999	UTIG	bad hydrophone
M115_145-1	**OBS103**	18°36.359'	N	81°41.953'	W	5024	UTIG	
M115_146-1	**OBS104**	18°33.174'	N	81°42.030'	W	4825	UTIG	
M115_147-1	**OBS105**	18°30.949'	N	81°42.093'	W	4922	UTIG	
M115_148-1	**OBS106**	18°26.237'	N	81°42.193'	W	5108	UTIG	
M115_149-1	**OBS107**	18°25.573'	N	81°42.221'	W	5148	UTIG	
M115_150-1	**OBH108**	18°22.861'	N	81°42.324'	W	4662	GEOMAR	
M115_151-1	**OBH109**	18°20.136'	N	81°42.401'	W	4444	GEOMAR	Sercel, spikes
M115_152-1	**OBH110**	18°17.465'	N	81°42.477'	W	5076	GEOMAR	
M115_153-1	**OBH111**	18°09.369'	N	81°42.690'	W	5413	GEOMAR	poor data
M115_154-1	**OBH112**	18°06.684'	N	81°42.738'	W	5076	GEOMAR	
M115_155-1	**OBS113**	18°03.981'	N	81°42.832'	W	5142	UTIG	
M115_156-1	**OBS114**	18°01.282'	N	81°42.902'	W	4659	UTIG	
M115_157-1	**OBS115**	17°58.596'	N	81°42.960'	W	4055	UTIG	
M115_158-1	**OBS116**	17°55.907'	N	81°43.048'	W	4918	UTIG	
M115_159-1	**OBS117**	17°45.113'	N	81°43.340'	W	5404	UTIG	lost
M115_160-1	**OBS118**	17°42.416'	N	81°43.413'	W	4434	UTIG	
M115_161-1	**OBS119**	17°39.750'	N	81°43.497'	W	3549	OBIF	
M115_162-1	**OBS120**	17°37.002'	N	81°43.574'	W	2707	OBIF	
M115_163-1	**OBS121**	17°34.300'	N	81°43.668'	W	2678	OBIF	
M115_164-1	**OBS122**	17°31.609'	N	81°43.717'	W	2653	OBIF	
M115_165-1	**OBS123**	17°28.917'	N	81°43.806'	W	2243	OBIF	
M115_166-1	**OBS124**	17°26.222'	N	81°43.883'	W	1709	OBIF	
M115_167-1	**OBS125**	17°23.528'	N	81°43.951'	W	1446	OBIF	
M115_168-1	**OBS126**	17°20.823'	N	81°44.035'	W	1313	OBIF	
M115_169-1	**OBS127**	17°18.128'	N	81°44.104'	W	1894	OBIF	
M115_170-1	**OBS128**	17°15.436'	N	81°44.179'	W	1103	OBIF	
M115_171-1	**OBS129**	17°12.733'	N	81°44.200'	W	1103	OBIF	
M115_172-1	**OBS130**	17°10.009'	N	81°44.314'	W	1088	OBIF	
M115_173-1	**OBS131**	17°07.369'	N	81°44.396'	W	999	OBIF	
M115_174-1	**OBS132**	17°04.669'	N	81°44.458'	W	890	OBIF	

Table 6.2 Ocean-bottom seismographs deployed along profile P1.

METEOR station	Gear Station	Latitude		Longitude		Depth in m	Type	Remarks
M115_213-1	**OBS201**	18°19.417'	N	82°09.391'	W	3751	OBIF	
M115_214-1	**OBS202**	18°19.829'	N	82°06.582'	W	3355	OBIF	
M115_215-1	**OBS203**	18°20.234'	N	82°03.767'	W	4203	OBIF	
M115_216-1	**OBS204**	18°20.645'	N	82°00.957'	W	4568	OBIF	
M115_216-1	**OBS205**	18°21.054'	N	81°58.148'	W	3349	OBIF	
M115_217-1	**OBS206**	18°21.490'	N	81°55.354'	W	3523	OBIF	
M115_218-1	**OBS206b**	18°21.513'	N	81°55.236'	W	3582	OBIF	
M115_219-1	**OS207**	18°21.885'	N	81°52.512'	W	3240	OBIF	
M115_220-1	**OBS208**	18°22.304'	N	81°49.740'	W	2187	OBIF	
M115_221-1	**OBS208b**	18°22.307'	N	81°49.606'	W	2237	OBIF	
M115_222-1	**OBS209**	18°22.714'	N	81°46.932'	W	2529	OBIF	
M115_223-1	**OBS210**	18°23.123'	N	81°44.110'	W	3594	UTIG	
M115_224-1	**OBS211**	18°23.508'	N	81°41.316'	W	5063	UTIG	
M115_225-1	**OBS212**	18°23.895'	N	81°38.480'	W	4520	UTIG	
M115_226-1	**OBS213**	18°24.295'	N	81°36.549'	W	3573	UTIG	
M115_227-1	**OBS214**	18°24.697'	N	81°32.875'	W	3978	UTIG	
M115_228-1	**OBH215**	18°25.115'	N	81°30.047'	W	3678	GEOMAR	
M115_229-1	**OBH216**	18°25.516'	N	81°27.258'	W	4184	GEOMAR	
M115_230-1	**OBH217**	18°25.907'	N	81°24.421'	W	4678	GEOMAR	
M115_231-1	**OBH218**	18°26.348'	N	81°21.631'	W	4674	GEOMAR	
M115_232-1	**OBH218b**	18°26.348'	N	81°21.631'	W	4674	GEOMAR	poor coupling

Table 6.3 Ocean-bottom seismographs deployed along profile P2.

METEOR station	Gear Station	Latitude		Longitude		Depth in m	Type	Remarks
M115_233-1	**OBH301**	18°36.057'	N	81°21.367'	W	3719.9	GEOMAR	
M115_234-1	**OBH302**	18°35.667'	N	81°24.196'	W	3730.4	GEOMAR	Sercel, spikes
M115_235-1	**OBS303**	18°35.264'	N	81°27.005'	W	3256	UTIG	
M115_236-1	**OBS304**	18°34.865'	N	81°29.826'	W	3555	UTIG	
M115_237-1	**OBS305**	18°34.447'	N	81°32.638'	W	4068	UTIG	
M115_238-1	**OBS306**	18°34.060'	N	81°35.444'	W	4027	UTIG	
M115_239-1	**OBS307**	18°33.651'	N	81°38.287'	W	3986	UTIG	
M115_240-1	**OBS308**	18°33.268'	N	81°41.051'	W	5060	UTIG	
M115_241-1	**OBH309**	18°32.866'	N	81°43.860'	W	5017	GEOMAR	
M115_242-1	**OBH310**	18°32.465'	N	81°46.698'	W	4977.7	GEOMAR	
M115_243-1	**OBH311**	18°32.044'	N	81°49.519'	W	4485.9	GEOMAR	
M115_244-1	**OBH312**	18°31.670'	N	81°52.301'	W	4381	GEOMAR	
M115_245-1	**OBH313**	18°31.231'	N	81°55.113'	W	5220	GEOMAR	
M115_246-1	**OBH314**	18°30.871'	N	81°57.985'	W	4175	GEOMAR	
M115_247-1	**OBS315**	18°30.393'	N	82°00.793'	W	4450	OBIF	
M115_248-1	**OBS316**	18°30.021'	N	82°03.577'	W	4263	OBIF	
M115_249-1	**OBS317**	18°29.612'	N	82°06.363'	W	4470	OBIF	
M115_250-1	**OBS318**	18°29.126'	N	82°09.223'	W	4744	OBIF	

Table 6.4 Ocean-bottom seismographs deployed along profile P3.

METEOR station	Gear Station	Latitude		Longitude		Depth in m	Type	Remarks
M115_290-1	**OBH401**	18°38.362'	N	82°29.449'	W	5509	GEOMAR	
M115_291-1	**OBH402**	18°35.676'	N	82°29.132'	W	5304	GEOMAR	
M115_292-1	**OBH403**	18°32.976'	N	82°28.827'	W	5015	GEOMAR	
M115_293-1	**OBH404**	18°30.298'	N	82°28.486'	W	4846	GEOMAR	
M115_294-1	**OBH405**	18°27.617'	N	82°28.188'	W	4849	GEOMAR	
M115_295-1	**OBH406**	18°24.927'	N	82°27.858'	W	4712	GEOMAR	
M115_296-1	**OBH407**	18°22.263'	N	82°27.523'	W	4491	GEOMAR	
M115_297-1	**OBH408**	18°19.583'	N	82°27.223'	W	4438	GEOMAR	
M115_298-1	**OBS409**	18°16.903'	N	82°26.870'	W	4409	GEOMAR	
M115_299-1	**OBS410**	18°14.223'	N	82°26.542'	W	3977	OBIF	
M115_300-1	**OBS411**	18°11.223'	N	82°26.242'	W	4250	OBIF	
M115_301-1	**OBS412**	18°08.878'	N	82°25.910'	W	4237	UTIG	
M115_302-1	**OBS413**	18°06.208'	N	82°25.561'	W	4225	UTIG	
M115_303-1	**OBS414**	18°03.519'	N	82°25.262'	W	4287	UTIG	
M115_304-1	**OBS415**	18°00.845'	N	82°24.933'	W	4472	UTIG	
M115_305-1	**OBS416**	17°58.186'	N	82°24.584'	W	4444	UTIG	
M115_306-1	**OBS417**	17°55.471'	N	82°24.274'	W	4105	UTIG	
M115_307-1	**OBS418**	17°52.807'	N	82°23.957'	W	3747	UTIG	
M115_308-1	**OBS419**	17°50.112'	N	82°23.624'	W	5187	UTIG	
M115_309-1	**OBH420**	17°47.417'	N	82°23.352'	W	5342	GEOMAR	
M115_310-1	**OBH421**	17°44.792'	N	82°22.989'	W	5759	GEOMAR	
M115_311-1	**OBS422**	17°42.069'	N	82°22.672'	W	5420	GEOMAR	no data
M115_312-1	**OBS423**	17°39.408'	N	82°22.351'	W	4600	OBIF	
M115_313-1	**OBS424**	17°36.704'	N	82°22.020'	W	3455	OBIF	
M115_314-1	**OBS425**	17°34.031'	N	82°21.687'	W	3005	OBIF	
M115_315-1	**OBS426**	17°31.342'	N	82°21.397'	W	2696	OBIF	
M115_316-1	**OBS427**	17°28.668'	N	82°21.044'	W	2542	OBIF	
M115_317-1	**OBS428**	17°26.026'	N	82°20.705'	W	2195	OBIF	
M115_318-1	**OBS429**	17°23.342'	N	82°20.414'	W	2357	OBIF	
M115_319-1	**OBS430**	17°20.643'	N	82°20.082'	W	2284	OBIF	
M115_320-1	**OBS431**	17°17.944'	N	82°19.800'	W	1690	OBIF	
M115_321-1	**OBS432**	17°15.282'	N	82°19.455'	W	1344	OBIF	
M115_322-1	**OBS433**	17°12.572'	N	82°19.149'	W	1165	OBIF	
M115_323-1	**OBS434**	17°09.905'	N	82°18.835'	W	1252	OBIF	
M115_324-1	**OBS435**	17°07.212'	N	82°18.524'	W	1287	OBIF	
M115_325-1	**OBS436**	17°04.528'	N	82°18.196'	W	1154	OBIF	

Table 6.5 Ocean-bottom seismographs deployed along profile P4.

METEOR station	Gear Station	Latitude		Longitude		Depth in m	Type	Remarks
M115_375-1	**OBS501**	18°17.209'	N	80°38.998'	W	5239	UTIG	
M115_376-1	**OBS502**	18°16.888'	N	80°41.799'	W	4983	UTIG	
M115_377-1	**OBS503**	18°16.498'	N	80°44.634'	W	5171	GEOMAR	
M115_378-1	**OBS504**	18°16.166'	N	80°47.454'	W	4933	GEOMAR	
M115_379-1	**OBS505**	18°15.803'	N	80°50.297'	W	4904	GEOMAR	
M115_380-1	**OBS506**	18°15.625'	N	80°51.453'	W	4870	GEOMAR	
M115_381-1	**OBS507**	18°15.520'	N	80°52.525'	W	4676	GEOMAR	
M115_382-1	**OBS508**	18°15.393'	N	80°53.639'	W	5041	GEOMAR	
M115_383-1	**OBS509**	18°15.243'	N	80°54.786'	W	5047	GEOMAR	
M115_384-1	**OBS510**	18°15.083'	N	80°55.896'	W	5032	GEOMAR	
M115_385-1	**OBS511**	18°14.966'	N	80°57.015'	W	5293	GEOMAR	
M115_386-1	**OBH512**	18°14.786'	N	80°58.151'	W	5041	GEOMAR	no data
M115_387-1	**OBH513**	18°14.639'	N	80°59.275'	W	4761	GEOMAR	
M115_388-1	**OBS514**	18°14.492'	N	81°00.420'	W	4395	GEOMAR	
M115_389-1	**OBH515**	18°14.363'	N	81°01.514'	W	4174	GEOMAR	
M115_390-1	**OBH516**	18°14.221'	N	81°02.676'	W	3960	GEOMAR	
M115_391-1	**OBS517**	18°14.066'	N	81°03.803'	W	3862	GEOMAR	no data
M115_392-1	**OBH518**	18°13.925'	N	81°04.931'	W	3841	GEOMAR	
M115_393-1	**OBH519**	18°13.790'	N	81°06.058'	W	3787	GEOMAR	
M115_394-1	**OBS520**	18°13.641'	N	81°07.176'	W	4018	OBIF	
M115_395-1	**OBS521**	18°13.493'	N	81°08.295'	W	4121	OBIF	
M115_396-1	**OBS522**	18°13.353'	N	81°09.416'	W	3849	OBIF	
M115_397-1	**OBS523**	18°13.223'	N	81°10.522'	W	3576	OBIF	
M115_398-1	**OBS524**	18°13.068'	N	81°11.670'	W	3468	OBIF	
M115_399-1	**OBS525**	18°12.702'	N	81°14.481'	W	3571	UTIG	
M115_400-1	**OBS526**	18°12.333'	N	81°17.298'	W	3905	UTIG	
M115_401-1	**OBS527**	18°11.957'	N	81°20.109'	W	4083	UTIG	
M115_402-1	**OBS528**	18°11.591'	N	81°22.931'	W	4009	UTIG	

Table 6.6 Ocean-bottom seismographs deployed along profile P5.

METEOR station	Gear Station	Latitude		Longitude		Depth in m	Type	Remarks
M115_440-1	**OBS601**	18°06.640'	N	82°00.609'	W	4066	OBIF	
M115_441-1	**OBS602**	18°06.078'	N	82°04.520'	W	4066	OBIF	no data
M115_442-1	**OBS603**	18°05.577'	N	82°08.493'	W	2484	UTIG	
M115_443-1	**OBH604**	18°05.289'	N	82°10.422'	W	2468	GEOMAR	bad DPG, no data
M115_444-1	**OBS605**	18°05.023'	N	82°12.397'	W	3735	UTIG	
M115_445-1	**OBS606**	18°04.484'	N	82°16.349'	W	3410	UTIG	
M115_446-1	**OBS607**	18°03.952'	N	82°20.288'	W	3098	UTIG	
M115_447-1	**OBH608**	18°03.450'	N	82°24.210'	W	4188	GEOMAR	
M115_448-1	**OBH609**	18°02.921'	N	82°28.145'	W	4702	GEOMAR	
M115_449-1	**OBS610**	18°02.383'	N	82°32.056'	W	5062	GEOMAR	
M115_450-1	**OBH611**	18°01.800'	N	82°35.999'	W	4996	GEOMAR	

Table 6.7 Ocean-bottom seismographs deployed along profile P6.

METEOR station	Profile	No. Shots	date 1	time 1	Latitude 1		Longitude 1		date 2	time 2	Latitude 2		Longitude 2	
M115_179-1	**P01**	1307	04.04.15	22:02:00	17.0576	N	81.7410	W	05.04.15	19:48	18,9314	N	81,9314	W
M115_251-1	**P02**	701	09.04.15	12:53:00	18.4561	N	81.2670	W	10.04.15	00:13:00	18,3092	N	82,2579	W
M115_251-1	**P03**	734	08.04.15	22:45:00	18.4711	N	82.2604	W	09.04.15	10:39:00	18,6103	N	81,2877	W
M115_326-1	**P04**	1169	13.04.15	03:56:00	17.0784	N	82.2952	W	13.04.15	23:24:00	18,7119	N	82,4996	W
M115_403-1	**P05**	884	17.04.15	22:24:00	18.1777	N	81.5061	W	18.04.15	13:07:00	18,3002	N	80,5340	W
M115_451-1	**P06**	579	20.04.15	15:23:00	18.0172	N	82.6954	W	21.04.15	01:01:00	18,1232	N	81,9125	W

Table 6.8. Airgun operations during M115.

METEOR station	Profile	date 1	time 1	Latitude 1		Longitude 1		date 2	time 2	Latitude 2		Longitude 2	
M115_179-1	**P01**	04.04.15	22:02:00	17.0576	N	81.7410	W	05.04.15	19:48:00	18,9314	N	81,9314	W
M115_251-1	**P02**	09.04.15	12:53:00	18.4561	N	81.2670	W	10.04.15	00:13:00	18,3092	N	82,2579	W
M115_251-1	**P03**	08.04.15	22:45:00	18.4711	N	82.2604	W	09.04.15	10:39:00	18,6103	N	81,2877	W
M115_326-1	**P04**	13.04.15	03:56:00	17.0784	N	82.2952	W	13.04.15	23:24:00	18,7119	N	82,4996	W
M115_403-1	**P05**	17.04.15	22:24:00	18.1777	N	81.5061	W	18.04.15	13:07:00	18,3002	N	80,5340	W
M115_451-1	**P06**	20.04.15	15:23:00	18.0172	N	82.6954	W	21.04.15	01:01:00	18,1232	N	81,9125	W
M115_471-1	**Transit**	23.04.15	03:30:00	17.9350	N	81.9233	W	24.04.15	16:04:00	18,0522	N	75,6385	W

Table 6.9 Magnetic field measurements during M115.

7 Data and sample storage and availability

A Cruise Summary Report (CSR) is available at the Deutsches Ozeanographisches Datenzentrum, DOD (http://www.bsh.de/aktdat/dod/fahrtergebnis/2015/20150005.htm). The cruise was performed within territorial waters of the Cayman Islands / British jurisdiction. During transits data were collected in the waters of Jamaica. All data will be transferred to public databases and will be available two years after the cruise on 1st of May 2017. Table 8.1 lists the databases and responsible scientists.

Table 8.1: Data storage and availability

Type	Database	Available	Free Access	Contact
Bathymetry	www.bsh.de	Jan. 16	Jan. 16	bathymetrie@bsh.de
OBS data				
GEOMAR	PANGAEA	Nov. 16	May 17	igrevemeyer@geomar.de
OBIF	BODC	Jan. 16	May 17	christine.peirce@durham.ac.uk
UTIG	Seismic Portal	Nov. 16	May 17	harm@ig.utexas.edu
Gravity	BODC	Jan. 16	May 17	christine.peirce@durham.ac.uk
Magnetics	BODC	Jan. 16	May 17	christine.peirce@durham.ac.uk

PANGAEA: World Data Centre, Bremerhaven (htwww.pangaea.de)
BODC: British Oceanographic Data Centre (www.bodc.ac.uk/)
Seismic Portal: Seismic Portal of the Institute for Geophysics, Texas (www.ig.utexas.edu/sdc/)

8 Acknowledgements

We acknowledge the excellent and professional sea-going operations of the METEOR during M115, by Captain Rainer Hammacher and his crew. Furthermore, we acknowledge the assistance of Mark Maltby, installing the gravimeter and magnetometer in Kingston. Ship time has been funded by the Deutsche Forschungsgemeinschaft / German Science Foundation (DFG). In addition, German participants acknowledge funding from the DFG, supporting transportation, travelling and the operation of the PAM system. German OBSs were provided and funded by GEOMAR's OCEANS programme. The UK OBSs were provided by UK's Natural Environment Research Council's (NERC) Ocean-Bottom Instrumentation Facility (OBIF), the gravimeter and magnetometer were provided by NERC's National Marine Equipment Pool (NMEP). British participants acknowledge support from NERC under the grant NE/K/011162/1. USA participants acknowledge support from the National Science Foundation (NSF) under the grant OCE-1356895.

9 References

Baker, E. T., Y. J. Chen, J. Phipps Morgan, The relationship between near-axis hydrothermal cooling and the spreading rate of mid-ocean ridges, *Earth Planet. Sci. Lett*, *142*, 137-145, 1996.

Baker, E., C. German, On the global distribution of mid-ocean ridge hydrothermal vent-fields, *Geophys. Mono,, 148*, 245-266, 2004.

Blackman, D.K., J.P. Canales, A. Harding, Geophysical signatures of oceanic core complexes, *Geophys. J. Int., 178***,** 593–613, 2009

Canales, J.P., B.E. Tucholke, M. Xu, J.A. Collins, D.L. DuBois, Seismic evidence for large-scale compositional heterogeneity of oceanic core complexes, *G-cubed.,* 9, 2008

Cannat, M., D. Sauter, V. Mendel, E. Ruellan, K. Okino, J. Escartin, V. Combier, M. Baala, Modes of seafloor generation at a melt-poor ultraslow-spreading ridge, *Geology*, *34*(7), 605-608, 2006.

Cannat, M., D. Sauter, A. Bezos, C. Meyzen, E. Humler, M. Le Rigoleur, Spreading rate, spreading obliquity, and melt supply at the ultraslow spreading Southwest Indian Ridge, *G-cubed*, *9*, 26, 2008.

Dannowski, A., I. Grevemeyer, C.R. Ranero, G. Ceuleneer, M. Maia, J. Phipps Morgan, P. Gente, Seismic structure of an oceanic core complex at the Mid-Atlantic Ridge, 22°19' N, *J. Geophys. Res., 115*, B07106, doi:10.1029/2009JB006943, 2010

Dannowski, A., I. Grevemeyer, J. Phipps Morgan, C. R. Ranero, M. Maia, and G. Klein (2011), Crustal structure of the propagating TAMMAR ridge segment on the Mid-Atlantic Ridge, 21.5°N, Geochem. Geophys. Geosyst., 12, Q07012, doi:10.1029/2011GC003534.

deMartin, B.J., R.A. Sohn, J.P. Canales, S.E. Humphris, Kinematics and geometry of active detachment faulting beneath the Trans-Atlantic Geotraverse (TAG) hydrothermal field on the Mid-Atlantic Ridge, *Geology, 35*, 711-714, 2007.

DeMets, C., et al., Present motion and deformation of the Caribbean plate: Constraints from new GPS geodetic measurements from Honduras and Nicaragua, *GSA Special Paper*, *428*, 21-36, 2007.

Detrick, R.S., R.S. White, G.M. Purdy, Crustal structure of North Atlantic Fracture Zones, *Rev. Geophys., 31*, 439-458, 1993

Dick, H. J. B., J. Lin, H. Schouten, An ultraslow-spreading class of ocean ridge, *Nature*, *426*, 405-412, 2003.

Dick, J. B., et al., A long in situ section of the lower ocean crust: results of ODP Leg 176 drilling at the Southwest Indian Ridge. Earth and Planetary Science Letters 179, 31-51, 2000.

Collins, J.A., Blackman, D.K., Harris, A., Carlson, R.L., Seismic and drilling constraints on velocity structure and reflectivity near IODP hole U1309D on the central dome of Atlantis Massif, Mid-Atlantic Ridge 30◦N, *G-cubed., 10***,** 2009.

Edwards, R.A., Whitmarsh, R.B., Scrutton, R.A., The crustal structure across the transform continental margin off Ghana, eastern equatorial Atlantic, *J. Geophys. Res., 102*, 747–772, 1997.

Escartin, J., D. K. Smith, J. Cann, H. Schouten, C. H. Langmuir, S. Escrig, Central role of detachment faults in accretion of slow-spreading oceanic lithosphere, *Nature*, *455*, 790-795, 2008.

Escartín, J., C. Mével, C. J. MacLeod, A. M. McCaig, Constraints on deformation conditions and the origin of oceanic detachments: The Mid-Atlantic Ridge core complex at 15°45'N, *Geochemistry, Geophysics, Geosystems*, *4, 2003*.

Ewing, J., J. Antoine, M. Ewing, Geophysical Measurements in the Western Caribbean Sea and in the Gulf of Mexico, *J. Geophys. Res.*, *65, 1960*.

German, C. R., et al., Hydrothermal exploration of the Mid-Cayman Spreading Centre: Isolated evolution on Earth's deepest Mid-Ocean Ridge?, in *AGU Fall Meeting*, Session OS21B-08, 2009.

Greenroyd,C.J., C. Peirce, M. Rodger, A. B. Watts, R. W. Hobbs, Demerara Plateau – the structure and evolution of a transform passive margin, *Geophys. J. Int.,172*, 549–564, 2008.

Grevemeyer, I., W. Weigel, R.B. Whitmarsh, F. Avedik, G.A. Dehghani, The Aegir Rift: Crustal structure of an extinct spreading axis, *Mar. Geophys. Res., 19*, 1-23, 1997

Grevemeyer, I., W. Weigel, C. Jennrich, Structure and ageing of oceanic crust at 14°S on the East Pacific Rise, *Geophys. J. Int. 135*, 573-584, 1998

Grevemeyer, I., T.J. Reston, and S. Moeller, Microseismicity of the Mid-Atlantic Ridge at 7°S-8°15'S and at the Logatchev Massif oceanic core complex at 14°40'N-14°50'N, Geochem. Geophys. Geosyst., 14, 3532-3554, doi:10.1002/ggge.20179, 2013.

Holcombe, T. L., G. F. Sharman, Post-Miocene Cayman Trough evolution: a speculative model, *Geology*, *11*, 714-717, 1973.

Hyman, N.W., N.R. Grindlay, M.R. Perfit, P. Mann, Oceanic core complex development at the ultraslow spreading Mid-Cayman Spreading Centre, *G-cubed*, in press, 2011

Ildefonse, B., D. K. Blackman, B. E. John, Y. Ohara, D. J. Miller, C. J. MacLeod, Oceanic core complexes and crustal accretion at slow-spreading ridges, *Geology*, *35*, 623-626, 2007.

Karson, J. A., and P. J. Fox, Geological and geophysical investigation of the Mid-Cayman spreading centre: seismic velocity measurements and implications for the constitution of Layer 3, *Geophys. J. Astron. Soc.*, *85*, 389-412, 1986.

Karson, J. A., E. A. Williams, G. L. Früh-Green, D. S. Kelley, D. R. Yoerger, M. Jakuba, Detachment shear zone on the Atlantis Massif Core Complex, Mid-Atlantic Ridge 30°N, *G-cubed*, *7*, 2006.

Kelly, D. S. et al. An off-axis hydrothermal-vent field near the Mid-Atlantic Ridge at 30° N. *Nature 412*, 145-149, 2001.

Klein, E. M., C. H. Langmuir, Global correlations of ocean ridge basalt chemistry with axial depth and crustal thickness, *J. Geophys. Res.*, *92*, 8089-8115, 1987.

Leroy, S., A. Mauffret, P. Patriat, B. Mercier de Lepinay, An alternative interpretation of the Cayman Trough evolution from a re-identification of magnetic anomalies, *Geophys. J. Int. 141* 539-557, 2000.

Lomax, A., Virieux, A. J., Volant, P., Berge, C. 2000, Probabilistic earthquake location in 3D and layered models: Introduction of a Metropolis-Gibbs method and comparison with linear locations, in Advances in Seismic Event Location, pp. 101-134, eds. Thurber, C. H. and Rabinowitz, N., Kluwer, Amsterdam, 2000.

Mann, P., Overview of the tectonic history of northern Central America, *GSA Special Paper*, *428*, 1-19, 2007.

Michael, P.J., et al., Magmatic and amagmatic seafloor generation at the ultraslow-spreading Gakkel Ridge, Arctic Ocean: Nature, v. 423, p. 956-961, 2003.

Muller, M.R., Robinson, C.J., Minshull, T.A., White, R.S., Bickle, M.J.. Thin crust beneath Ocean Drilling Program borehole 735B at the Southwest Indian Ridge?, *Earth planet. Sci. Lett.,* 148, 93–107, 1997.

Peirce, C., Whitmarsh, R.B., Scrutton, R.A., Pontoise, B., Sage, F., Mascle, J., Cote d'Ivoire-Ghana margin: seismic imaging of passive rifted crust adjacent to a transform continental margin, *Geophys. J. Int., 125***,** 781–795, 1996.

Planert, L., E.R. Flueh, F. Tilmann, I. Grevemeyer, T.J. Reston, Crustal structure of a rifted oceanic core complex and its conjugate side at the MAR at 5°S: Implications for melt extraction during detachment faulting and core complex formation, *Geophys. J. Int., 181*, 113-126, doi: 10.1111/j.1365-246X.2010.04504.x, 2010.

Reid, I., H. R. Jackson, Ocean spreading rate and crustal thickness, *Mar. Geophys. Res.*, *5*, 165-172, 1981.

Reston, T.J., W. Weinrebe, I. Grevemeyer, E.R. Flueh, N.C. Mitchell, L. Kristein, C. Kopp, H. Kopp, participants of Meteor 47/2, A Rifted inside corner massif on the Mid-Atlantic Ridge at 5°S, *Earth Planet. Sci. Lett., 200,* 255-269,2002

Reston, T. J., and C. R. Ranero (2011), The 3-D geometry of detachment faulting at mid-ocean ridges, Geochem. Geophys. Geosyst., 12, Q0AG05, doi:10.1029/2011GC003666.

Reston, T.J., The structure, evolution and symmetry of the magma-poor rifted margins of the North and Central Atlantic: A synthesis, Tectonophysics 468, 6–27, 2009

Rosencrantz, E., R. I. Malcom, J. G. Sclater, Age and spreading history of the Cayman Trough as determined from depth, heat flow, and magnetic anomalies, , *J. Geophys. Res.*, *93*, 2141-2157, 1988.

Stroup, J. B., P. J. Fox, Geologic investigations in the Cayman Trough: Evidence for thin crust along the Mid-Cayman Rise, *J. Geol.*, *89*, 395-420, 1981.

ten Brink, U., D. Coleman, W. P. Dillon, The nature of the crust under Cayman Trough from gravity., *Mar. Petro. Geol.*, *19*, 971-987, 2002.

Yoshinobu, A. S., G. Hirth, Microstructural and experimental constraints on the rheology of partially molten gabbro beneath oceanic spreading centres, *J. Struct. Geol.*, *24*, 1101-1107, 2002.

Appendix 1

Installation and De-Installation of Gravimeter

The gravimeter was installed on 30th of April 2015 by Mark Maltby. The meter was locationed in the Gravimeter Room (Lab 12). The room had it's own air conditioning unit which was already set to provide a constant stable 20°C.

The gravimeter was installed on the wooden plinth in the gravimeter room. Power was provided from the red RFI protected sockets. On power up it was found that the bios had lost power so system time was set to GPS time and all bios setting were checked against the manufactures manual "Appendix F Bios Configuration". The Self Test, Clamp Meter and PreLevel routines where run successfully then the SEA_SysII software was started successfully. The control software counter was synchronized with the physical counter value indication on the sensor lid using the "Set Counter" routine. The meter was then unclamped and spring tension tracking enabled and the meter left to stabalise.

The GPS navigation feed that was provided comes from the ship's C-Nav 3050 GPS system, which is set up to deliver a UDP broadcast on the ships Network. The ships systems and electronic engineers used a Moxa to convert this broadcast into the required RS232 serial feed.

Beam Zero			**Beam Gain**		
Value	**Voltage**		**Value**	**Voltage**	
7.14	0.002		18.08	5.000	
Beam Scale Factor Check					
Initial Value	1.9917 (lab value)				
	Counter (cu)	**TC (cu)**	**QC Grav (mGals)**	**M Temp**	**M Pressure**
Still Reading	6828.2	2.4	6773.9	44.4	-0.92
Counter +50	6878.0	-46.6	6774.7	44.3	-0.93
Counter - 50	6778.2	52.5	6773.9	44.4	-0.92
Difference	99.8	99.1			
Final Value	1.9917 as TC difference is within 100 ±5%				

Tab. A1: Beam Zero, Gain and Scale Factor checks

The serial feed was initially set at the meters default baud rate setting of 4800, but it was found that as the feed contained all available NMEA GPS strings and not just the required RMC string the meter was buffering the serial feed and the update rate of the GPS feed into the software was erratic and quickly lagged. It was requested for the baud rate to be increased to 9600 in the MOXA and on the meter the settings were changed in the hardware configuration file ASII_HW.ini this solved the issue with the software then showing GPS time and position data refresh rate of 1Hz.

A Laptop with the "SEALOGGER" software installed was connected via a cross over serial cable to the data out port on the meter. This meant data could be logged remotely as well as locally on the meter for redundancy.

On 31st of April 2015 Beam Zero, Gain and Scale Factor checks were perform along with the required tie-in.

Gravimeter observations are non-absolute, being measured only with reference to other observations of the survey. In the case of marine surveys, observations made with the ship borne meter can be tied with a portable land gravimeter to absolute bases at ports of call. The process is done by first taking a set of land meter reading by the ship at a measured height above water level, second taking a set of land meter reading at the known absolute base station then third a second set of land meter reading by the ship at a measured height above water level. NMF then

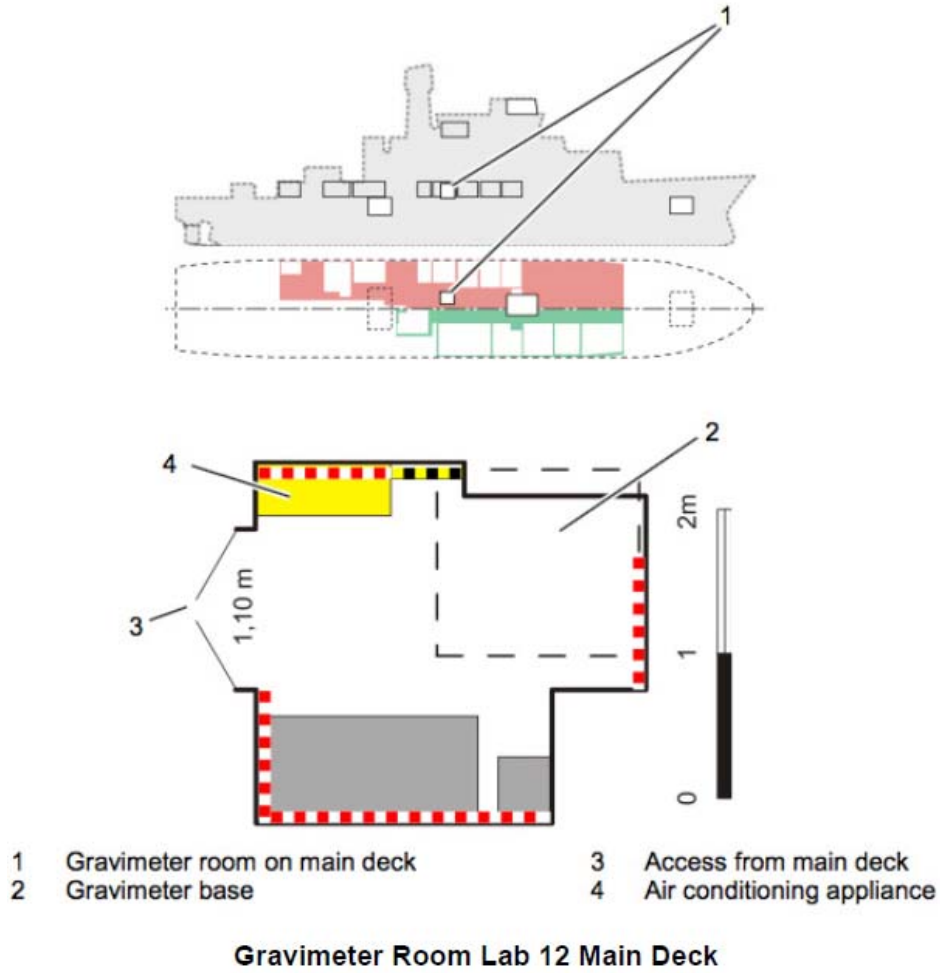

Fig. A1: Layout of the Gravimeter Lab on METEOR.

have a spreadsheet that these land gravimeter readings, Ship gravimeter reading and height above water level, absolute base station data and tidal data can then be input to calculate the tie-in / transfer of the absolute base station reference to the marine gravimeter. As in many ports of call most base stations around the world seem to have been established in the 1960 and 70's and many no longer exist due to building works etc. Kingston is such a place and the nearest known remaining base station on the island was found to be in Montego Bay ref ACIC 1030-0 IGB 04487A.

Mark Maltby and OBIC team member Andrew Clegg performed the tie-in. A set of land meter reading was taken at the shipside at South Terminal berth 4 Bollard 11 17 58.667N 076 49.813W taking the reading was difficult due to considerable vibrations through the quayside possibly from nearby operating machinery. Height above the water line was measured and

recorded. They were then transported by the ship's agent's driver to Montego Bay for the base station tie-in. The Latitude and Longitude of the base station taken in 1970 is only documented in degrees and whole minutes. This position places the base station outside Montego Bay so is too inaccurate to locate the position, so they went by the documentations description of the court house building and relied on the driver's local knowledge. They were taken to central downtown Montego Bay to the building locally known as the court house building which is now the Civic Hall and local museum. On arrival they walked around the outside of the building and couldn't recognise the building profile as in the base station description. After speaking to the building security guard and museum receptionist they were introduced to the museum curator. After stating why they were there and explaining that they couldn't pick out the detail in the description when walking around the outside of the building they were informed that the original wooden building burned down after 1970 (which is the date the base station was created) and the present building was rebuilt on the same footprint. Looking at the description against the building though there was no North entrance. On asking was there any other building that could be the court house they were told that this was the only building known as the court house. With this information it was decided to go ahead and take the reading offset from the center point of the Northern wall of the building. The reading was taken as measured from the center of the center window on the Northern wall 1.15m from the wall and 1.60m west towards the rear of the building, this lines up with the corners of the floor tiles.

Fig. A2: Picture of the Gravimeter room with meter installed on wooden plinth.

GPS location from the window was 18° 28.432' N 077° 55.383 W. Fig. A3 shows the diagram and photograph of the gravity tie location.

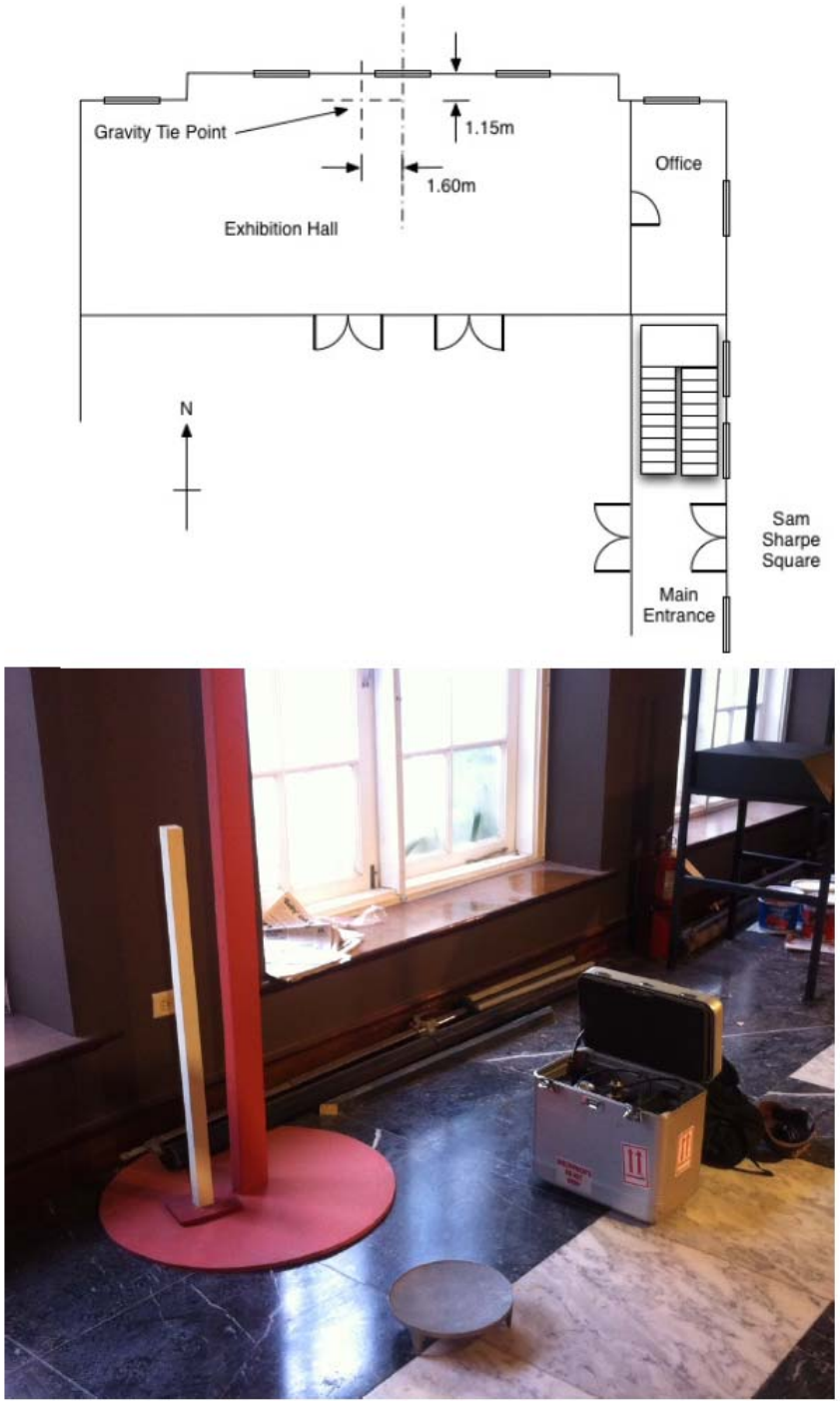

Fig. A3: Photo and Diagram of Gravity Tie location in Montego Bay

In Point-à-Pitre a second tie was obtained by Christine Peirce and Andrew Clegg at 16° 13.978’N / 61° 32.782’W.

GRAVITY BASE STATION

LATITUDE 18° 30'N (1)	STATION DESIGNATION MONTEGO BAY
LONGITUDE 77° 53'W (1)	
ELEVATION 3 METERS (1)	COUNTRY/STATE Jamaica
REFERENCE CODE NUMBERS: ACIC 1030-0; IGB 04487A	ADOPTED GRAVITY VALUE: g= 978 673.86 mgals
	ESTIMATED ACCURACY: ± 0.2 mgals; DATE: MONTH/YEAR 7/70

DESCRIPTION AND/OR SKETCH

The gravity station is in Montego Bay, at the Court House building, in downtown Montego Bay. Court House is located south of the court house square. Station is inside the building, one meter west of the main north entrance, in a corner, on a stone block surface.

(1)

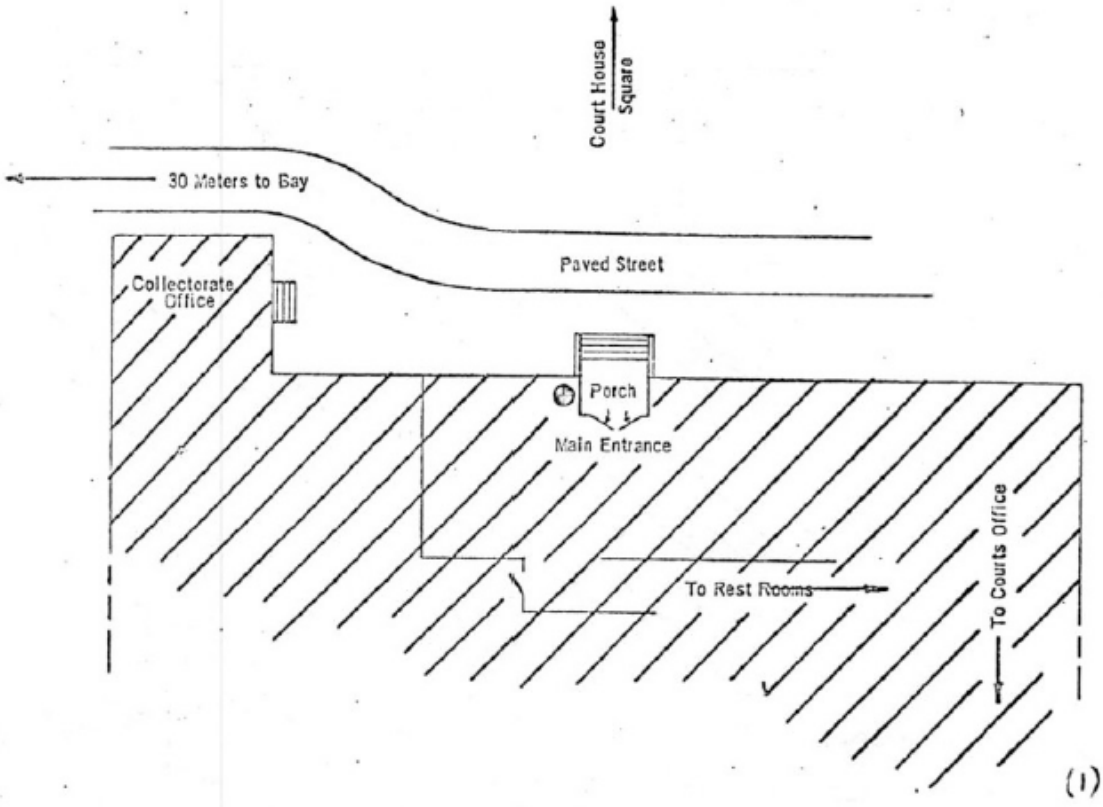

REFERENCE SOURCE

(1) 02752

ACIC HQ FORM FEB 69 0-415

Fig. A4: Gravity Tie in Montego Bay as defined in the 1970's

NMFD Gravitymeter Port Tie In Form

Ship: *Meteor* **Cruise:** *M115*

Principle Scientist: *C Peirce*

Details of Ship Fitted Gravity Meter:

Make: *Micro-g-Lacoste*
Type: *AirSea II*
Serial No: *S40*

Details of Land Gravity meter used for the tie in readings:

Make: LaCoste & Romberg
Type: *Model G*
Serial No: *G484*
Calibration factor (microgals / div): *1.02228*

Location where Tie In needs to be calculated:

Port: *Kingston*
Berth No:
Coordinates (Lat / Long): *17 58.667N 076 49.813W*

Location of Known Gravity Base Station:

ISGN Station No: *ACIC 1030-0 IGB 04487A*
Address: *Montego Bay*
Court House Building

Contact Person (If any):
Tel no. / e-mail:
Coordinates (Lat / Long): *18 28.432N 077 55.383W*

Absolute gravity value in milliGals: *978673.86*

Comments:

Readings Page

Date: 31/03/15 **Julian Day No:** 121

First set of readings on quay wall adjacent to ship:

Counter Reading 1:	2046.2	**@ time:**	15:26
Counter Reading 2:	2046.3	**@ time:**	15:28
Counter Reading 3:	2046.0	**@ time:**	15:29
Counter Reading 4:		**@ time:**	
Counter Reading 5:		**@ time:**	

Height of Gravity Meter above water level (h1): 2.02 **meters**

Set of readings at the known base station:

Counter Reading 1:	2124.5	**@ time:**	20:34:50
Counter Reading 2:	2124.6	**@ time:**	20:36:30
Counter Reading 3:	2124.6	**@ time:**	20:39:45
Counter Reading 4:		**@ time:**	
Counter Reading 5:		**@ time:**	

Second set of readings on quay wall adjacent to ship:

Counter Reading 1:	2046.3	**@ time:**	02:11
Counter Reading 2:	2046.2	**@ time:**	02:35
Counter Reading 3:	2046.3	**@ time:**	02:37
Counter Reading 4:	2046.2	**@ time:**	02:38
Counter Reading 5:		**@ time:**	

Height of Gravity Meter above water level (h2): 2.13 **meters**

Height of ships GM above static water line (h3): 3.23 **metres**

Digital Gravity Reading shown on ships GM display: 6773.9 **02:42**

Calculations page

Tidal Calculations: (Obtain (a),(b) and (d) below from UK Hydrographic tables)

Height of last Low Water (a):	*0.30* metres
Height of next High Water (b):	*0.40* metres
Tidal Range (c):	*0.10* metres
Height of tide above LW at average time of readings (d):	*0.39* metres
Height of tide above mean sea level ((d-c/2) =e):	*0.34* metres
Average height of Land GM above waterline ((h1+h2)/2=f):	*2.08* metres
Average height of Land GM above mean sea level (e + f =g):	*2.42* metres
Difference in height between Land GM and Ship GM (f - h3):	*-1.16* metres
Free Air corrected value for height difference (0.31 x (f-h3)):	*-0.36* metres

---

Average of the first set of quay wall readings (S1);	*2046.2* Counter divs
Average of the second set of quay wall readings (S2):	*2046.2* Counter divs
Average of the Known base station readings (S3):	*2124.5* Counter divs
Difference in minutes between first and second sets of quay wall readings (ST2 - ST1):	*665.0* Mins
Drift of Land GM ((S1-S2)/ST2-ST1 = k):	*-0.0001* divs/min
Difference in minutes between Known Base station readings and first quay wall readings (ST3):	*308.0* Mins
Corrected quay wall reading at the time of Base station reading: (S1 + (ST3 x k)=m):	*2046.1* Counter divs
Difference between quay wall reading and known base (S2-m-S3 =N):	*-78.4* Counter divs
Converted value (calibration factor x N):	*-80.2* milliGals

Absolute value at the quay wall (Known value + converted value): ***978593.69*** **milliGals**

Absolute value at ships GM (abs. quay wall value + free air corrected value): ***978593.33*** **milliGals**

NMFD Gravitymeter Port Tie In Form

Ship: *Meteor* **Cruise:** *M115*

Principle Scientist: *C Peirce*

Details of Ship Fitted Gravity Meter:

Make: *Micro-g-Lacoste*
Type: *AirSea 2*
Serial No: *S40*

Details of Land Gravity meter used for the tie in readings:

Make: LaCoste & Romberg
Type: *Model G*
Serial No: *G484*
Calibration factor (microgals / div): *1.02228*

Location where Tie In needs to be calculated:

Port: *Pointe-a-Pitre Cruise Terminal*
Berth No: *3 or 4*
Coordinates (Lat / Long): *16^14.158N, 61^32.322W*

Location of Known Gravity Base Station:

ISGN Station No: *ISGN71*
Address: *Pointe-a-Pitre West Side*

Contact Person (If any):
Tel no. / e-mail:
Coordinates (Lat / Long): *16^13.978N, 61^32.782W*

Absolute gravity value in milliGals: *978542.78*

Comments:

Readings Page

Date: *27/04/2015* **Julian Day No:** *117*

First set of readings on quay wall adjacent to ship:

Counter Reading 1:	*2011.8*	**@ time:**	*23:51*
Counter Reading 2:	*2011.8*	**@ time:**	*23:52*
Counter Reading 3:	*2011.7*	**@ time:**	*23:53*
Counter Reading 4:	*2011.8*	**@ time:**	*23:54:00*
Counter Reading 5:	*2011.8*	**@ time:**	*23:55:00*

Height of Gravity Meter above water level (h1): *1.68* **meters**

Set of readings at the known base station:

Counter Reading 1:	*2009.2*	**@ time:**	*00:25:00*
Counter Reading 2:	*2009.1*	**@ time:**	*00:26:00*
Counter Reading 3:	*2009.2*	**@ time:**	*00:27:00*
Counter Reading 4:	*2009.2*	**@ time:**	*00:27:00*
Counter Reading 5:	*2009.2*	**@ time:**	*00:28:00*

Second set of readings on quay wall adjacent to ship:

Counter Reading 1:	*2011.8*	**@ time:**	*00:52*
Counter Reading 2:	*2011.7*	**@ time:**	*00:54*
Counter Reading 3:	*2011.8*	**@ time:**	*00:55*
Counter Reading 4:	*2011.8*	**@ time:**	*00:56*
Counter Reading 5:	*2011.7*	**@ time:**	*00:56*

Height of Gravity Meter above water level (h2): *1.78* **meters**

Height of ships GM above static water line (h3): *2.93* **metres**

Digital Gravity Reading shown on ships GM display: *6471.4*

Calculations page

Tidal Calculations: (Obtain (a),(b) and (d) below from UK Hydrographic tables)

Height of last Low Water (a):	0.40 metres
Height of next High Water (b):	0.60 metres
Tidal Range (c):	0.20 metres
Height of tide above LW at average time of readings (d):	0.50 metres
Height of tide above mean sea level ((d-c/2) =e):	0.40 metres
Average height of Land GM above waterline ((h1+h2)/2=f):	1.73 metres
Average height of Land GM above mean sea level (e + f =g):	2.13 metres
Difference in height between Land GM and Ship GM (f - h3):	-1.20 metres
Free Air corrected value for height difference (0.31 x (f-h3)):	-0.37 metres

---

Average of the first set of quay wall readings (S1);	3352.9 Counter divs
Average of the second set of quay wall readings (S2):	2514.7 Counter divs
Average of the Known base station readings (S3):	3348.6 Counter divs
Difference in minutes between first and second sets of quay wall readings (ST2 - ST1):	665.0 Mins
Drift of Land GM ((S1-S2)/ST2-ST1 = k):	1.2605 divs/min
Difference in minutes between Known Base station readings and first quay wall readings (ST3):	308.0 Mins
Corrected quay wall reading at the time of Base station reading: (S1 + (ST3 x k)=m):	3741.2 Counter divs
Difference between quay wall reading and known base (S2-m-S3 =N):	392.6 Counter divs
Converted value (calibration factor x N):	401.3 milliGals

Absolute value at the quay wall
(Known value + converted value): **978944.11** **milliGals**

Absolute value at ships GM
(abs. quay wall value + free air corrected value): **978943.74** **milliGals**

Appendix 2

Report on Marine Mammal Observation

Seiche Limited
Bradworthy Industrial Estate
Langdon Road, Bradworthy
Holsworthy, Devon EX22 7SF
United Kingdom
Tel: +44 (0) 1409 404050
Email: info@seiche.com
Web: www.seiche.com

Seiche Limited
10355 Centrepark Dr
Suite 240
Houston TX77043
United States of America
Tel: +1 713 201 5726
Email: info@seiche.com
Web: www.seiche.com

Marine Mammal Observer Report
M115 CaySeis Survey

Prepared for:
GEOMAR Helmholz Centre for Ocean Research
Kiel, Germany

Prepared by:
Seiche Limited
Rebecca Snyder
Contact E-mail: r.snyder@seiche.com

01 April to 28 April 2015

TABLE OF CONTENTS

1. EXECUTIVE SUMMARY 1
2. INTRODUCTION 2
2.1. Project Location and Operational Parameters 2
2.2. Regulatory Framework 3
3. MITIGATION REQUIREMENTS 4
3.1. Mitigation Zone 4
3.2. Soft Start 4
3.3. Soft Start Delay 4
4. OBSERVER METHODOLOGY 5
4.1. Visual Monitoring 5
4.2. Passive Acoustic Monitoring 6
4.2.1. Passive Acoustic Monitoring Equipment 7
4.2.2. Deployment 7
4.2.3. *PAMGUARD* Configuration 8
5. SEISMIC SOURCE OPERATIONS 11
6. MONITORING EFFORT 13
6.1. Visual Monitoring 13
6.1.1. Weather Conditions 13
6.2. Acoustic Monitoring 15
7. WILDLIFE SUMMARY 17
7.1. Marine Mammal Detections 17
7.1.1. Visual Detections 17
7.1.2. Acoustic Detections 17
7.2. Other Notable Wildlife 17
8. MITIGATION ACTION SUMMARY 18
9. ACKNOWLEDGEMENTS 19
10. REFERENCES 20

LIST OF FIGURES

Figure 1: CaySeis survey area showing the location of each of the six active profiles (identified as P1, P2, P3, P4, P5, and P6) and the approximation position of OBS (black circles) deployed along each profile. 2
Figure 2: 5th superstructure deck on the Meteor, with detailed images of the port (top right) and starboard (bottom right) observation areas. 5
Figure 3: Acoustic monitoring station in laboratory 9 on the Meteor. 6
Figure 4: Hydrophone cable deployed off the stern of the Meteor. 7
Figure 5: PAMGUARD spectrogram display, showing a low (bottom) and mid frequency (top) spectrogram panels. 9
Figure 6: PAMGUARD spectrogram display with dolphin whistles that have been detected by the whistle and moan detector as evidenced by the color overlays. 9
Figure 7: PAMGUARD click detector display with detected sperm clicks from multiple individuals on the amplitude/time display (top), click waveform (bottom left), click spectrum (bottom second from left), trigger threshold window (bottom second from right), and Wigner plot (bottom right) 10
Figure 8: Source activity throughout the CaySeis survey 11
Figure 9: Summary of airgun operations while the source was active. 12
Figure 10: Visual monitoring effort while the source array was active and inactive. 13
Figure 11: Rain shower activity during visual monitoring. 14
Figure 12: Beaufort wind force during visual monitoring. 14
Figure 13: Sea surface conditions during visual monitoring. 15
Figure 14: Swell during visual monitoring. 15
Figure 15: Acoustic monitoring effort while the source array was active and inactive 16
Figure 16: Avifauna observed during the CaySeis survey, including barn swallow (A), gray kingbird (B), brown booby (C), cattle egret (D), and merlin (E). 17

1. EXECUTIVE SUMMARY

Three institutions, GEOMAR Helmholz Centre for Ocean Research, the University of Durham, and the University of Texas collaborated to conduct the CaySeis survey in the Caribbean Sea, along the Cayman Trough from 01 through 28 April 2015. During this period, active and passive seismic data were acquired through the use of ocean bottom seismometers and an airgun array (active portion).

Visual and acoustic marine mammal observations were conducted during the survey as directed by the Cayman Island's Department of the Environment, which required operations to be conducted under the Joint Nature Conservation Committee's guidelines for seismic operations.

Visual monitoring was conducted for 236 hours 54 minutes, while acoustic monitoring, which took place only during the period immediately preceding soft start, was conducted for 5 hours 49 minutes. The majority of the monitoring effort, both visual and acoustic, took place while the source (airgun) array was inactive and corresponded to periods of OBS deployment and recovery. The source array was active for 92 hours 21 minutes.

Marine mammals were visually detected on two occasions, bottlenose dolphin on 07 April and unidentified blackfish during the transit on 25 April. Mitigation actions were not required during either detection. Marine mammals were not detected acoustically during the survey.

2. INTRODUCTION

2.1. PROJECT LOCATION AND OPERATIONAL PARAMETERS

The CaySeis survey was conducted in the Cayman Trough of the Caribbean Sea between 01 and 28 April 2015, as a collaborative effort by three institutions, GEOMAR Helmholz Centre for Ocean Research Kiel, the University of Durham in conjunction with the Ocean Bottom Instrumentation Consortium (OBIC), and the University of Texas Institute of Geophysics (UTIG). The team of scientists utilized both active and passive ocean bottom seismometers (OBS) to study the crustal and upper mantle structure of the Cayman Trough and to record natural, local seismic activity.

The active portion of the survey, which utilized an airgun array as the sound source was conducted along six profiles, two north/south profiles and four east/west profiles (Figure 1). Active OBS were deployed along each profile before conducting the active survey and were recovered upon the completion of each profile. Passive OBS were deployed throughout the survey area upon at the start of the CaySeis survey and remained deployed throughout the majority of the survey, with some units recovered before completing the final two profiles.

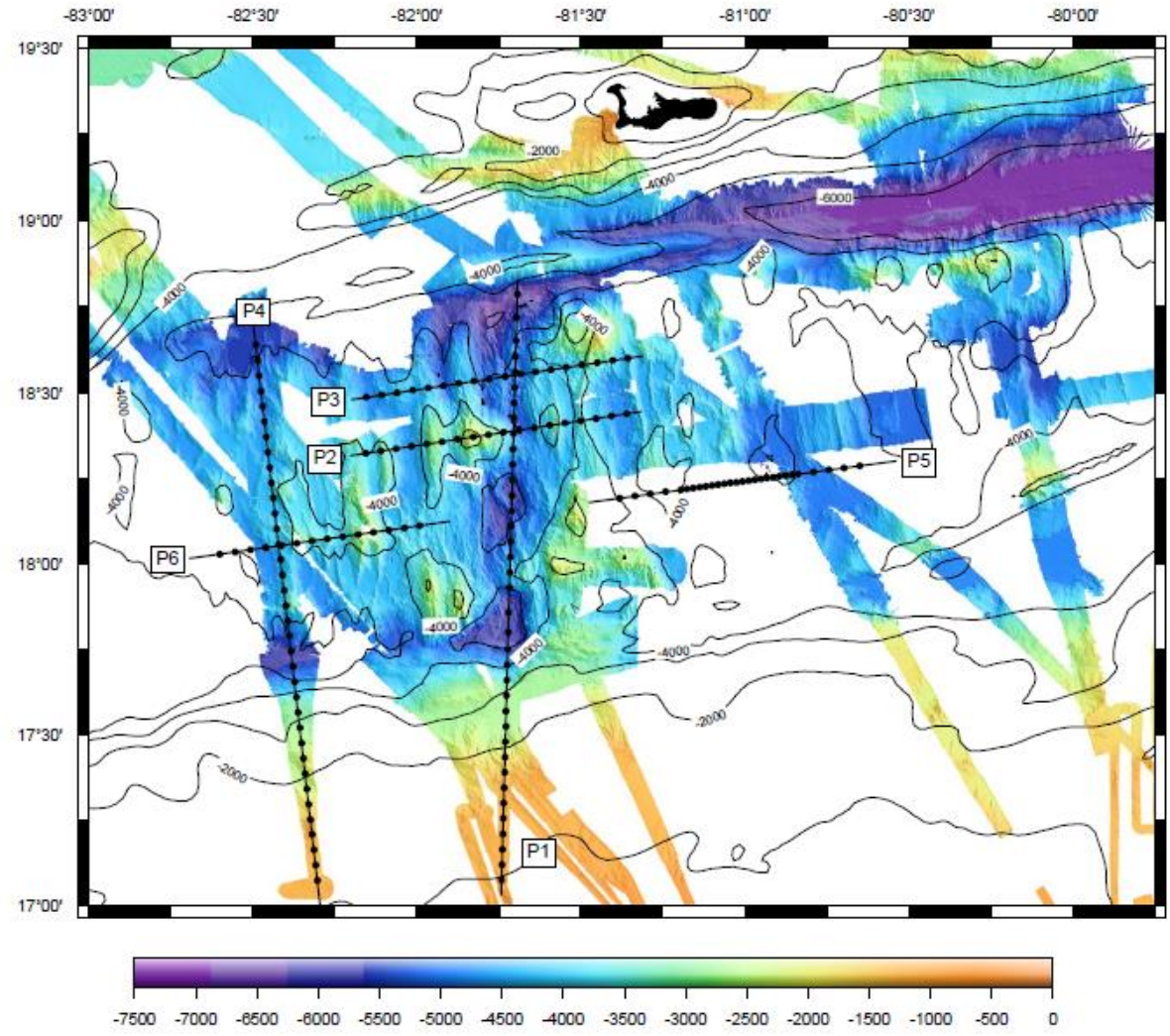

Figure 1: CaySeis survey area showing the location of each of the six active profiles (identified as P1, P2, P3, P4, P5, and P6) and the approximation position of OBS (black circles) deployed along each profile. Water depth in meters is represented by the color scale key. Map provided courtesy of GEOMAR.

A single vessel, the research vessel *Meteor* was used to conduct the CaySeis survey. The *Meteor* is approximately 98 meters long, with accommodation for 35 crew and 28 scientists.

The sound source used for the survey was a 12 airgun, 5440 in^3 array. The source array consisted of two sub-arrays, each with six airguns ranging in volume from 250 in^3 to 520 in^3. The estimated source level of the array was 51.7 bar meters (peak to peak) and the frequency ranged from 2 to 75 Hertz. The airgun array was deployed approximately 80 meters astern of the *Meteor* and towed at a depth of approximately 7.5 meters.

The airgun array was deployed approximately 90 minutes prior to the start of each profile and was recovered shortly after the completion of each profile. The only exception was during the line change between profiles 2 and 3, during which data was collected during the turn and the airguns remained deployed and active. The source array was activated every 60 seconds or about every 150 meters.

OBS units were deployed and recovered during the periods in between profiles, with deployments taking roughly a day to complete and recovery approximately two days on average. During these periods, the vessel would often undergo multiple direction changes and would traverse the area at variable speeds.

2.2. REGULATORY FRAMEWORK

Under the jurisdiction of the Cayman Island's Department of the Environment, the *Joint Nature Conservation Committee (JNCC) guidelines for minimizing the risk of injury and disturbance to marine mammals from seismic surveys* (*JNCC Guidelines*) was used as for the mitigation and monitoring protocol for the CaySeis survey.

3. MITIGATION REQUIREMENTS

The main purposes of the vessel-based monitoring program was to ensure that provisions of the *JNCC Guidelines* were satisfied with respect to mitigation, disturbances to marine mammals were minimized, and marine mammal observations during the survey were documented.

The primary purposes of the monitoring and mitigation program are:

Monitoring: Visual and/or acoustic observations to determine whether marine mammals are present inside the 500 metre mitigation zone and document behaviors as best as practically possible.

Mitigation: An action or activity implemented to minimize the risk of a potential impact occurring to a marine mammal observed or detected inside the 500 metre mitigation zone for example: seismic source array soft start procedure and delay to the start a sound source as per the *JNCC Guidelines*.

The following mitigation measures were adopted for visual and acoustic monitoring for marine mammals during the CaySeis survey. The mitigation measures implemented included:

- mitigation zone,
- soft start procedures, and
- soft start delay procedures.

3.1. MITIGATION ZONE

A 500 metre mitigation zone was implemented around the center of the seismic source (airgun) array and was monitored for the presence or absence of marine mammals by a marine mammal observer (MMO). The mitigation zone was monitored both visually and/or acoustically depending on visibility (only acoustically if during reduced visibility, such as at night and during period of heavy rain, fog, or large swells) prior to soft start and visually during profiles. Additionally, the entire visible area was monitored by a MMO during the deployment and recovery of OBS during daylight hours.

3.2. SOFT START

The intent of soft start is to warn marine mammals in close proximity to a source array of pending fully active seismic source operations and to allow sufficient time for those animals to leave the immediate vicinity. Under normal conditions, animals sensitive to these activities are expected to move away from an activated source array.

When required, soft start began with the smallest airgun in the array (250 in^3). Airguns were added in a sequence such that the sound source level of the array gradually increased over a minimum 20 minute period until the full output of the array was reached.

3.3. SOFT START DELAY

Prior to initiating the seismic source, the mitigation zone was visually and acoustically monitored for the presence of marine mammals for a minimum of 60 minutes during daylight hours with good visibility and acoustically monitored for a minimum of 60 minutes during periods of reduced visibility when the 500 metre mitigation zone could not be monitored visually (darkness, fog, heavy rain, and large swells).

If marine mammals were detected within the safety zone either visually and/or acoustically, soft start was delayed until 20 minutes had elapsed from the last visual or acoustic detection of marine mammals in the mitigation zone.

4. OBSERVER METHODOLOGY

4.1. VISUAL MONITORING

Visual observations for marine mammals were conducted by JNCC trained MMOs during daylight hours with good visibility using both the naked eye and binoculars of 7 times magnification. Observations were conducted from the 5th superstructure deck (Figure 2) approximately 16 meters above the sea surface.

Figure 2: 5th superstructure deck on the *Meteor*, with detailed images of the port (top right) and starboard (bottom right) observation areas. Photo on left credit to Steffen Sanstrup.

Distance to observed marine species was estimated by using a range stick. Species were identified based upon physical characteristics and behaviors. Identification was facilitated by consulting relevant field guides or by observer experience.

Upon making a visual detection, the MMO determined whether the presence of the marine species immediately warranted a mitigation action. The MMO maintained visual contact with the animal until the marine mammal could no longer be observed, whether because the animal sounded or the distance at which the MMO could maintain visual contact had been exceeded. Mitigation actions were implemented when appropriate and were made through the bridge office on duty or to the chief scientist by the intra-vessel phone system or direct verbal communications. Notes on the detection, such as behavior of the animal, distance to the animal from the seismic source, bearing to the animal, animal direction of travel, number of individuals, etc. were maintained by the MMO throughout their monitoring shift using print outs of the data forms or field notebooks. Details on operations, vessel position, and weather conditions are also recorded during the monitoring shift. All data were recorded electronically in the *JNCC Marine Mammal Recording Forms* spreadsheet.

Monitoring began no less than 60 minutes prior to the start of soft start and continued until seismic operations ceased or sighting conditions no longer allowed for observation of the sea surface (darkness, fog, rain, etc.). Monitoring also took place between all profiles, during OBS deployment and recovery; however monitoring did not take place during the transits between Jamaica and the survey site and between the survey site and Guadeloupe.

Monitoring shifts were established such that one of the two MMOs onboard was observing for marine

mammals at all times during daylight hours with good visibility. Each MMO monitored for no more than three consecutive hours (exception being for pre-soft start monitoring periods when two MMOs were on watch – one visual and one acoustic).

4.2. PASSIVE ACOUSTIC MONITORING

Acoustic monitoring for marine mammals was conducted by trained MMOs during all pre-soft start monitoring periods. The passive acoustic monitoring (PAM) system consisted of a hydrophone array cable with a single embedded hydrophone, a deck cable, an electronics processing unit, two laptop computers equipped with an acoustic analysis package, and headphones (Figure 3). *PAMGUARD* is the standard acoustic analysis package included with the system, but the *International Federation for Animal Welfare* (*IFAW*) software was provided as an alternative if required. Acoustic monitoring was conducted from laboratory 9 on the main deck of the *Meteor*.

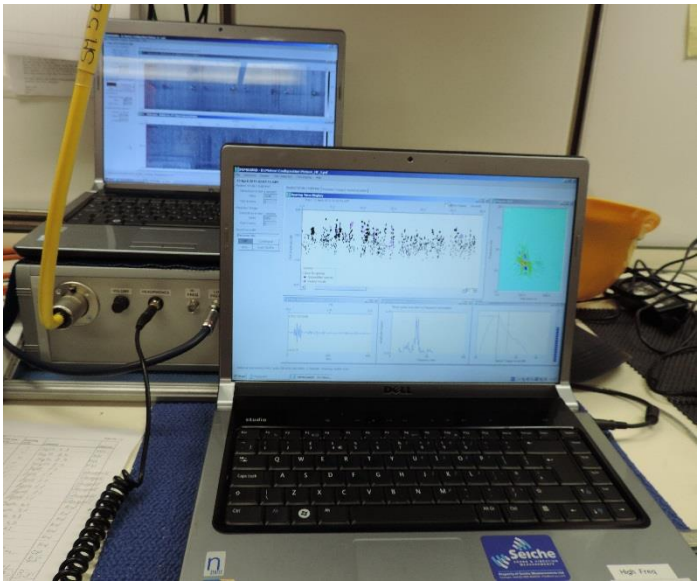

Figure 3: Acoustic monitoring station in laboratory 9 on the *Meteor*.

During an acoustic monitoring shift, the MMO aurally monitored the signal from the hydrophone while monitoring pertinent visualization modules in *PAMGUARD*. Upon making an acoustic detection of marine mammal vocalizations, the MMO determined whether the detection immediately warranted a mitigation action based upon the frequency component of the vocalization or through a subjective rating of signal amplitude. The MMO continued to monitor for vocalizations until vocalizations were no longer detected aurally and/or visually in *PAMGUARD*.

Mitigation actions were implemented when appropriate and were made direct to the bridge officer on duty or to the chief scientist by the intra-vessel phone system or direct verbal communications. Audio recordings of marine mammal detection events were collected, as well as screen images of the *PAMGUARD* visualization modules. Notes on the detection including vocalization type, frequency, amplitude, duration, etc., as well as other notable events or observations were maintained by the MMO throughout their monitoring shift in a notebook and later transcribed into an electronic log and associated data forms. Details on operations, vessel position, and weather conditions are also recorded during the monitoring shift.

Range estimates were obtained by using a subjective scale based on signal amplitude, with high amplitude signals presumed to be closer than lower amplitude signals. As only a single hydrophone element was contained within the array, details on bearings to vocalizing marine mammals were not

obtained and therefore could not be used to provide more accurate range estimates.

Monitoring began no less than 60 minutes prior to the start of soft start (daylight and reduced visibility) and continued until soft start began.

4.2.1. Passive Acoustic Monitoring Equipment

The PAM system used on the CaySeis survey was designed and manufactured by Seiche Limited from Bradworthy, Devon, England. The system consisted of hydrophone array cable with a single embedded hydrophone, a deck cable, an electronics processing unit, two laptop computers with an acoustic analysis package, and headphones.

The hydrophone array was 100 meters in length and contained one broadband hydrophone element, with a frequency response (3 dB points) of 5 Hertz to 150 kilohertz. The frequency range provided for the hydrophone element represented the flat response of the hydrophone between the two 3 dB points. The 3 dB points are the frequency at which the power output has been reduced by half the maximum output. Although the minimum and maximum frequencies were set to 5 Hertz and 150 kilohertz the hydrophones were sensitive to vocalizations below the minimum frequencies and above the maximum frequency. Hydrophone sensitivity was -157dB re 1V/µPa.

The 100 m deck cable was used as an interface between the hydrophone array cable and the acoustic monitoring station. The interface thus allows for nearly the full length of the hydrophone cable to be deployed.

The electronics processing unit contained two external sound cards used for sampling the raw audio from the hydrophones. Power to the hydrophone array is also provided by the electronics processing unit. One sound card, the National Instruments DAQ card, was used to sample audio up to 500 kilohertz while the second sound card, ASIO4All, is used to sample audio at 48 kilohertz. Use of the two sound cards allows for audio to be sampled at rates consistent with low, mid, and high frequency cetacean vocalizations.

4.2.2. Deployment

Approximately 80 meters of the hydrophone array was deployed directly off the stern of the *Meteor*. The cable was hand-deployed from a spool that was supported by a frame and secured to the main deck. While deployed, the hydrophone cable was positioned in between the two airgun sub-arrays (Figure 4). The magnetometer cable was also deployed between the airgun sub-arrays.

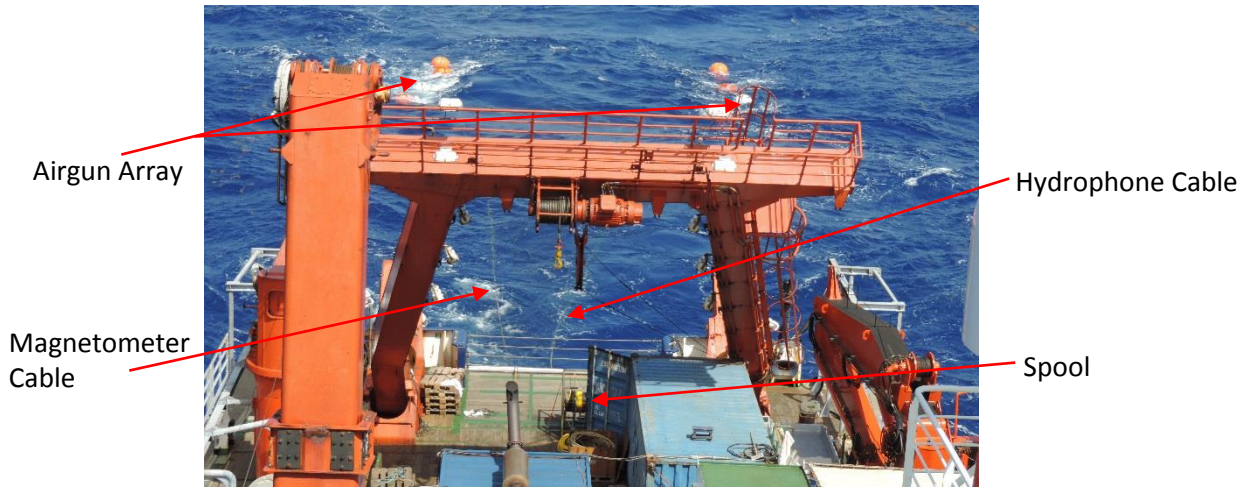

Figure 4: Hydrophone cable deployed off the stern of the Meteor.

Due to the location near the stern of the vessel, the potential for masking of cetacean vocalizations did exist particularly in relation to low frequency vessel noise.

4.2.3. *PAMGUARD* Configuration

PAMGUARD is an open source software program for passive acoustic monitoring developed with the support from the OGP E&P Sound and Marine Life Program. The software can be configured by the user to meet any specific project requirements. The user can add in various modules that will allow for visualization of the raw and/or filtered signal from the hydrophone, implementation of detectors for tonal and pulsed vocalizations, permit recording of raw or filtered audio, and provide tracking and localization capabilities when using multiple hydrophones.

The PAM system was configured to monitor for low, mid, and high frequency cetacean vocalizations. Two click detectors were incorporated, one for low/mid frequency clicks produced by delphinids, beaked whales, and sperm whales and one for high frequency clicks produced by delphinids, *Kogia*, phocoenids, and beaked whales. General classifiers for beaked whales, phocoenids, and *Kogia* were included in the high frequency click detector. Click waveforms, spectrums, and Wigner plots were also available through the click detector for further analysis and potential identification/confirmation of cetacean group or in some cases species.

Two tonal detectors or whistle and moan detectors were also incorporated to the *PAMGUARD* configuration. One whistle and moan detector was configured to detect low frequency tonal calls from baleen whales and the second was configured to detect low/mid frequency whistles. The detectors do often mark non-biological sources as clicks and/or tones, so it was important that an operator maintain focus while monitoring. Two spectrogram displays were incorporated to cover the wide range of frequencies used by marine mammals.

Further details on the various *PAMGUARD* modules are provided below.

4.2.3.1. Spectrogram

Spectrograms provide information on frequency and amplitude of the acoustic signals received by the hydrophone element. The *PAMGUARD* settings file developed for the CaySeis survey contained two spectrogram displays, each configured for the detection of cetacean vocalizations within different frequency ranges. One spectrogram was configured for low frequency baleen whale vocalizations (up to 3 kilohertz) and one for mid frequency sperm whale and delphinid vocalizations (up to 24 kilohertz; Figure 5).

The two spectrograms utilized a Hanning window FFT (fast Fourier transform, algorithm used for signal processing and spectrogram visualization) lengths of 2048, with 50% hop and were set to a window length of 20 seconds.

The amplitude range was adjusted as necessary to maximize the operator's ability to detect marine mammal vocalizations over background noise present with the minimum amplitude set between 50 and 70 dB and the maximum amplitude set between 150 and 200 dB.

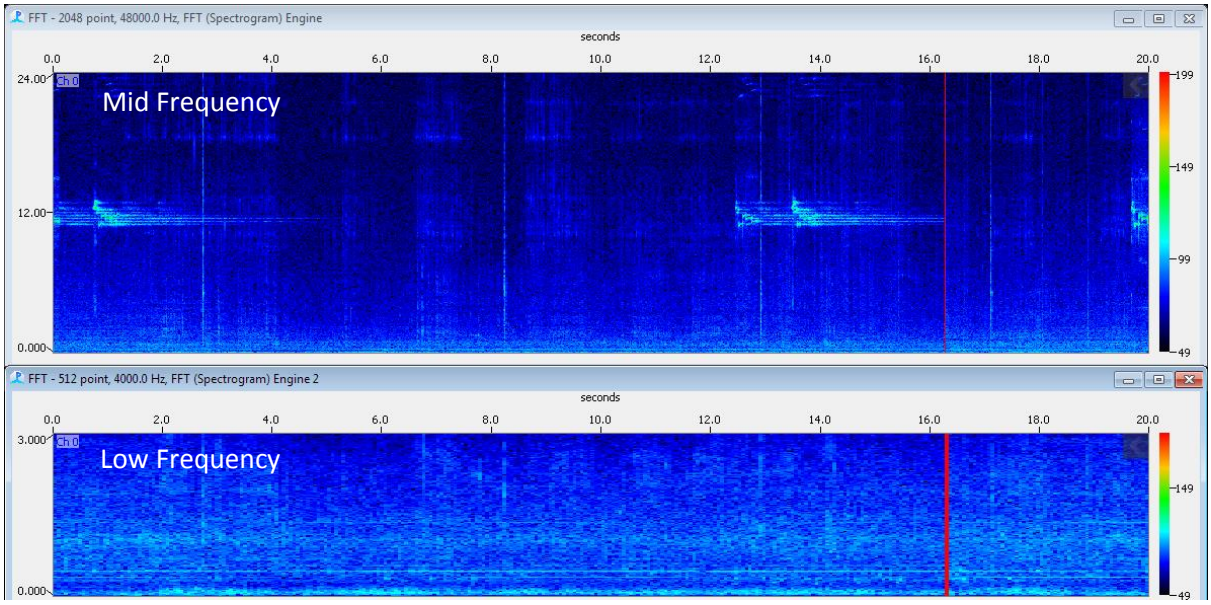

Figure 5: *PAMGUARD* spectrogram display, showing a low (bottom) and mid frequency (top) spectrogram panels.

4.2.3.2. Whistle and Moan Detector

The whistle and moan detector was configured to automatically detect tonal sounds, including baleen whale calls and delphinid whistles, from FFT spectrogram engine noise free FFT data. The detector processed the spectrogram to remove noise, establish thresholds, create binary maps of the regions above the threshold, and connect the regions of the binary map to create sounds. Two separate whistle and moan detectors were used for the detection of low and mid frequency tonal vocalizations.

With the proper spectrogram overlays, detected tonal sounds were highlighted with various color contour overlays (Figure 6). The detectors were configured to search for and connect tones along the all sides and diagonals, thus increasing the probability of detecting tonal sounds. However using 8 tries to connect instead of 4 also increased the number of false detections. False detections were ruled as such by the operator. The low frequency moan detector was set to search for tonal sounds between 5 Hertz and 3 kilohertz, while the mid frequency whistle detector was set to search for tonal sounds between 3 and 24 kilohertz.

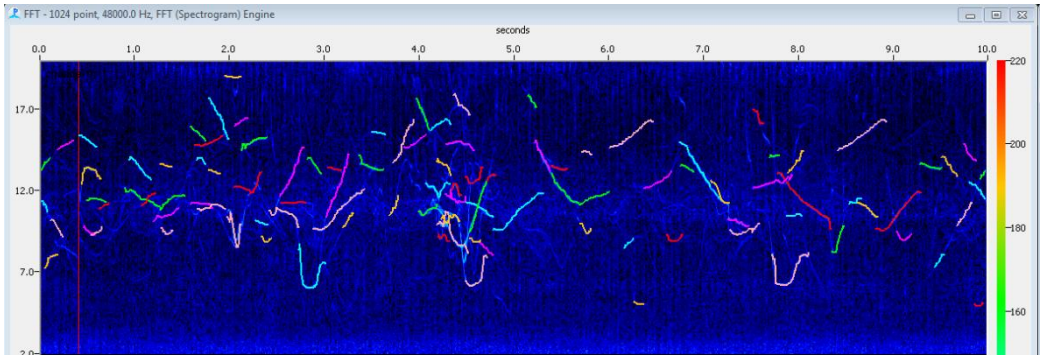

Figure 6: *PAMGUARD* spectrogram display with dolphin whistles that have been detected by the whistle and moan detector as evidenced by the color overlays. Please note the file used to generate the screen image was not obtained during the CaySeis survey.

4.2.3.3. Click Detector

Two click detectors, one for low/mid frequency clicks and one for high frequency clicks were incorporated into the *PAMGUARD* settings files used on the CaySeis survey. The high frequency click

detector was run in a separate settings file from the low/mid frequency click detector. The click detectors were configured to receive the raw input from the hydrophone.

The raw signal from the hydrophone was filtered through a Butterworth high pass filter for the low/mid frequency click detector or a Butterworth band pass filter for the high frequency click detector. The high pass filter searched for pulsed vocalizations with a minimum frequency of 4 kHz. The band pass filter for the high frequency click detector searched for pulsed vocalizations between 10 and 200 kHz. Filtered audio then had to exceed the designated threshold value of 10dB to be plotted on the amplitude/time display of the click detector module (Figure 7).

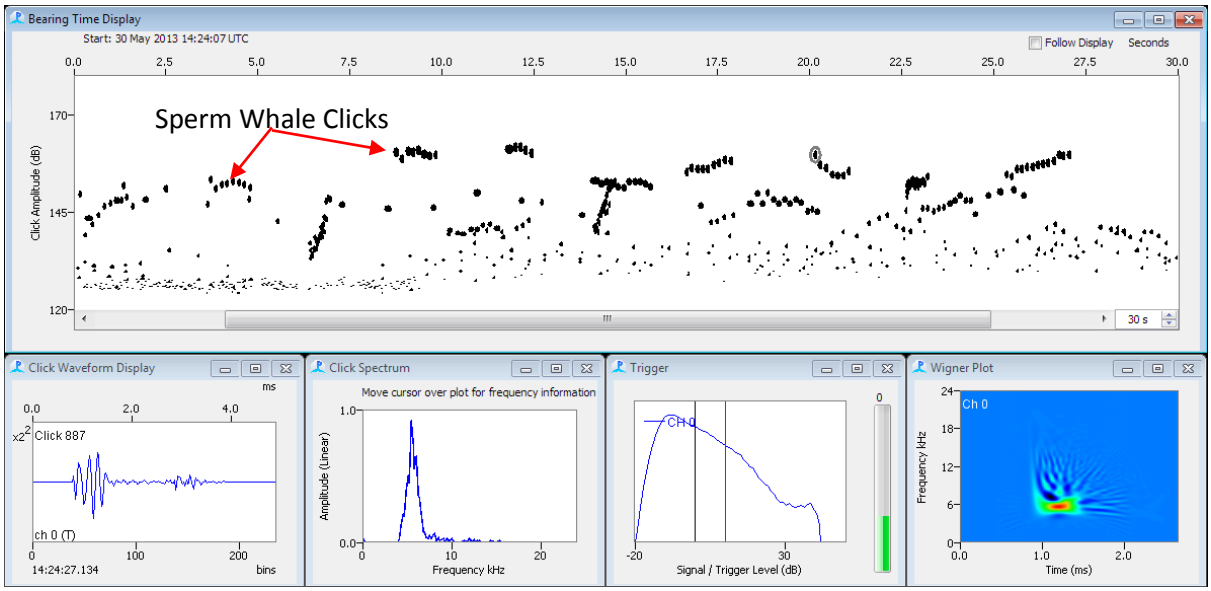

Figure 7: *PAMGUARD* click detector display with detected sperm clicks from multiple individuals on the amplitude/time display (top), click waveform (bottom left), click spectrum (bottom second from left), trigger threshold window (bottom second from right), and Wigner plot (bottom right). Please note the file used to generate the screen image was not obtained during the CaySeis survey.

A conservative threshold value of 10dB was utilized for the detector so as to limit the possibility of missing cetacean clicks, but resulted in numerous false clicks. As with false tonal sounds, false clicks were determined to be non-biological by the operator through aural monitoring and analysis of the individual click waveform, spectrum, and Wigner plot.

5. SEISMIC SOURCE OPERATIONS

Over the course of the survey, the source array was active for 14% of the total time (day and night; Figure 8). OBS deployment and recovery were conducted while the source array was inactive and accounted for the majority of the survey time.

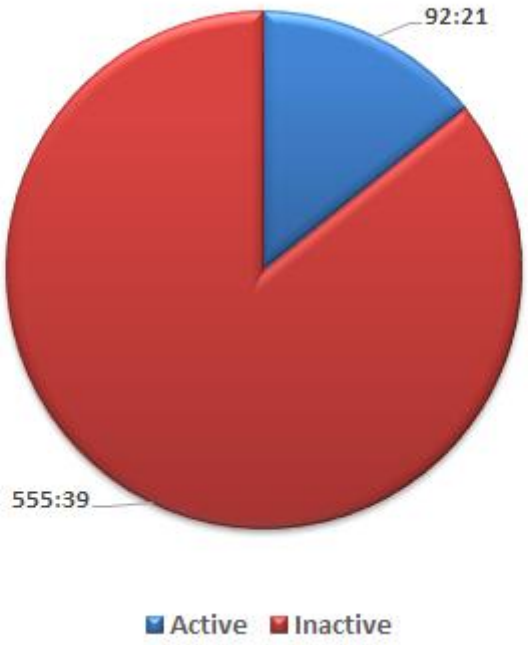

Figure 8: Source activity throughout the CaySeis survey.

The seismic source array was in operation for a total of 92 hours 21 minutes, of which 93% was at full power while on profile (Figure 9). The remaining 7% of airgun operations was composed of soft start (3%) and full power operations approaching the start the start of the profile or immediately after completion of the profile (4%). The airguns were ramped up from silence five times during the CaySeis survey, four during daylight hours after 60 minute visual and acoustic pre-soft start surveys and one at night after 60 minutes of acoustic monitoring.

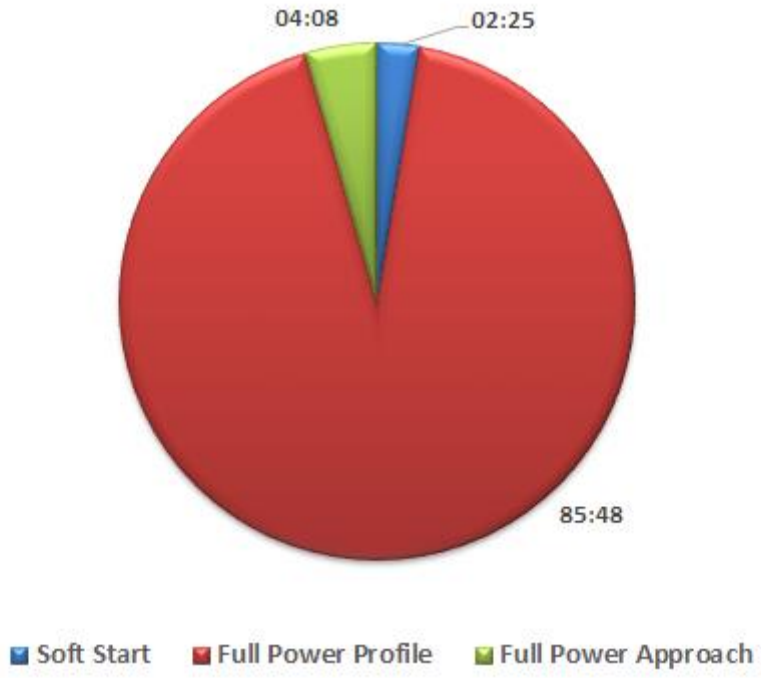

Figure 9: Summary of airgun operations while the source was active.

6. MONITORING EFFORT

6.1. VISUAL MONITORING

Visual monitoring for marine mammals was conducted for 236 hours 54 minutes over the course of the survey, 21% of which took place while the source array was active (Figure 10).

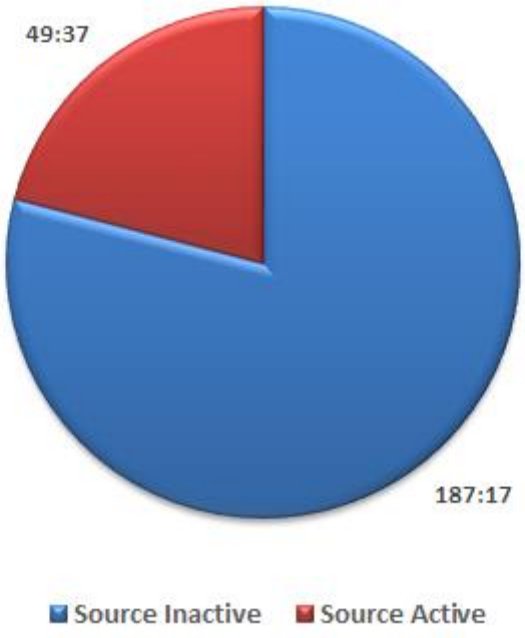

Figure 10: Visual monitoring effort while the source array was active and inactive.

6.1.1. Weather Conditions

Weather conditions were fairly consistent throughout the CaySeis survey, however there were occasional periods during which detection of marine mammals at or near the surface were hindered by large swells and choppy sea conditions. Visibility was greater than 5 kilometers for most of the survey and was only reduced to 3 to 4 kilometers during short periods of rain, which lasted anywhere from a few minutes to 30 minutes. Rain was predominantly light, with 71% of all rain showers consisting of light rain (Figure 11). Heavy precipitation, which had the greatest impact on visibility, occurred for only 22 minutes.

The Beaufort wind force averaged 4 (winds between 5.5 and 7.9 m/s), with a minimum of 1 (winds between 0.3 and 1.5 m/s) and maximum of 6 (winds between 10.8 and 13.8 m/s). The majority of visual observations were conducted during Beaufort 4 or 5 wind states (Figure 12).

Seas were slight (Figure 13), with swells less than 2 meters (Figure 14) during the majority of the survey.

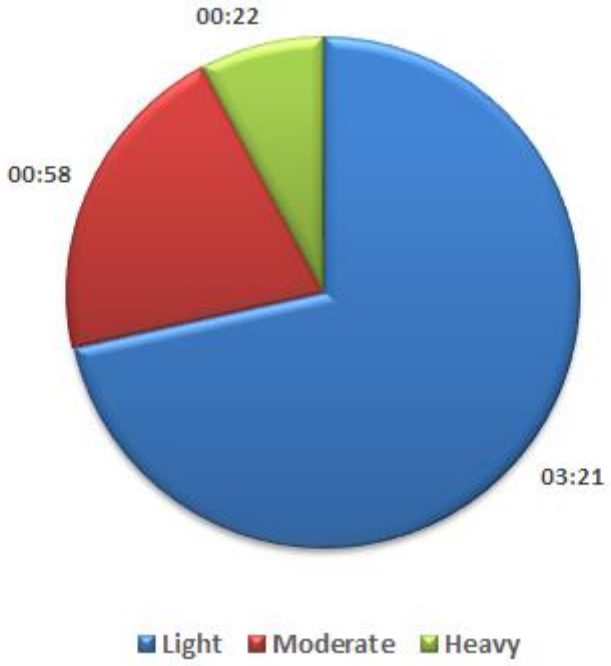

Figure 11: Rain shower activity during visual monitoring.

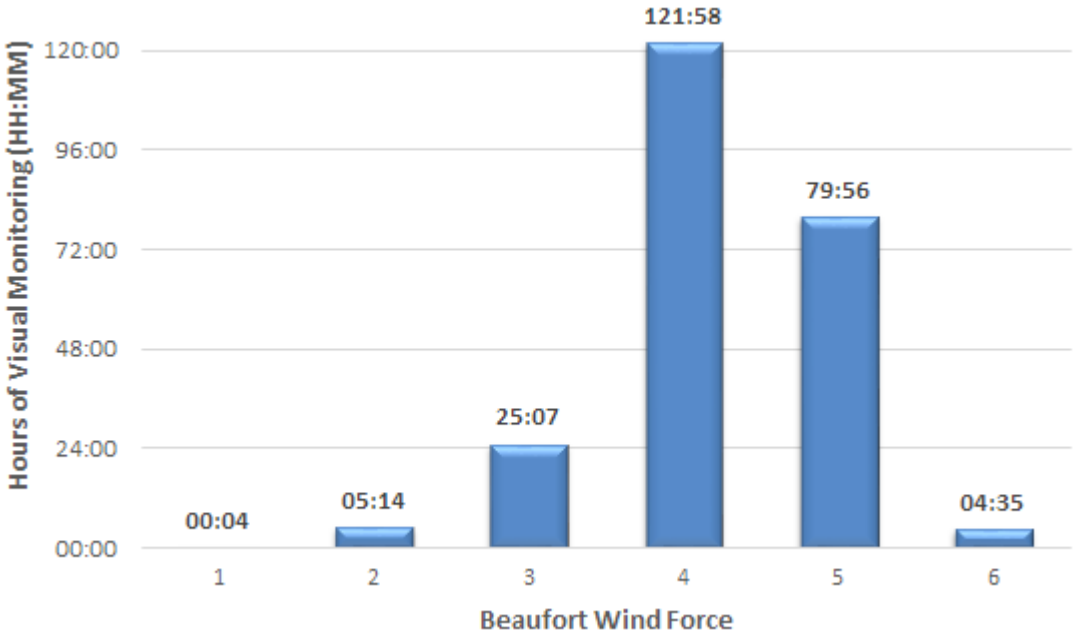

Figure 12: Beaufort wind force during visual monitoring.

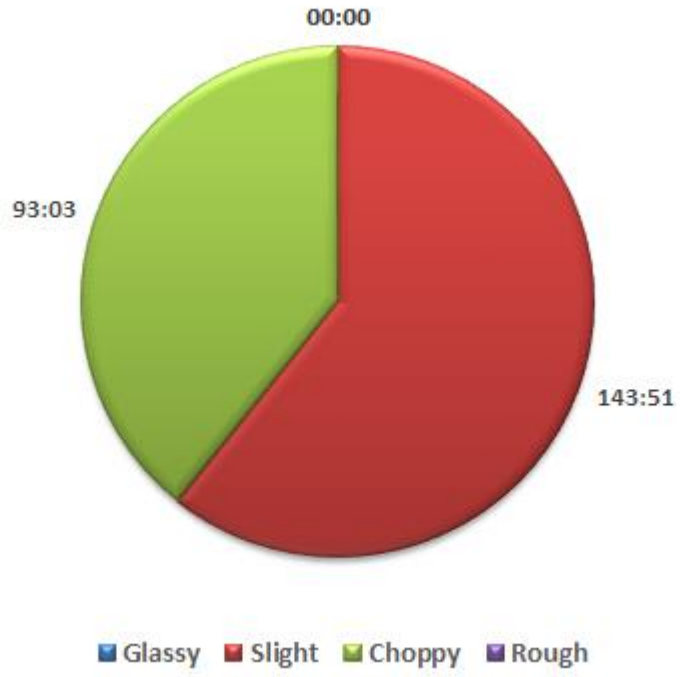

Figure 13: Sea surface conditions during visual monitoring.

Figure 14: Swell during visual monitoring.

6.2. ACOUSTIC MONITORING

Acoustic monitoring for marine mammal vocalizations was conducted for 5 hours 49 minutes over the course of the survey, the majority (89%) of which took place while the source array was inactive (Figure 15).

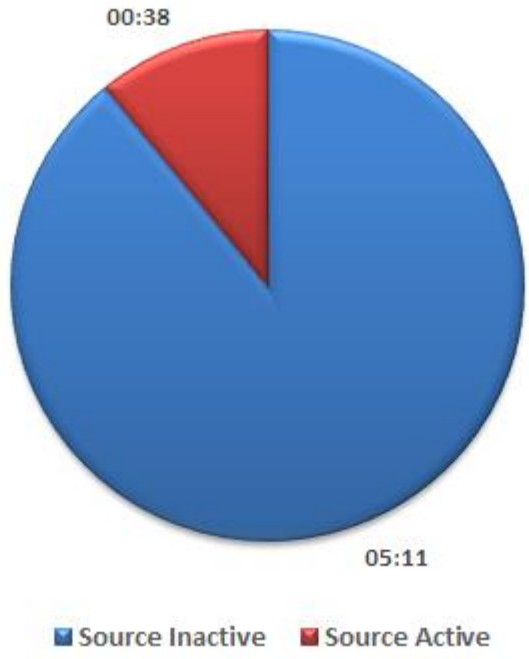

Figure 15: Acoustic monitoring effort while the source array was active and inactive

7. WILDLIFE SUMMARY

7.1. MARINE MAMMAL DETECTIONS

7.1.1. Visual Detections

Two visual detections of marine mammals were recorded during the CaySeis survey, both of delphinid species.

A small pod of bottlenose dolphin were observed on 07 April 2015, while in the survey area. The pod of eight adult dolphin approached the bow of the *Meteor* coming within 50 meters of the vessel and briefly remained in the area before heading away from the vessel. The airgun array was on deck at the time of the detection and the crew was in the process of recovering OBS units.

Approximately five unidentified blackfish were briefly observed by one of the members of the science team during the transit to Guadeloupe on 25 April 2015. The blackfish (short-finned pilot whale, false killer whale, or melonheaded whale) were travelling in the opposite direction of the vessel, approximately 30 meters off the starboard side. Identification was hindered due to the brevity of the detection and vessel speed (12 knots).

7.1.2. Acoustic Detections

Marine mammals were not detected acoustically during the CaySeis survey.

7.2. OTHER NOTABLE WILDLIFE

Numerous flying fish, as well as a few mahi mahi were observed during the CaySeis survey.

However, most notable were the observations of avifauna that used the *Meteor* as a temporary resting place. Several barn swallows made their home on the vessel and were soon found by a few species of falcon, including a merlin and a peregrine falcon. Other species of birds observed included cattle egrets, brown booby, magnificent frigatebirds, and a gray kingbird. Figure 16 provides a few examples of the avifauna observed on the *Meteor* during the CaySeis survey.

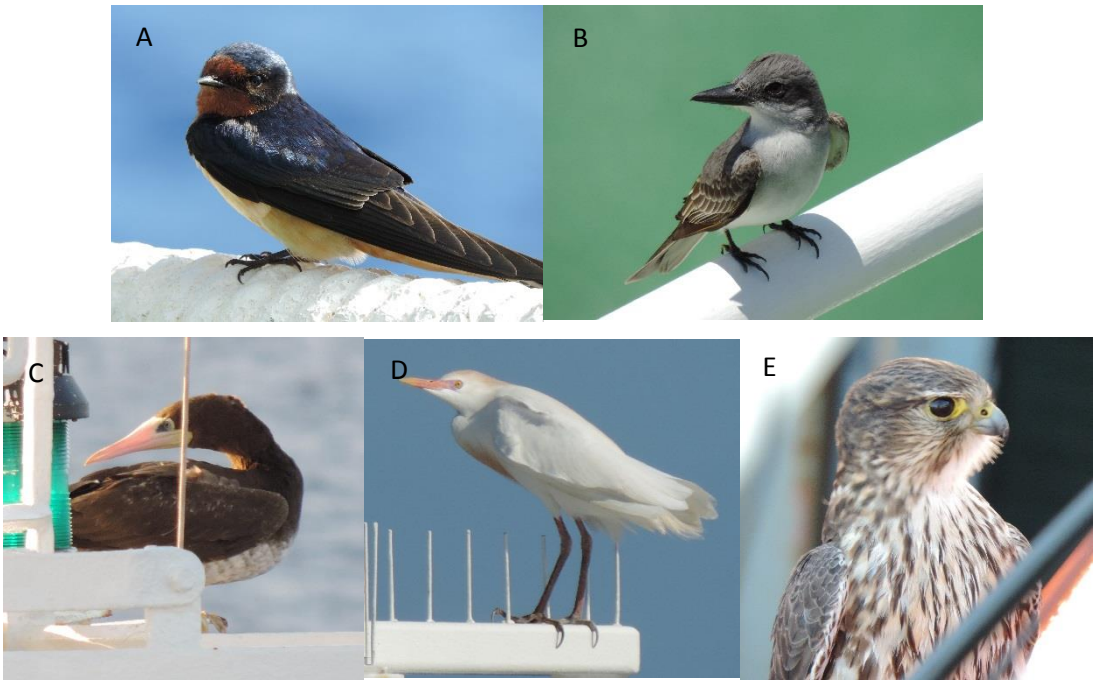

Figure 16: Avifauna observed during the CaySeis survey, including barn swallow (A), gray kingbird (B), brown booby (C), cattle egret (D), and merlin (E).

8. MITIGATION ACTION SUMMARY

Mitigation actions (soft start delays) were not required on the CaySeis survey.

9. ACKNOWLEDGEMENTS

The maritime and scientific crew on the *Meteor* was extremely helpful the to the marine mammal observer team. Both crews assisted with the deployment of the hydrophone array cable, maintained good communications throughout the survey, and were constantly on the lookout for marine mammals.

The scientific team complied with any requests associated with the mitigation and monitoring program for the CaySeis survey.

10. REFERENCES

Cayman Islands Government, Department of the Environment Memo. 26 September 2014.

JNCC guidelines for minimising the risk of injury and disturbance to marine mammals from seismic surveys. August 2010.